Regulation of Theiler's Virus Induced Cell Death

BY

SEVIM YILDIZ ARSLAN

M.S., University of Illinois at Chicago, 2008
B.S., Halic University, Istanbul, Turkey, 2004

THESIS

Submitted as partial fulfillment of the requirements

for the degree of Doctor of Philosophy in Microbiology and Immunology

in the Graduate College of the

University of Illinois at Chicago, 2013

Defense Committee:

Howard Lipton, Chair and Advisor

Nancy Freitag

Yee-Kin Ho, Biochemistry and Molecular Genetics

Alan McLachlan

Deepak Shukla

David Ucker

ACKNOWLEDGMENTS

I would like to thank my thesis advisor, Dr. Howard L. Lipton, for his constant encouragement and guidance. Dr. Lipton provided a research environment in which I was continuously pushed to become a better scientist with larger ideas and a greater understanding of virology. Over the years, as I developed as a PhD Candidate, I learned to think critically about my work. Through the directed guidance of Dr. Lipton, I am armed with the investigative research problem-solving skills to establish collaborations.

The members of the Lipton Lab have also been tremendous in their support and friendship: The mentorship of Dr. Kyung-No Son has proven invaluable in my professional development and opened my mind to the power of discussion. A great deal of thanks is owed to Patricia Kallio, whose help and strict supervision of laboratory practices and procedures led to a productive research environment. I would also like thank Dr. Shannon Hertzler and Dr. Zhiguo Liang for their precious time and advice in helping me accomplish my research goals.

To my Dissertation Committee members for their innovative ideas, critical discussion and research insight: Dr. Alan McLachlan, Dr. David Ucker, Dr. Deepak Shukla, Dr. Nancy Freitag and Dr. Yee-Kin Ho.

To Chicago Biomedical Consortium (CBC) that exposed me to immense networking and funding opportunities.

Lastly, I am grateful to my family. It would not have been accomplished without their support. It is with them all in mind, I can begin each day with the same passion for success.

Table of Contents

LIST OF FIGURES

LIST OF FIGURES (continued)

LIST OF FIGURES (continued)

LIST OF TABLES

LIST OF ABBREVIATIONS

Apaf-1	Apoptotic protease activating factor 1
CARD	Caspase-recruitment domain
CMV	Cytomegalovirus
CNS	Central nervous system
CSF	Cerebrospinal fluid
CTL	Cytolytic T lymphocyte
DD	Death domain
DED	Death effector domain
DISC	Death-inducing signaling complex
DR	Death receptors
EMCV	Encephalomyocarditis virus
FACS	Fluorescence activated cell sorting
FADD	Fas-associated death domain
FCV	Feline calicivirus
H_2DCFDA	2′,7′-dichlorodihydrofluorescein diacetate
HIV-1	Human immunodeficiency virus type-1
HSV-1	Herpes simplex virus type-1
IRES	Internal ribosome entry site
KSHV	Kaposi's sarcoma-associated herpesvirus
L	Leader protein
MCMV	Murine cytomegalovirus

LIST OF ABBREVIATIONS (continued)

MOI	Multiplicity of infection
MOMP	Mitochondrial outer membrane permeabilization
MS	Multiple sclerosis
Nec-1	Necrostatin-1
pi	Post-infection
PRRs	Pattern recognition receptors
RHIM	Homotypic interaction motif
RIP	Receptor interacting protein
ROS	Reactive oxygen species
TMEV	Theiler's murine encephalomyelitis virus
TO	Theiler's Original
TRADD	Tumor necrosis factor receptor type 1-associated death domain
UTRs	Untranslated regions
VV	Vaccine virus
WNV	West nile virus

CHAPTER 1

1. Introduction

1.1 Theiler's murine encephalomyelitis viruses (TMEV)

Theiler's murine encephalomyelitis viruses (TMEV), members of the *Cardiovirus* genus in the family *Picornaviridae*, are enteric pathogens of mice. In 1934, TMEV was isolated by Max Theiler, who was awarded a Nobel Prize for developing the first effective vaccine against yellow fever [1, 2]. It has an 8.1 kb positive-sense RNA genome that is highly cytolytic, causing a persistent central nervous system (CNS) infection and immune-mediated demyelination in susceptible strains of mice. This provides a relevant experimental animal model for multiple sclerosis (MS) [3]. MS is an inflammatory disorder of the CNS with a lifetime risk of one in 500 and around 2.5 million affected individuals worldwide. It is a common cause of neurological disability in young adults [4]. Different modalities of immunosuppression, including cytoxan, anti-CD4 antibodies, tolerization to Theiler's virions, and macrophage-depletion reduce pathologic changes and clinical signs (spastic paralysis). However, there is no known cure or vaccination against TMEV-induced demyelinating disease. It is essential to understand the mechanism of virus-host interaction to facilitate the development of novel antiviral strategies.

1.2 Life cycle of TMEV

Cell to cell spread of TMEV is required for persistence *in vivo* and *in vitro [5]*. After entry of the virus into the host cell, TMEV will immediately begin the replication cycle in the host cell cytoplasm. The RNA strand is polyadenylated at the 3' end. At the 5' end it contains a small protein covalently linked termed, VPG [6]. TMEV RNA includes a large open reading frame (ORF) that encodes a 2309 amino acid flanked by untranslated regions (UTRs) (Fig. 1). During translation, the chain is cleaved into 12 mature proteins by autoproteolytic activity. Translation of the open reading frame is initiated by the internal ribosome entry site located at the 5' non-coding region. The persistent strains of TMEV have an additional open reading frame that encodes an 18-kDa leader (L) protein. The function of the L protein was shown to facilitate in the infection of Theiler's virus and viral persistence [3, 7]. TMEV also contains 4 polypeptide chains VP1, VP2, VP3, and VP4 that assemble to form the viral capsid. The role of protein 2A is unknown; however, some picornaviruses such as poliovirus use 2A to cleave VP1 from the newly translated polyprotein [6]. 3B also termed VPG is covalently linked to the 5' end, and 3B is used during encapsulation and replication. 3C is the proteinase that is responsible for the majority of the polyprotein cleavages. 3D is the RNA-dependent RNA polymerase, and proteins 2B, 2C, and 3A are used in the replication cycle (Fig. 2).

BeAn Virus Gene products

Protein	RNA Loci	No. A.A	MW (kDa)
L (P8)	1065	76	8.5
1A(VP4)	1293	71	7.1
1B(VP2)	1506	267	29.4
1C(VP3)	2307	232	25.5
1D(VP1)	3003	276	30.6
2A	3831	143	16.4
2B	4257	127	14.8
2C	4638	326	36.8
3A	5616	88	9.9
3B	5880	20	2.2
3C	5940	217	23.6
3D(P56)	6591	461	52.2

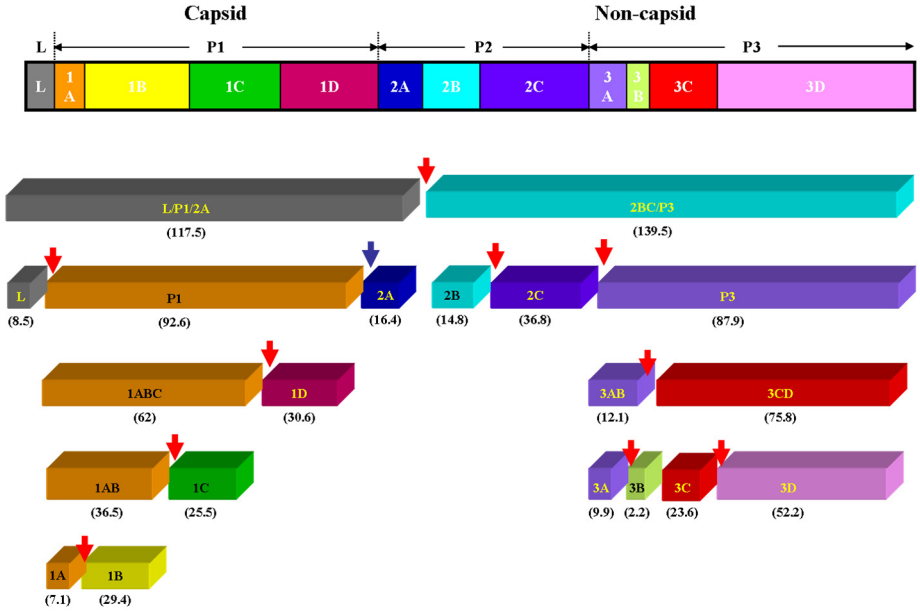

Figure 1. Theiler's virus genomic organization. It codes for 12 structural (VP1, VP2, VP3, & VP4, used in capsid assembly) and non-structural proteins (2A, 2B, 2C, 3A, 3B, 3C, & 3D). It has IRES at 5' end for translation initiation of polypeptide chain, used in replication cycle.

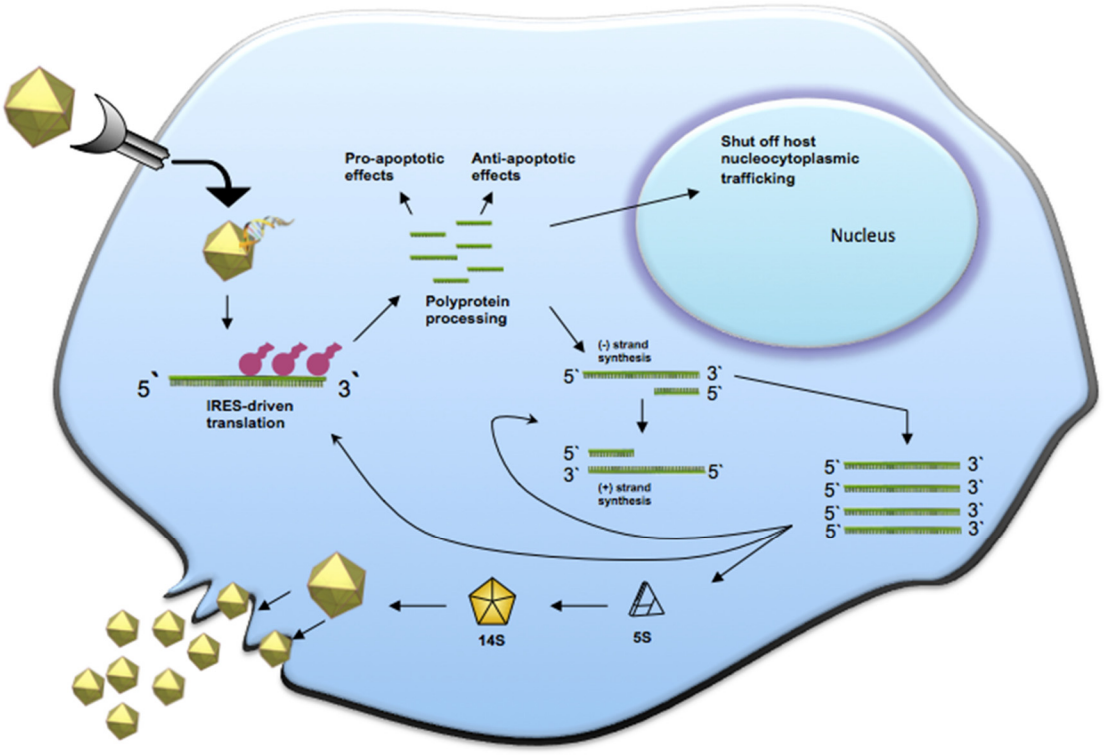

Figure 2. TMEV life cycle**.** Following binding to the cognate receptor, the virus undergoes uncoating, and the viral genome is released. TMEV is positive-sense RNA virus that codes for 12 proteins. This cap is absent from the 5′ end of picornavirus RNAs, which therefore cannot undergo cap-dependent translation, and translational initiation in these viruses instead depends on the IRES (internal ribosome entry site). The viral polyprotein is rapidly processed both during and after translation. Most picornaviruses effectively terminate host-cell translation and transcription. Capsid assembly starts with formation of a protomer that consists of four viral capsid proteins. Five protomers then are linked together with hydrophobic interactions to form the pentamer. 12 pentamers associate by means of electrostatic interactions to form the mature virion.

1.3 Pathogenesis of TMEV infection

Theiler's virus is a naturally occurring enteric pathogen of mice and in early disease causes poliomyelitis-like flaccid paralysis in mice [8]. Theiler's viruses are divided into two subgroups: GDVII and Theiler's Original (TO). The GDVII subgroup viruses (FA and GDVII) are extremely neurovirulent and cause necrotizing encephalitis and death in the murine host within 7 days of intracerebral (i.e.) infection even at very low doses, resulting in acute fatal polioencephalomyelitis without demyelination [9]. Intracerebral infection of mice with TO subgroup viruses (DA and BeAn) induces acute encephalitis between days 5 and 10 post-injection (pi) in all strains of mice. Virus replicates primarily in neurons during acute phase of infection and viral titers escalate rapidly [10]. Within two weeks of infection, virus is cleared from the gray matter of mouse strains resistant to persistent infection (H-$2^{d,\ b}$) by a strong cytolytic T lymphocyte (CTL) response directed against the VP2 viral capsid protein [11-15]. Infection of these animals results in no obvious functional deficits, leading to a quick recovery. In contrast, some strains of mice are unable to efficiently clear the virus from the CNS and a persistent infection is established in the white matter of the brain and spinal cord, where demyelination and chronic inflammation develops. The infiltrate is comprised of CD4- T cells, CDR+ T cells, B cells, and activated microglia/macrophages. Macrophages are the main reservoir of BeAn virus in chronically infected mice. Low levels of virus can also be detected in oligodendrocytes [16, 17], microglia/macrophages [10, 18, 19], and astrocytes [17, 19].

TMEV persistence in mice is recognized as a relevant experimental animal model for multiple sclerosis [20, 21]. The initial demyelination in the TMEV model is due to direct viral damage to the myelin-producing oligodendrocytes. Ongoing chronic demyelination is a result of autoimmune responses to previously sequestered self-epitopes, known as epitope spreading phenomenon [22, 23]. Clinical signs of chronic TMEV infection such as weakness, spasticity, incontinence, and paralysis are similar to those observed in patients with chronic progressive MS [10]. TMEV infection of susceptible strains of mice results in intrathecal antibody production similar to the oligoclonal hands found in the cerebrospinal fluid (CSF) of MS patients [24].

1.4 Cell death.

1.4.1 Apoptosis.

Apoptosis, or type 1 programmed cell death, occurs normally during the life cycle of an organism to maintain homeostasis of cell populations in tissues. It is triggered in response to a wide variety of stimuli during development and in the event of severe cellular stress, viral infection or damage. Aberrant regulation of apoptotic cell death mechanisms has been implicated in a number of human diseases.

Apoptosis is characterized by the activation of pathways leading to the activation of a family of proteases: caspases that will then cleave a number of substrates [25], resulting in the biochemical and morphological changes typical of this form of death. Caspases are divided into two groups, the upstream initiator caspases

(caspase-9, caspase-2, caspase-8, and caspase-10) and the downstream executioner caspases (caspase-3, caspase-6, and caspase-7) [26]. Activation of caspases results in the cleavage of downstream substrates that result in apoptosis. During this process, dying cell initially shows nuclear and cytoplasmic condensation, followed by blebbing of the plasma membrane that are phagocytosed by macrophages, parenchymal cells, or neoplastic cells and degraded within phagolysosomes [27].

There are two main subtypes of apoptosis that are signaled through different biochemical routes (Fig. 3). The extrinsic apoptotic pathway is a mechanism of transmitting extracellular signals through death receptors, collectively known as death receptors (DR) belonging to the TNFα/NGF family that activate intracellular apoptotic machinery. Ligand binding to the receptor recruits cytoplasmic adapter proteins, such as FADD (Fas-associated death domain) TRADD (tumor necrosis factor receptor type 1-associated death domain) and RIP (receptor interacting protein), with corresponding death domains to the death receptors. Adaptor proteins then associate with the N terminal domain of initiator caspases, procaspase-8 or -10 via dimerization of the death effector domain (DED). This triggers conformational changes allowing the assembly of a large multi-protein complex, known as the death-inducing signaling complex (DISC), resulting in the auto-catalytic cleavage and activation of initiator caspases that can directly cleave and activate the effector caspase-3 and inducing apoptosis.

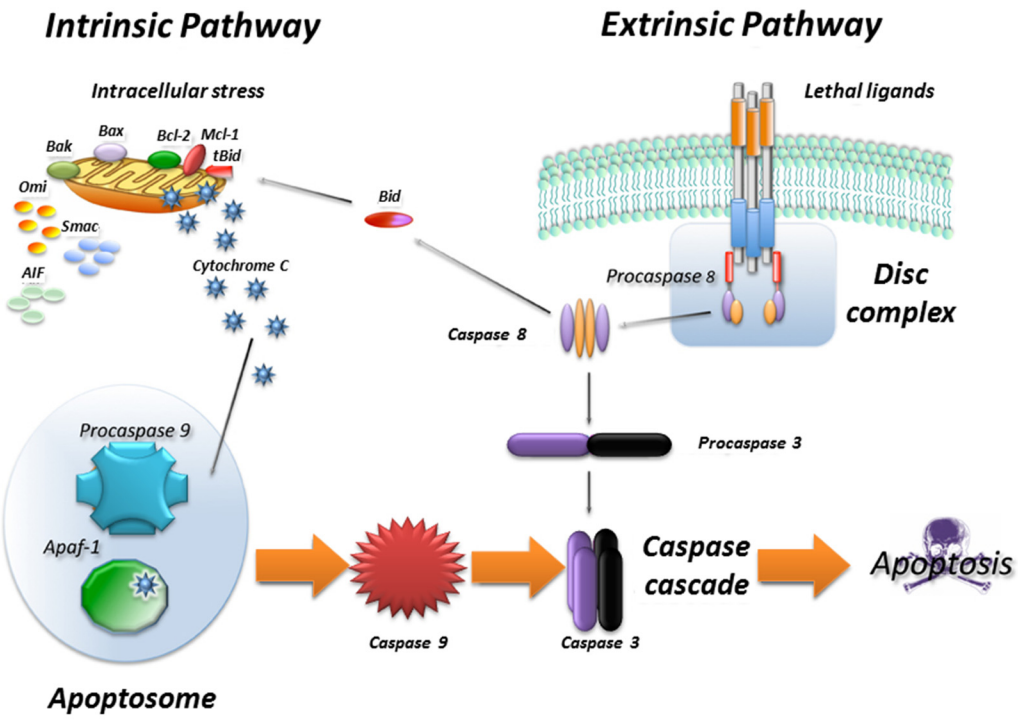

Figure 3. Intrinsic and extrinsic apoptosis pathways. Both the intrinsic (left panel) and extrinsic (right panel) pathways use related principles in receiving an apoptotic signal and executing apoptosis. In the intrinsic pathway, an apoptotic stimulus in the cell causes to the assembly of a signaling network, the apoptosome, which activates the initiator caspase-9. However the extrinsic apoptotic pathway is mediated by binding of an extracellular ligand to a transmembrane receptor (lethal ligands), leading to the formation of the death-inducing signalling complex (DISC), which is capable of activating the initiator caspase-8. Caspase-8 and -9 then activate downstream caspases such as caspase-3 and -7, which represents the execution level of the caspase cascades and resulting in cell death (Adapted from Favaloro *et al*. [28]).

The intrinsic pathway is activated in response to a number of stressing conditions including include DNA damage, reactive oxygen species (ROS), radiation, viral infection, hypoxia, and toxins as well as loss of apoptotic suppression and cell survival factors. In all cases this multiple forms of stress that induce a signaling cascade that ultimately results in mitochondrial outer membrane permeabilization (MOMP), resulting in dissipation of the mitochondrial membrane potential and therefore in cessation of ATP production as well as release of a number of proteins that contribute to caspase activation. Apoptosome formation is caused by binding of cytochrome c to the C terminal region of Apaf-1 (Apoptotic protease activating factor 1), a cytosolic protein with an N-terminal caspase-recruitment domain (CARD) and a nucleotide-binding domain [29]. Once assembled, the apoptosome can bind and caspase-9, which cleaves and activates the effector caspase-3 [30]. Members of the Bcl-2 family include critical effectors and regulators of the intrinsic apoptotic pathway [31]. The Bcl-2 family members control the process of mitochondrial outer membrane permeabilization by a coordinated effort between anti-apoptotic (Bcl-2, Bcl-xL, Bcl-w, Mcl-1 and A1), pro-apoptotic effector (Bak and Bax) and pro-apoptotic BH3-only proteins (Puma, Noxa, Bim, etc.). Pro-apoptotic members of the family mediate apoptosis by disrupting membrane integrity either directly forming pores or by binding to mitochondrial channel proteins such as VDAC or ANT, while anti-apoptotic family members block apoptosis by negatively regulating Bax and Bak until their protective effect is countered by the binding of proapoptotic BH3-only proteins [32, 33]. In some cell types where only a small

amount of active caspase-8 is produced, the apoptotic signal can be amplified by cleavage of the BH3 domain containing Bcl-2 family member BID in the proapoptotic fragment tBID. Cleaved tBID then translocated to the mitochondria and results in the aggregation of Bax and Bak on the mitochondria releasing cytochrome c, which stimulates the apoptosome and promotes activation of caspase-9 and subsequent cleavage and activation of the apoptosis effector caspase-3 [34].

The anti-apoptotic Bcl-2 family member Mcl-1, initially isolated from a human myeloblastic leukemia cell line [35], reportedly predominates in differentiated human macrophages [36] and protects against apoptosis during the initial steps of differentiation [37, 38]. Whether Mcl-1 is the key anti-apoptotic protein that regulates and determines the mechanism of TMEV-induced cell death in other cells remains to be determined. Its expression levels may not only provide greater protection against TMEV-induced apoptosis but also may point to specific upstream pro-apoptotic BH3-only activators, Puma and Noxa, which sense cellular damage and engage Mcl-1 to overcome the block to Bax or Bak activation [39]. Identifying upstream signals involved in the intrinsic apoptotic pathway during TMEV infection may eventually permit experiments to modulate and prevent apoptosis during viral infection in the mouse CNS. The tumor suppressor protein p53 is one of many proteins that contribute to the activation of the intrinsic signaling pathway upon exposure to cellular stress. Both Puma and Noxa are transcriptionally up-regulated by p53 in response to DNA damage [37, 40-42].

Preliminary data in our laboratory revealed an increase in total p53 and phosphorylated p53 (ser15) during TMEV infection in M1-D and BHK-21 cells (data not shown), suggesting that the p53 pathway is important in regulation of Mcl-1 and modulating cell death in TMEV infection.

1.4.1.1 Virus-induced apoptosis.

Many DNA and RNA viruses such as chicken anemia virus [43], varicella-zoster virus [44], human immunodeficiency virus [45], Sindbis virus [46, 47], influenza virus [48], and reovirus [49], have been shown to induce apoptotic cell death as the result of productive infection. In contrast, other viruses, including adenovirus [50], poxviruses [51], Epstein-Barr virus [52], baculovirus [53], and African swine fever virus [54], have evolved mechanisms to subvert the apoptotic process, presumably to allow cell survival and continued virus replication. Further, it is known that the fate of cells infected with picornaviruses such as poliovirus depends on the balance of host and viral anti-apoptotic factors [55].

TMEV induces two distinct cell death programs, necrosis and apoptosis, which result in substantial differences in infectious viral yields. All rodent cell types except for macrophages undergo necrosis because of the high viral yields produced [56]; in contrast, murine macrophages undergo apoptosis with restricted viral yields, producing only a few plaque-forming units (pfu) of virus per cell [57]. Further, TMEV infection of mouse M1-D macrophages induces apoptosis by activating the intrinsic apoptotic pathway [57, 58]. In those cells, TMEV infection

results in activation of p38 mitogen-activated protein kinase by 2-3 h post-infection (pi), followed by phosphorylation of tumor suppressor protein p53 Ser 15 at 3 to 6 h pi and stable p53 levels until 6 h pi; activated p53 up-regulates the transcription of the pro-apoptotic *puma* and *noxa* genes at 2 to 4 h pi, and levels of pro-survival Mcl-1 and A1 proteins become undetectable at 4 to 10 h pi [58, 59]. Specific inhibition of phospho-p38 and inhibition of p53 by a genetic suppressor element led to a significant decrease in apoptosis [59]. Degradation of pro-survival proteins was also shown to release Bax [58, 59], which forms homo-oligomers and translocates into and permeabilizes the mitochondrial outer membrane, releasing cytochrome c and initiating the caspase cascade.

It is reported that over-expression of Bcl-2 in TMEV-infected M1-D cells provided significant, albeit modest, cell protection; whereas over-expression of Bcl-xL did not have a salutary effect on cell survival [58]. Furthermore, expression profiles of Bcl-2 and Bcl-xL were not distinguishable in macrophage and rodent cell lines (data not shown) suggesting that other anti-apoptotic proteins may be essential in regulation of TMEV-induced cell death. Overexpression of Mcl-1 in TMEV-infected M1-D cells reduced the cleavage of caspases-3 and -9 to their active forms and inhibited apoptosis [59]. Whether Mcl-1 endogenously regulates TMEV-induced cell death in other cells remains to be determined.

1.4.2 Necroptosis.

Apoptosis is a well-established caspase-dependent host defense pathway triggered through cell-intrinsic or/and cell-extrinsic signals cell-intrinsic in response to pathogens [60, 61]. On the other hand, caspase-independent cell death, or programmed necrosis (necroptosis), has emerged as an alternative death pathway that dominates under specific conditions [62]. Necroptosis is a form of programmed necrosis induced by death receptors (DR) that is independent of caspases but dependent on receptor-interacting protein kinase 1 (RIP1; also known as RIPK1) [63, 64] and RIP3 (also known as RIPK3) [65-67], and it requires the active disintegration of mitochondrial, lysosomal and plasma membranes. Necroptosis is known as an alternative pathway to apoptosis, and is triggered when caspase-8 activation has been suppressed or is absent (Fig. 4) [64].

RIP1 is the founding member of a serine-threonine PK family that transduces inflammatory and cell-death signals following DR ligation, activation of pattern recognition receptors (PRRs), and DNA damage [64]. An amino-terminal PK domain in RIP1 is critical for DR-induced necroptosis [68] and is the target of the inhibitor necrostatin-1 (Nec-1) [32]. RIP1 has a carboxy-terminal death domain (DD) that binds to other DD-containing proteins, an intermediate domain important for NF-kB activation [64] and RHIM-dependent signaling [69]. The RIP1 family member, RIP3 has been identified as a key mediator of caspase-independent cell death [65-67]. RIP3 possesses an N-terminal kinase domain and physically interacts with RIP1 owing to a C-terminal RIP homotypic interaction motif (RHIM)

[69]. The expression levels of RIP3 have been shown to correlate with the propensity of cells to respond to TNFR1 ligation in the presence of caspase-inhibiting agents by undergoing necroptosis [66]. RIP3 has a positive impact on DAI-induced, RIP1 RHIM-dependent NF-kB activation [70, 71], as well as in RHIM-dependent necroptosis induced by TNFα [65-67]. Although mice lacking RIP1 die within 3 days postnatally [72], RIP3-deficient mice are viable and display neither developmental defects nor altered NF-kB signaling triggered by lipopolysaccharide (LPS) or TNFα [73]. Experiments with cells that have been stably or temporarily depleted of RIP3 unequivocally demonstrated that RIP3 is required for TNFR1-elicited necroptosis [65-67].

Beside cytokines, infection with viruses i.e. west nile virus (WNV) [74], human immunodeficiency virus type-1 (HIV-1) [75, 76], murine cytomegalovirus (MCMV) [77] results in necrotic cell death. Whereas cell viability upon HSV-1 infection is increased in the presence of RIPK1 kinase inhibitor Nec-1 [78], RIPK1 deficiency does not protect HIV-1-infected T cells from necrosis [79]. On the other hand, WNV envelope protein has been demonstrated to inhibit the antiviral response by interfering with dsRNA-induced RIPK1 polyubiquitination and NF-kB activation. However, whether WNV-induced necrosis is RIPK1-dependent remains to be determined [80]. One recent report described that vaccine virus (VV) infection sensitizes TNF-resistant cells to TNF-induced cell death [65, 81, 82] and this sensitization requires the presence of RIPK1 and RIPK3. Further, VV infection of RIPK3-deficient mice do not induce necrosis and liver inflammation [65], indicating

that RIPK1- and RIPK3-dependent necroptosis act as a critical pathway, regulating the inflammatory response against virus infections.

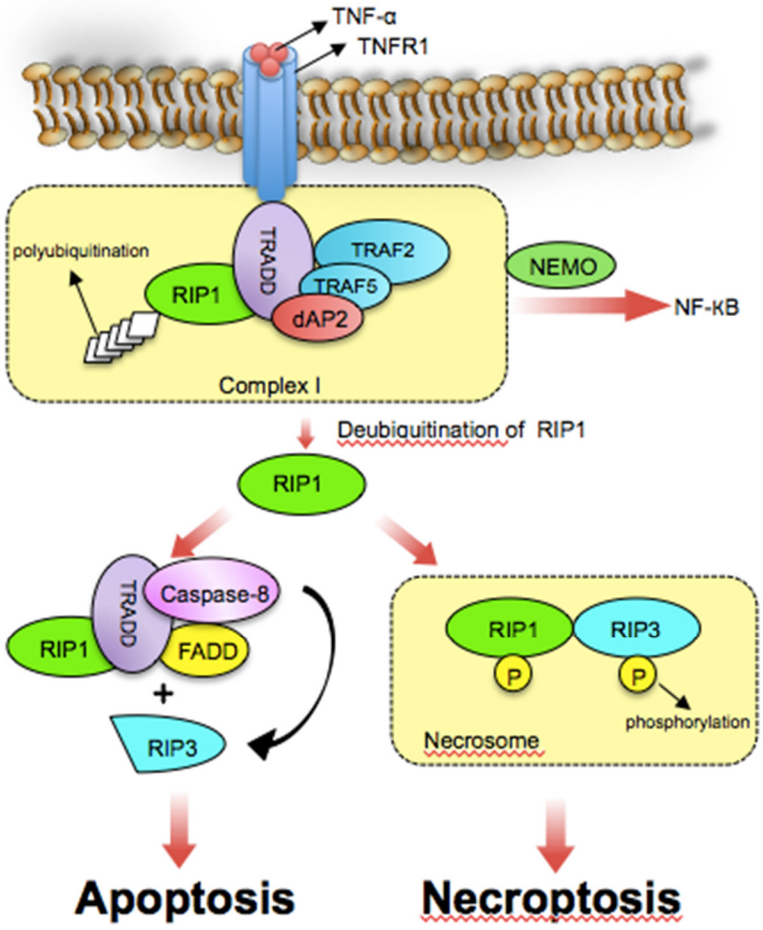

Figure 4. Formation of necrosome. After binding to TNF-α, the intracellular domain of TNFR1 summons a series of proteins, including TNF receptor-associated death domain (TRADD), receptor-associated death protein1 (RIP1), and Fas-associated death domain (FADD). Meanwhile, several E3 ligases, such as TNF receptor associated factor 2/5 (TRAF2/5), inhibitor of apoptosis proteins (IAPs) cIAP1 and

cIAP2 are also recruited to TNFR1. Those proteins mentioned above form “complex I”. RIP1 is ubiquitilatized in complex I, and has the ability to activate of the IκB kinase (IKK) complex and NF-κB essential modulator (NEMO), leading to the activation of prosurvival NF-κB pathway in consequence. When RIP1 is deubiquitilitized by cylindromatosis (CYLD), it is released to the cytoplams, and forms complex II with TRADD, FADD, RIP3 and caspase-8. While caspase-8 is activated, it would cleave RIP3 and induce apoptosis through caspase cascade. However, when caspase-8 is blocked, phosphorylated RIP1 and RIP3 form necrosome and initiate necroptosis. (Adapted from Wu *et al.* [83]).

CHAPTER 2

2.1 Hypothesis and Aims

Theiler's virus is a highly cytolytic RNA virus that causes a persistent CNS infection and immune-mediated demyelination in susceptible strains of mice, providing a relevant experimental animal model MS. TMEV infected macrophages undergo apoptosis and restrict virus replication (<10 pfu/cell). This stands in contrast to TMEV infection in other rodent cells, including neurons and oligodendrocytes, which produce necrotic cell death with high virus yields (200-500 pfu/cell). The contrasting outcomes of TMEV infection suggest the existence of distinct virus-induced cell death pathways. However, the factors that are critical in regulation of the two distinct TMEV-induced cell death pathways are not well known. These studies will provide knowledge toward the dynamic and nature of TMEV regulation by apoptosis that may give rise to development of novel antiviral strategies against persistence CNS infection.

The overall objective of this study is to gain an understanding of the molecular events in TMEV infection culminating in cell death. The type of cell death may directly influence pathogenesis and disease. Based on preliminary findings in the course of the work, four specific aims were proposed to test the hypothesis:

1. To gain insight into the upstream signaling events that lead to apoptosis by examining the role of each non-structural proteins of Theiler's virus.

2. To investigate the role of Mcl-1 on the regulation of BeAn-induced cell death and identify upstream signals, such as p53, that are involved in the intrinsic apoptotic pathway.

3. To characterize the role of RIP1 on BeAn-induced necroptotic cell death that generates high yields of infectious virus.

4. To study the mechanism of how apoptosis results in loss of infectivity.

CHAPTER 3

3.1 Materials and Methods

3.1.1 Cells and Viruses.

BHK-21 cells were grown in Dulbecco's modified Eagle medium supplemented with 10% fetal bovine serum (FBS), 7.5% tryptose phosphate, 2 mM L-glutamine, 100 U/ml penicillin, and 100 μg/ml streptomycin at 37°C in 5% CO^2. Cells of the immature myelomonocytic cell line M1, derived from the SL mouse strain, were induced to differentiate into macrophages with supernatants from L929 and P388D1 cells as described previously [56]. N20.1 mouse oligodendrocytes were grown in Dulbecco modified Eagle medium (DMEM)/F-12 medium containing 100 μg of streptomycin, 100 U of penicillin per ml, and 10% FBS at 37°C in 5% CO_2 (37); the cells at this temperature were undifferentiated and consisted of immature oligodendrocytes. The origin and passage history of the BeAn virus stock have been described [84]; generation of BeAn virus with mutation in the L-protein Zn finger domain is described below.

3.1.2 Reagents.

The following reagents and antibodies were purchased commercially: the pancaspase inhibitor qVD-OPh and rabbit anti-caspase 8 (R&D Systems, Minneapolis, MN); mouse anti-caspase 9, rabbit anti-caspase 3, rabbit anti-poly(ADP-ribose) polymerase (PARP), rabbit anti-Bak, rabbit anti-Flag M2, and rabbit antiactin antibodies (Cell Signaling Technology, Beverly, MA); mouse anti-Bax, Mcl-1 siRNA, and Mcl-1 short hairpin RNA (Santa Cruz Biotechnology Inc.,

Santa Cruz, CA); goat anti-mouse immunoglobulin G (IgG)-horseradish peroxidase and goat anti-rabbit IgG-horseradish peroxidase (BD Pharmingen, San Diego, CA); anti-rabbit IgG–Alexa Fluor 568 and puromycin (Invitrogen, Carlsbad, CA); enhanced chemiluminescence solution (Amersham, Piscataway, NJ); cell-permeative proteasome inhibitor MG132 (Calbiochem, Darmstadt, Germany); and actinomycin D (Sigma, St. Louis, MO). Active recombinant mouse caspase -3 used for capsid protein cleavage studies were purchased from Biovision.

3.1.3 Virus infections.

After virus adsorption at a multiplicity of infection of 10 for 45 min at 24°C, cell monolayers were washed twice with phosphate-buffered saline (PBS) containing 1 mM $CaCl_2$ and 0.5 mM $MgCl_2$ and incubated in Dulbecco's modified Eagle medium containing 1% FBS at 37°C for various times. The end of the adsorption period was designated as time zero.

3.1.4 Virus titers.

Virus titers of clarified lysates of infected cells were determined by standard plaque assay [84] or by tissue culture infectious dose 50 ($TCID_{50}$) in BHK-21 cells. Briefly, cell monolayers (2 x 10^4 cells/well) in 96-well plates were infected with serial 10-fold dilutions of virus and the viral cytopathic effect (CPE) was monitored under an inverted light microscope. On day 5 of incubation, the 50% tissue culture infective dose was calculated as the reciprocal of the lowest 10-fold dilution resulting in CPE in more than 50% of the monolayers [85].

3.1.5 Cell viability assay.

WST-1 reagent (Roche Applied Science, Indianapolis, IN), a tetrazolium salt, was added to the medium of monolayer cultures in 96-well microtiter plates at the indicated times, and plates were incubated for 1 to 2 h at 37°C in 5% CO_2. Cell viability was determined based on the absorbance of samples at 420 nm (reference wavelength, 610 nm) measured with a Vmax kinetic microplate reader (Molecular Devices, Sunnyvale, CA), indicating cleavage of the tetrazolium salt to formazan against background and medium-alone controls. Cell death values were calculated as the ratio of BeAn virus-infected to mock-infected cultures.

3.1.6 Fluorescence-activated cell sorting (FACS).

At various times post-transfection, cell monolayers were washed with PBS and detached with trypsin, and 5 x 10^5 cells were stained with propidium iodide (PI) and annexin V–fluorescein isothiocyanate (Calbiochem, Darmstadt, Germany) according to the manufacturer's instructions. Incubation of cell monolayers with puromycin (2 μg/ml) and actinomycin D (1 or 3 μg/ml) provided positive controls for apoptosis. For each sample, 10,000 events were analyzed using a Beckman Coulter Epics Elite ESP and FlowJo 8.8.3 software.

3.1.7 Plasmid construction.

Overlap extension PCR [86] was used to assemble internal ribosome entry site (IRES) constructs expressing a BeAn virus nonstructural protein(s) by joining the

3’ end of the BeAn virus IRES to nucleotides encoding each of seven nonstructural proteins (2A, 2B, 2C, 3A, 3C, and 3D and the precursor 3CD) with an AUG codon at the N terminus and a Flag epitope at the C terminus. The IRES and each virus protein were amplified from a full-length infectious BeAn virus clone [87] using the primer pairs 1 plus 3 and 2 plus 4, respectively (Fig. 1). The two PCR products were gel purified, mixed in equimolar amounts, and PCR amplified with the primer pair 1 plus 2. The resulting products were digested with NheI and NotI and ligated into the pIRES vector, replacing the encephalomyocarditis (EMCV) IRES with that of BeAn virus. For assembly of the pIRES-L plasmid, the IRES and L were amplified from a full-length infectious BeAn virus clone (19) using the primer pair 1 and 2; for the pL plasmid, L was amplified with primers 1B and 2. The resulting PCR products were digested with NheI and NotI, gel purified and ligated into pIRES digested with the same restriction enzymes. All recombinant plasmids were recovered from transformed Escherichia coli, and the nucleotide sequences of the inserts were confirmed by dideoxynucleotide sequencing.

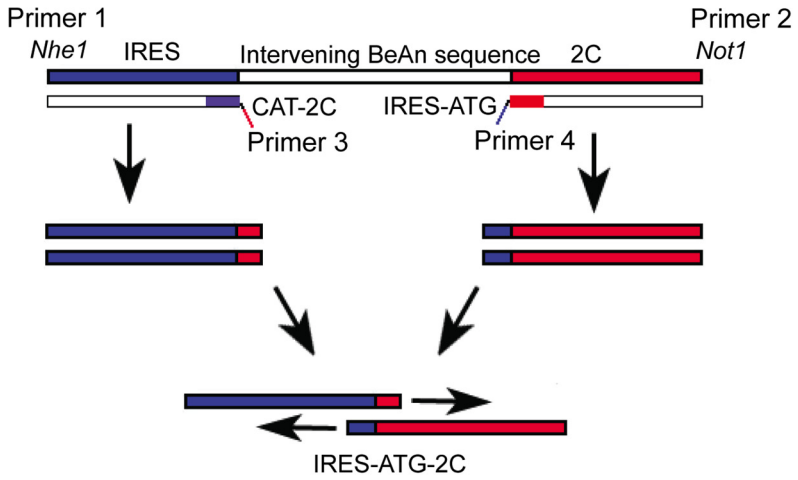

Figure 1. The IRES (blue color) and each virus protein (red color; examples given here is for 2C) were amplified from a full-length infectious BeAn virus clone [88] using primer pairs 1 and 3 and 2 and 4, respectively. The two PCR products were gel-purified, mixed in equimolar amounts, and PCR-amplified with primer pairs 1 and 2. The resulting products were digested with *Nhe*1 and *Not*1 and ligated into the pIRES vector, replacing the encephalomyocarditis (EMCV) IRES with that of BeAn virus.

3.1.8 Leader protein mutagenesis.

Another overlap extension PCR-based method [89] was used to introduce nucleotide changes into the sequence of the L-protein CHCC Zn finger motif in a plasmid containing the full-length wild-type BeAn virus cDNA in pGEM4 (Promega, Madison, WI). The mutagenic primers were as follows: reverse, 5'-ACGGCTGTGCGAATAGTGCGCACATCTGGG-3', and forward, 5'-CAGATGTGCGCACTATTCCACAGCCGTTG-3'. The outside forward primer containing an *Nru*I site was 5'-CCATCGCGACGTGGTTGGAGAT-3' and the

reverse primer containing a *Sal*I site was 5'-AGAGTCGACCAACAGTAGATT-3'. Final PCR products were separated by electrophoresis, gel purified, and cloned into *Nru*I and *Sal*I restriction sites in the BeAn virus full-length plasmid.

3.1.9 Transfection.

Subconfluent monolayers of BHK-21 cells in 35-mm six-well plates were transfected with reaction mixtures consisting of 2 to 3 μg of DNA of an expression vector and Lipofectamine 2000 (Invitrogen) at a 2.5:1 ratio of reagent to DNA. Complexes incubated for 20 min at 24°C were added to cell monolayers for 4 h at 37°C, the growth medium was replaced, and incubation was continued for 24 to 48 h at 37°C in 5% CO_2. For M1-D cell transfection, 2 x 10^6 cells were washed and suspended in 100 μl nucleofection solution (Amaxa, Gaithersburg, MD), 2 μg of pmaxGFP or pIRES construct DNA was added, and samples were transferred into certified cuvettes and transfected with the Amaxa Nucleofector using the program D-23. M1-D transfection medium (RPMI, 1% FBS, 0.1 mM nonessential amino acids) with 1% FBS (500 μl) warmed to 37°C was added immediately after transfection to each cuvette, and cells were collected and dispensed into wells of 12-well plates containing 1 ml prewarmed M1-D transfection medium. Plates were incubated at 37°C in 5% CO_2 for the indicated times and assessed for cell viability in the presence of WST-1 or for apoptosis by flow cytometry.

3.1.10 Preparative in vitro RNA transcription.

DNA clones oriented with the 5' end of the IRES or L nucleotide sequence

downstream of the T7 promoter (Fig. 1) were linearized at the NotI site within the vector downstream of the 3' end of the BeAn virus nonstructural genes, and RNA transcripts were synthesized using the RiboMax(R) large-scale RNA production system (Promega). Reaction mixtures contained 2 mM spermidine, 80 mM HEPES-KOH (pH 7.5), 24 mM $MgCl_2$, 7.5 mM rNTPs, 40 mM dithiothreitol, and 5 µl of enzyme mix (T7 RNA polymerase, recombinant RNasin and recombinant inorganic pyrophosphatase; Promega) in 100 µl. Incubations were for 4 h at 37°C, and RNAs were analyzed for integrity and quantity on 1% native RNA agarose gels with or without prior DNase treatment.

3.1.11 *In vitro* translation.

In vitro translation in rabbit reticulocyte lysate (RRL) (Red Nova lysate kit; Novagen, Madison, WI) was carried out in 12.5 µl reaction mixtures after salt and RNA concentrations had been optimized. Mixtures containing 20 mM HEPES-KOH (pH 7.5), 0.1 mM KCl, 0.1 mM $MgSO_4$, 2 mM dithiothreitol, 8 mM creatine phosphate, a methionine-free amino acid mixture, and 20 µg/ml RNA in the presence of 10 µCi [^{35}S]methionine and [^{35}S]cysteine (Tran^{35}S-label; ICN Biomedicals, Inc., Irvine, CA) were incubated for 1 h at 30°C. Incorporation of [^{35}S]methionine was calculated from trichloroacetic acid precipitates, and samples were analyzed by sodium dodecyl sulfate-polyacrylamide gel electrophoresis (SDS-PAGE) using 12% NuPAGE bis-Tris minigels (Invitrogen), which were dried and exposed to X-ray film (Denville Scientific Inc., Metuchen, NJ).

3.1.12 Apoptosis assay.

The number of apoptotic cells was determined using DAPI (4',6'-diamidino-2-phenylindole) staining. Briefly, M1-D cells grown and infected on glass coverslips (Fisher Scientific Co., Pittsburgh, PA) were fixed in 4% paraformaldehyde for 15 min at room temperature, washed twice in PBS (pH 7.2), and incubated with DAPI for 5 min at a final concentration of 0.5 µg/ml. Coverslips were washed with 0.5% Tween 20 in PBS and distilled H_2O and viewed with a Zeiss digital confocal microscope. At least three randomly chosen fields containing cells were photographed at x200 magnification and the percentage of cells with condensed chromatin and fragmented nuclei were determined by a blinded observer; each experiment was repeated twice.

3.1.13 Caspase activity assay.

Caspase-8 and -9 activities were assayed with Caspase-Glo reagent (Promega, Madison, WI) in BHK-21 cells seeded in six-well plates (3 x 10^5 cells per well), infected 24 h later with BeAn virus (MOI=10), and harvested at 12 h pi. An equal volume of Caspase-Glo reagent containing MG132 was added to infected cell pellets, which were transferred to white-walled 96-well plates, and incubated at room temperature for 1 h, and the luminescence was measured in a plate-reading luminometer (GloMax-multi detection system; Promega).

3.1.14 Assay for reactive oxygen species (ROS).

Cellular ROS production was measured by flow cytometry using the ROS-sensitive dye 5- (and 6-) chloromethyl-2',7'-dichlorodihydrofluorescein diacetate, acetyl ester (CM-H_2DCFDA) (Molecular Probes, Eugene, OR). Infected BHK-21 cells (12 h pi) were incubated with infection media containing 5 µmol of CM-H2DCFDA/liter for 30 min in the dark at 37°C before harvesting. Cells were treated with trypsin, washed with DMEM without pyruvate X2, suspended in 0.5 ml of PBS, and subjected to flow cytometry.

3.1.15 Northern hybridization.

Total RNA from cell cultures was ethanol-precipitated, resuspended in RNA loading buffer (MOPS buffer), heated for 5 min at 95°C, and electrophoresed in a 1.2% agarose gel at 85 V for 2 h. The gel was soaked in 10X SSC for 15 min. RNA was passively transferred to a Hybond-N+ membrane (Amersham, Piscataway, NJ, USA), treated with short-wavelength UV light for 2 min and prehybridized with hybridization solution (Clontech, Mountain View, CA, USA) for at least 1 h at 68°C. A random-primed DNA probe specific for BeAn virus was derived from a 1.5-kb *Bcl*I/*Nci*I fragment of BeAn cDNA spanning nucleotides 4952 to 6492 by using the Prime-a-gene Labeling System (Promega). The [α-^{32}P]-labeled probe was added to the prehybridization solution and hybridization was carried out overnight at 42°C. Membranes were washed once with 2X SSC-0.05% SDS for 30 min and three times with 0.1X SSC-0.1% SDS at 24°C for 20 min each time, dried, and exposed

to a Molecular Dynamics PhosphorImager screen to detect BeAn virus with the [α-^{32}P] dNTP-labeled hybridized probe.

3.1.16 Pulse-labeling virus proteins.

Cell monolayers were infected with BeAn (MOI=50) for 4 h with infection medium containing 2 µg/ml actinomycin D. After rinsing, cells were incubated with methionine-free DMEM and 2 µg/ml actinomycin D for 1 h followed by incubation for 5 min in medium containing 30 µCi of [^{35}S]methionine. Cells were rinsed and chased in the presence of 10 mM methionine for 0, 1, 5, 10 and 20 min. Next, cells were harvested, lysed with 0.1 ml of lysis buffer [1% NP-40, 0.5% Na-deoxycholate, 0.1% sodium deoxycholate, 150 mM NaCl, 1 mM EDTA, 50 mM Tris (pH 7.5)] and centrifuged at 13,000 rpm for 20 min at 4°C. Aliquots were analyzed by 12% SDS-PAGE, followed by autoradiography.

3.1.17 Labeling of viral proteins.

BHK-21 and M1-D cell monolayers were infected with virus for 3.5 h. One hour prior to addition of label, medium was removed and cells after rinsing, were covered with DMEM deficient in methionine and cysteine, or RPMI deficient in methionine and cysteine, and incubated for 1 h. Medium was then replaced by that containing 30 µCi of [35S]methionine or [3H]leucine and incubated for 1 h. Then, cells were harvested after removal of medium and two rinses with phosphate-buffered saline. Cell lysates were prepared in 0.4 ml of lysis buffer (20 mM Tris pH 7.6, 1% NP-40, 10% Glycerol, 137 mM NaCl, 2 mM EDTA) and

centrifuged at 4°C in an Eppendorf Microfuge for 10 min. Supematants were then layered on sucrose gradients.

3.1.18 Sucrose gradients.

Cell lysates were fractionated on 11-ml 5 to 20% sucrose gradients prepared in lysis buffer. Gradients were centrifuged in an SW41 (Beckman) rotor at 35,000 rpm for 16 h (5 to 20%). Fractions (0.5 ml) were collected from the top of the gradient and then immunoprecipitated.

3.1.19 Immunoprecipitation

Fractions of sucrose gradients were incubated with shaking overnight at 4°C with 5 µl rabbit polyclonal anti-BeAn antibody. Samples were then incubated with 30 µl of a suspension of protein A/G at 4°C for 2 h with shaking. After centrifugation for 5 min, pellets were resuspended in lysis buffer and the washes were repeated twice. Final pellet were suspended in 50 µl of reducing sample buffer (1.4 M 2-mercaptoethanol, 4.6% SDS, 125 mM Tris [pH 6.8], 20% glycerol) and boiled for 3 min. Aliquots were quantitated for radioactivity in a scintillation counter or analyzed by 12% SDS-PAGE followed by autoradiography.

3.1.20 Virus purification.

Virus was purified as described with modifications [90]. Specifically, following virus adsorption, infected BHK-21 monolayers (in 100-mm dishes) were incubated in

maintenance medium for 4 h at 37°C, washed twice with DMEM deficient in methionine and cysteine, and incubated in this medium for 60 min at 37°C, and then deficient DMEM medium containing 20 to 30 µCi of ^{35}S-Trans label (ICN) per ml was added. Infection was allowed to progress from 10 to 24 h post infection. HEPES and $MgCl_2$ were added to the cells and supernatant to concentrations of 25 mM and 20 mM, respectively, and bovine pancreatic DNase I (Sigma Chemical) was added to a concentration of 10 µg/ml, and the lysate was incubated for 30 min at 24°C. NaCl was added to 0.5 M and PEG-8000 to 10% (wt/vol) to the lysate, stirred for 2 h at 4°C, and centrifuged in a Beckman HB-6 rotor at 10,000 × *g* for 30 min at 4°C. After resuspension of the pellet in high-salt TNE buffer (20 mM Tris-HCl [pH 7.6], 0.5 M NaCl, 2 mM EDTA) (hereafter designated hsTNE) containing 1% bovine serum albumin (BSA), 0.1% 2-mercaptoethanol (2ME), 1% (wt/vol) Sarkosyl and 0.4% 1,1,1,2,3,4,4,5,5,5-Decafluoropentane, the supernatant was layered over a 0.5 ml 30% sucrose cushion in 20 mM Tris-HCl pH 7.6, 1.0 M NaCl, 2 mM EDTA pH 8.0, 1% BSA and centrifuged in a SW55 Ti rotor at 45,000 rpm for 90 min at 15°C. The pellet, resuspended in 0.5 ml of hsTNE containing 0.1% 2ME, was layered on a 20 to 70% sucrose gradient in hsTNE and centrifuged in a SW41 rotor at 35,000 rpm for 3 h at 10°C. Gradients were fractionated from the top into 0.5-ml aliquots, and radioactivity was measured in a Beckman LS5000TD scintillation counter.

3.1.21 Estimation of the physical particle/pfu ratio.

To obtain an estimate of the physical particle/infectious particle ratio, the BeAn

virus RNA concentration was determined from virus purified on sucrose gradients. The number of physical particles was calculated assuming that 1 mg of picornavirus RNA is equivalent to $7.2x10^{13}$ virus genomes and to an equivalent number of virus particles. The number of physical particles was then related to the titer of purified virus, as determined by a standard plaque assay.

3.1.22 *In vitro* cleavage of capsid proteins by caspases.

Purified BeAn were incubated either alone or with purified recombinant caspase-3 in a final volume of 40 µl of caspase assay buffer (50 mM HEPES (pH 7.4), 50 mM NaCl, 0.1% 3-[(chlolamidopropyl) dimethylammonio]-1-propanesulfonate (CHAPS), 10 mM EDTA, 5% glycerol, 10 mM dithiothreitol) for 1 h at 37°C. Parallel tubes were also incubated with cytosolic extracts of infected M1-D cells. Viral proteins were analyzed by SDS-PAGE and immunoblotting with the anti-BeAn antibody. Titers from plaque assays were performed in triplicate and averaged for the data shown.

3.1.23 Electron microscopy.

M1-D cells were harvested and fixed with 3% glutaraldehyde in PBS and then in aqueous 2% osmium tetroxide, stained with 0.5% aqueous uranyl acetate, dehydrated with a graded ethanol series and embedded in Epoxy Resin LX112 for processing and staining as described [58, 59].

3.1.24 Statistical analysis.

Paired Student's *t*-test was used to compare groups; and differences were considered significant at $p<0.05$.

CHAPTER 4

THEILER'S MURINE ENCEPHALOMYELITIS VIRUS LEADER PROTEIN IS THE ONLY NONSTRUCTURAL PROTEIN TESTED THAT INDUCES APOPTOSIS WHEN TRANSFECTED INTO MAMMALIAN CELLS

4.1 Background

TMEV are highly cytolytic RNA viruses. Mice experimentally infected with a low-neurovirulence TMEV, such as BeAn virus, develop persistent infection in the CNS and an inflammatory demyelinating disease, providing an experimental analogue for multiple sclerosis. BeAn virus persists primarily in macrophages in the CNS of infected mice. Schlitt et al. [91] found that 74% of TUNEL-positive cells in infected spinal cords (primarily in CNS lesions) were T and B lymphocytes and 8% were macrophages, although virus genomes were detected in <1% of apoptotic cells, consistent with infection of only a low percentage of macrophages and the fact that TMEV does not infect T or B lymphocytes in culture. Thus, some means other than direct infection was responsible for apoptosis of most CNS macrophages, including TMEV triggering apoptosis through tumor necrosis factor alpha or tumor necrosis factor alpha-related apoptosis-inducing ligand by binding death receptors on activated macrophages in vitro, as reported elsewhere [92].

Infection of mouse macrophages induces apoptosis [93, 94] mediated by Bax through the intrinsic or mitochondrial pathway and severely restricts the yield of progeny virus [58]. Thus, apoptosis may be a mechanism to attenuate the virus yet promote macrophage-to-macrophage spread through phagocytosis of infected

apoptotic blebs during persistence [58]. In contrast, TMEV infection in other rodent cells tested thus far, including baby hamster kidney (BHK-21) cells, produces necrotic cell death with high virus yields. The contrasting outcomes of TMEV infection point to the existence of two distinct virus-induced cell death programs.

The genes of an increasing number of RNA viruses have been shown to encode proteins that trigger apoptosis. Among picornaviruses, coxsackievirus B3 1B (VP2) [95, 96], avian encephalomyocarditis virus 1C (VP3) [97] and 2C [98], enterovirus 71 2A [99], and poliovirus 2A [100] and 3C protease (3Cpro) [101] induce apoptosis, mostly through the intrinsic pathway. Coxsackievirus B3 VP2 has been shown to interact with the proapoptotic Siva protein in a yeast two-hybrid screen [95], but exactly how the VP2-Siva interaction or any of the other picornavirus proteins initiates the apoptotic cascade remains unknown.

To gain insight into the upstream signaling events that lead to apoptosis, we tested the ability of individual BeAn virus nonstructural genes to induce apoptosis in uninfected BHK-21 cells. Only the leader (L) protein resulted in apoptosis and mutation of the CHCC Zn finger motif in L significantly reduced L protein-induced apoptosis.

4.2 Results

4.2.1 Translation of virus nonstructural proteins in RRL.

Because genes of RNA viruses may be subject to RNA splicing when expressed from a polymerase II promoter in mammalian cells, the products of BeAn virus nonstructural gene constructs were first authenticated by translation in RRL. In vitro transcription of the pIRES constructs containing individual BeAn virus nonstructural genes and the 3CD precursor gene generated RNAs of the expected sizes upon electrophoresis in agarose gels (data not shown). SDS-PAGE analysis of RNAs translated in RRL revealed [^{35}S]methionine-labeled cognate proteins for L, 2A, 2B, 2C, and 3A (data not shown) as well as 3D polymerase (3Dpol) and 3CD but not the BeAn virus 3Cpro (Fig. 1). The latter result was not unexpected in light of the reported rapid degradation in RRL of the related cardiovirus EMCV 3Cpro protein. The presence of a 10-amino-acid sequence, LLVRGRTLVV, near the EMCV 3Cpro N terminus, which is recognized as a signal for ubiquitin/26S proteasomal degradation [102], and a homologous degradation sequence, LLLRAHLFVV, in BeAn virus 3Cpro would likely render 3Cpro unstable. Translation of BeAn virus 3Cpro in RRL in the presence of 100 μM lactacystin, a proteasome inhibitor that binds to a 20S subunit, revealed a faint 3Cpro protein band on SDS-PAGE (data not shown). In contrast, translation of BeAn virus 3CD in RRL revealed proteins bands for 3CD, 3Dpol, and 3Cpro on SDS-PAGE (Fig. 2). It has been reported that the presence of EMCV 3Dpol in the precursor 3CD masks the 3Cpro signal for ubiquitination, contributing to greater 3Cpro stability in RRL [103].

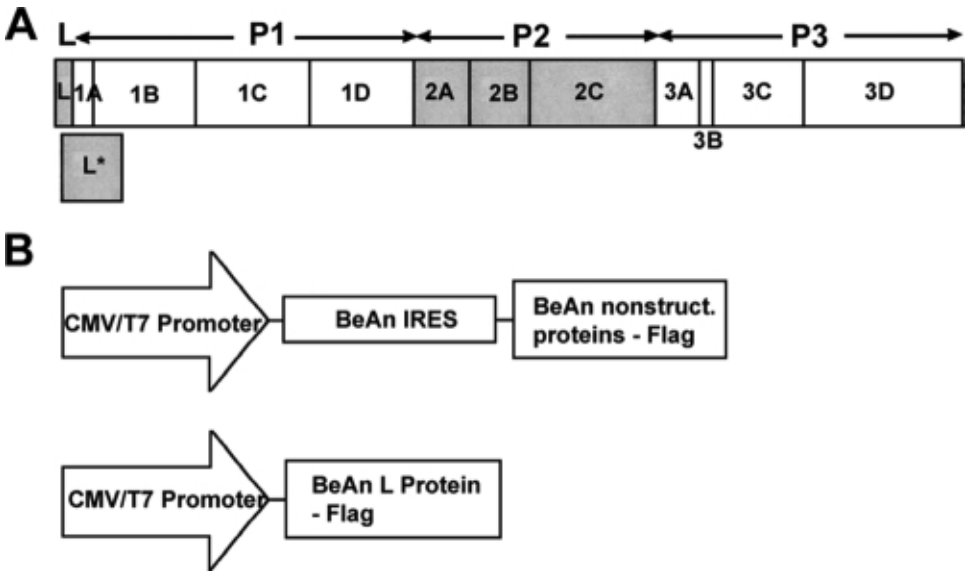

Figure 1 (A) TMEV final gene products arranged on the polyprotein in a standard picornavirus format of the L protein: four P1 capsid proteins and three P2 and four P3 nonstructural proteins. The 18-kDa out-of-frame L* protein, which is initiated 13 nucleotides downstream of the authentic polyprotein AUG, is shown below the polyprotein. (B) All of the BeAn virus nonstructural proteins except the 20-amino-acid 3B (VPg) were assembled using overlap extension PCR into the pIRES vector downstream of the BeAn virus IRES so that each protein is translated from a 5′ AUG codon and contains a C-terminal Flag sequence. The L protein was also assembled into the same vector without an IRES for cap-dependent translation.

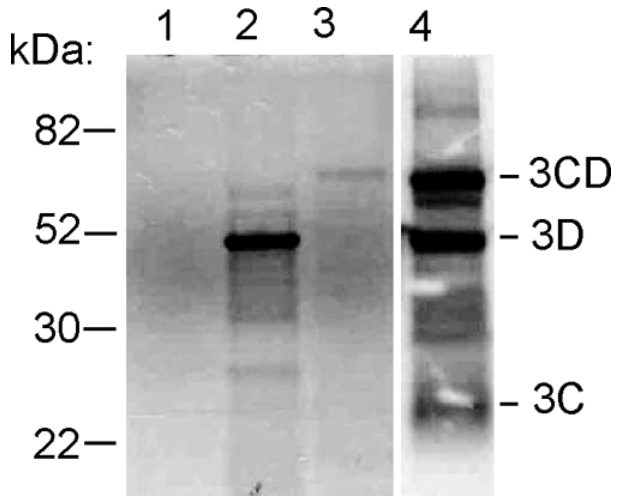

Figure 2 SDS-PAGE analysis of in vitro-translated RNAs transcribed from pIRES-3C, -3D, and -3CD plasmids in RRL in the presence of [^{35}S]methionine. Translation of pIRES-3Cpro reveals no apparent labeling of 3Cpro (lane 1); pIRES-3Dpol shows labeling of the 53-kDa 3Dpro (lane 2); pIRES-3CD shows labeling of the 65-kDa 3CD (lane 3); and when pIRES 3CD is overexposed, labeling of 3CD, 3Dpro, and 23-kDa 3Cpro is shown (lane −4).

4.2.2 Expression of virus nonstructural proteins in BHK-21 cells.

The pIRES nonstructural protein plasmids (Fig. 1B) were transfected into BHK-21 cells with Lipofectamine, and lysates were prepared at 24 and 48 h posttransfection, electrophoresed on 12% SDS-polyacrylamide gels, transferred to membranes, and immunoblotted with rabbit polyclonal anti-Flag antibody to detect the Flag sequences. Transfection efficiency in these experiments was >80%, as determined by FACS analysis of cells cotransfected with pIRES-GFP and pIRES nonstructural protein plasmids. As shown in Fig. 3A, immunoblotting revealed

expression of BeAn virus L, 2A, 2B, 2C, 3A, and 3D. BeAn virus L was expressed at 24 h, but expression had decreased at 48 h, whereas expression of 2A, 2B, 2C, and 3A at 24 h was maintained or increased at 48 h. BeAn virus 3Cpro was undetectable by immunoblotting, presumably because 3Cpro undergoes proteasomal degradation in vivo, as noted above for EMCV 3Cpro [104]. Indeed, 3Cpro accumulated to detectable levels at 12 to 24 h after transfection of pIRES-3Cpro in the presence of 20 μM of the reversible proteasome inhibitor z-Leu-Leu-Leu CHO (MG132) (Fig. 3B), suggesting that 3Cpro is highly susceptible to in vivo degradation by the ubiquitin/26S proteasome. The decline in 3Cpro band intensity likely reflects progressive cell death. The BeAn virus precursor 3CD was not detected after transfection of pIRES-3CD, even in the presence of MG132, for reasons presently unresolved.

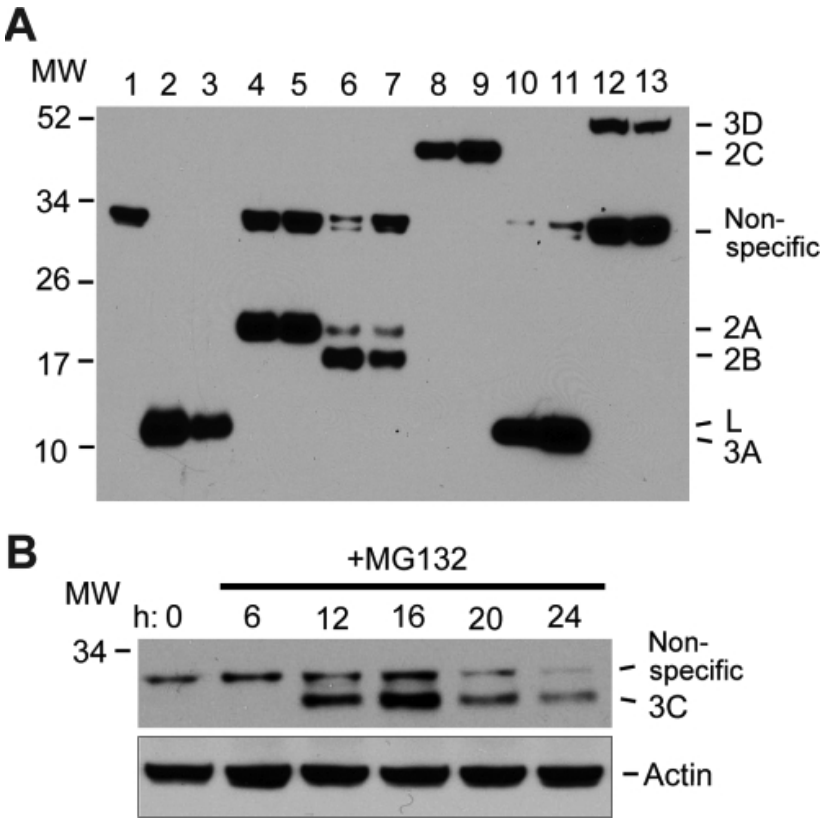

Figure 3 SDS-PAGE of the expression of pIRES-BeAn virus nonstructural gene constructs in transiently transfected BHK-12 cells. A) Immunoblot analysis at 24 h (even lanes) and 48 h (odd lanes) posttransfection. Lanes: 1, empty vector; 2 and 3, L; 4 and 5, 2A; 6 and 7, 2B; 8 and 9, 2C; 10 and 11, 3A; 12 and 13, 3D polymerase. B) Time course of the expression of 3Cpro in the presence of 20 μM of the reversible 26S proteasome inhibitor MG132. MW, molecular weight (in thousands).

4.2.3 Expression of L but not other nonstructural proteins in BHK-21 cells is cytotoxic.

We used BHK-21 cells transfected with individual BeAn virus nonstructural genes (except 3B) to screen for cytotoxicity with the intent of testing constructs positive for apoptosis in M1-D cells. Transfection of BeAn virus pIRES-L but not pIRES constructs for 2A, 2B, 2C, 3A, and 3Dpol produced significant cell death at 24 h ($P<0.5$) and 48 h ($P<0.01$) compared to transfection of pIRES-empty vector (Fig. 4A). Efforts to assess cell death by 3Cpro in the presence of MG132 were complicated by MG132-dependent cytotoxicity [105]. Cytopathic effect was observed by light microscopy as early as 12 to 16 h of incubation with MG132 alone, and cell death beyond that induced by MG132 alone was detected in the WST-1 cell survival assay from 24 to 48 h after transfection of 3Cpro in the presence of MG132 ($P<0.05$), although the amount of cell death exceeding that of MG132 was not impressive. Thus, BeAn virus 3Cpro in the absence of 26S proteasomal degradation appears to be cytotoxic, as reported for poliovirus 3Cpro (3). Transfection of BHK-21 cells with the pL plasmid construct (Fig. 1B), in which L expression is cap dependent, also led to progressive cytotoxicity at 24 h ($P<0.05$) and 48 h ($P<0.01$) compared to transfection with pEV (Fig. 4B). Temporal analysis of the expression of L by immunoblotting first revealed L expression at 12 h, with increased expression at 16 to 20 h posttransfection as cell death commenced (Fig. 4D).

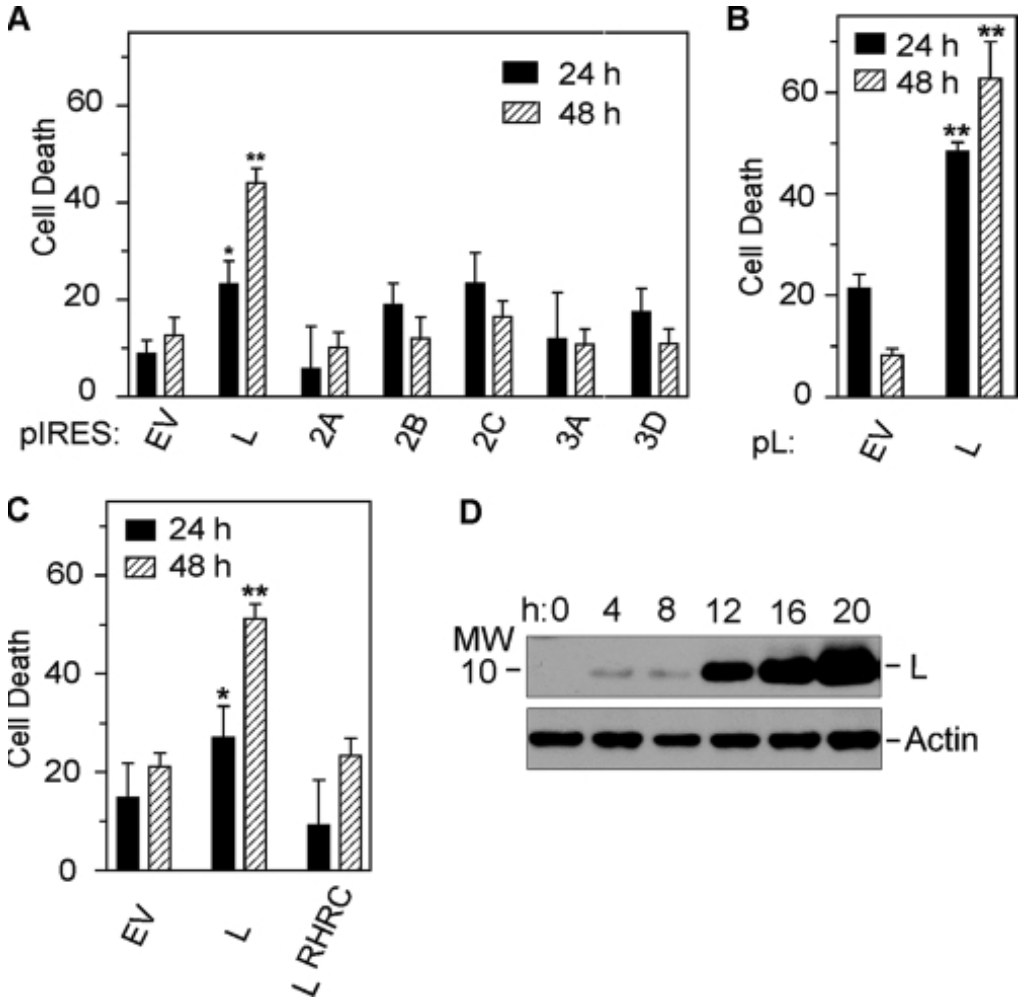

Figure 4 Cytotoxicity determined by the WST-1 assay at 24 and 48 h after transfection of plasmid BeAn virus nonstructural gene constructs in BHK-21 cells. *, $P<0.05$; **, $P<0.01$. A) Cell death after IRES-dependent expression of virus nonstructural genes (mean ± standard error; $n = 3$ to 6). B) Cell death after cap-dependent expression of L (mean ± standard error; $n = 3$). C) Comparison of cytotoxicity after cap-dependent expression of L and the L CHCC mutant (mean ± standard error; $n = 3$). D) Time course of cap-dependent expression of L up to 20 h posttransfection.

4.2.4 A BeAn virus L Zn finger mutant is not cytotoxic.

Inhibition of active nucleocytoplasmic trafficking by cardiovirus L was initially recognized as inhibition of innate immunity by blocking the type I interferon response [106-108]. Mutation of the TMEV L CHCC Zn finger motif compromises the antinucleocytoplasmic trafficking activity of L [109, 110]. To determine the role of the L Zn finger in cell death, we mutated the domain to RHRC without changing the amino acid sequence of the L* protein encoded by an alternative overlapping open reading frame (Fig. 1A), as initially reported for the TMEV DA strain [107]. The DA L* protein has been reported to be antiapoptotic [111, 112]. As shown in Fig. 4, transfection of a plasmid with a green fluorescent protein nuclear localization signal (pGFPNLS) followed 24 h later by transfection of pL resulted in efflux of GFP from the nucleus (Fig. 5A), whereas GFP accumulated and remained in the nucleus after transfection of only pGFPNLS (Fig. 4B) or after transfection of the pL mutant (Fig. 5C), indicating that the mutated L protein no longer disrupted the nuclear pore complex. Expression of L was also detected throughout the cytoplasm of transfected BHK-21 cells immunostained with anti-Flag antibody (Fig. 5D and E), but in some cells L was perinuclear. The BeAn virus pL mutant construct in transfected cells was not cytotoxic (Fig. 4C).

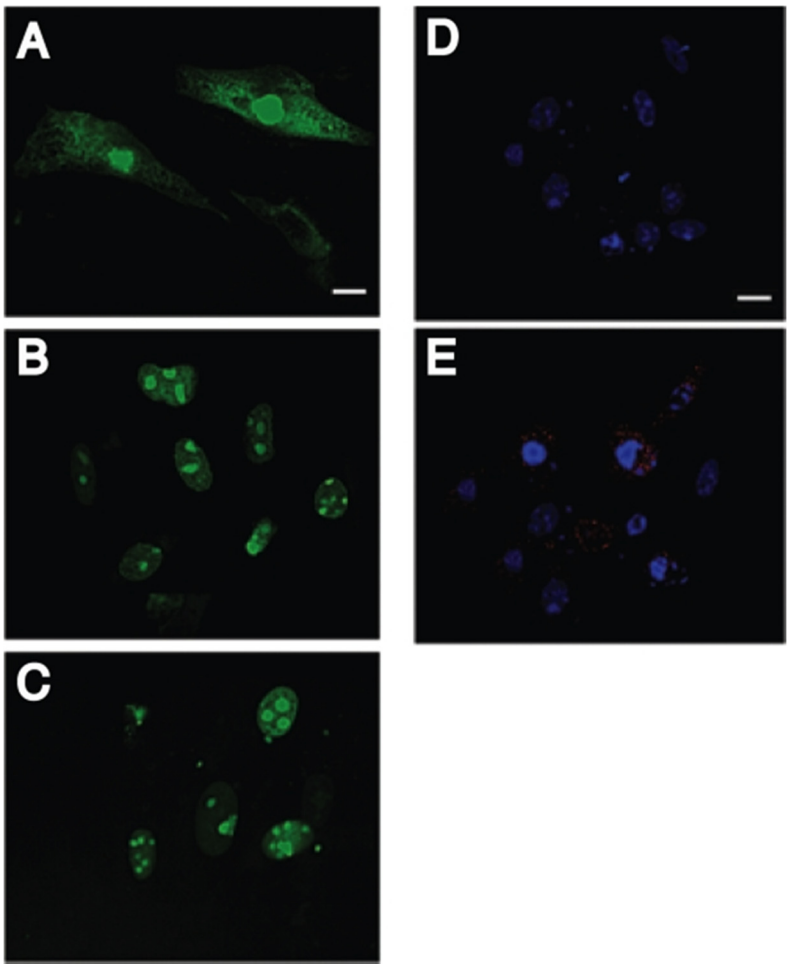

Figure 5 Digital confocal microscopic images of nuclei of cells loaded with the marker protein GFP (GFPNLS) (A to C) and Flag-tagged BeAn virus L (D and E) in BHK-21 cells 24 h posttransfection. Cells transfected with pL showed efflux of GFP from the nucleus to the cytoplasm A), whereas cells transfected with pEV B) and the pL mutant plasmid DNA C) retained GFP in the nucleus. Indirect immunofluorescent antibody staining of L in the cytoplasm of BHK-21 cells 24 h after pL transfection showed DAPI-stained nuclei (D) and L stained with rabbit anti-Flag M2 and anti-rabbit IgG-Alexa Fluor 568 and nuclei stained with DAPI E). Bars = 10 μm.

4.2.5 A portion of BeAn virus L cytotoxicity is due to apoptosis.

BHK-21 cells transfected with the pL and pL Zn finger mutant plasmids were assessed for apoptosis by FACS analysis of PI and annexin V-stained cells at 20 h. In a representative experiment whose results are shown in Fig. 6A, the percent PI negative, annexin V-positive cells (lower right quadrant) was elevated after pL compared to pEV transfection. PI-positive, annexin V-positive cells (upper right quadrant) are considered necrotic because of the potential exposure of phosphoserine on the inner leaflet of membrane fragments during necrosis. Use of only cells remaining on the monolayer for FACS (Fig. 6A) explains the marked difference in the percent necrotic cells compared to the WST-1 assay (Fig. 4A and 6B). In cells transfected with the pL mutant, the percent apoptotic cells was the same as that after pEV transfection, indicating that a functional Zn finger is necessary for L-induced apoptosis. The percent apoptotic cells for pEV, pL, and the pL mutant was 2.6 ± 0.62, 13.9 ± 2.74, and 5.9 ± 2.15 (mean ± standard deviation for five experiments; $P<0.001$ for differences between pEV and pL and between pL and the pL mutant). Immunoblot analysis revealed cleavage of PARP and caspases 3 and 9 to respective 17- and 37-kDa activated forms at 16 to 24 h after pL transfection (Fig. 6B). The less intense bands of the activated forms of caspases 3 and 9 after transfection of pEV and the pL mutant were probably due to the stress of transfection. The band reflecting cleavage of caspase 8 to its active 18-kDa form was inconsistently seen (Fig. 6B). Incubation of pL-transfected cells with the pan-caspase inhibitor qVD-OPh protected against apoptosis (Fig. 6C) and

prevented cleavage of PARP and caspase 3 (Fig. 6D). Electron microscopic examination of cells at 24 h after transfection of pL revealed necrotic debris, probably as the result of transfection and normal-appearing cells and some cells undergoing apoptosis (Fig. 5E, top), whereas only normal-appearing cells were observed after transfection with the pL mutant (Fig. 6E, bottom). Together, these results indicate that the transfected L gene induced apoptosis through the intrinsic apoptotic pathway and that removal of the Zn finger significantly reduced L-induced apoptosis.

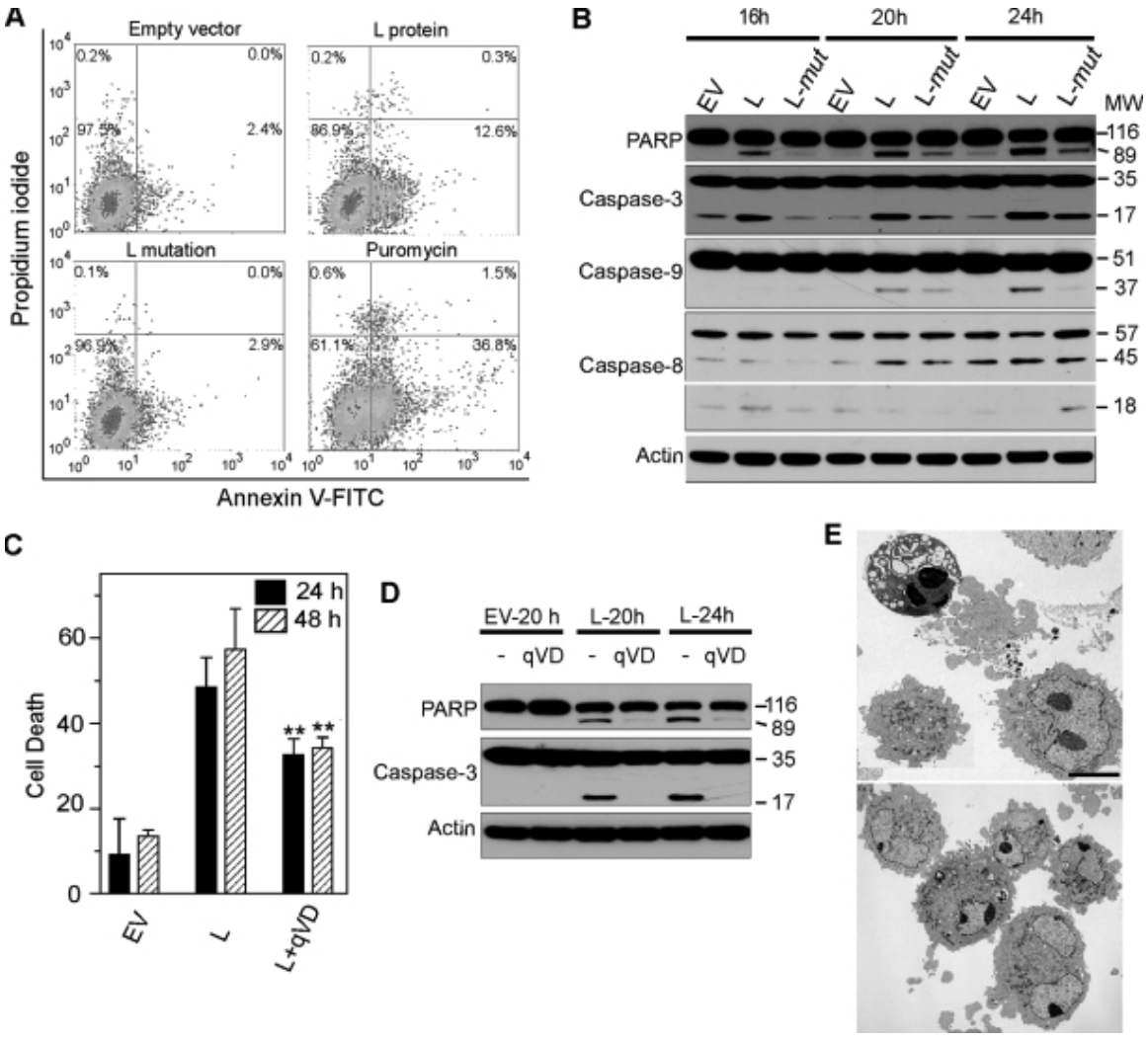

Figure 6 Effect of pL and the pL Zn finger mutant in transfected BHK-21 cells. A) FACS analysis of PI- and annexin V-stained cells at 24 h reveals increased numbers of apoptotic cells (right lower quadrant) after pL transfection but not after transfection with the pL mutant. B) Immunoblots revealing PARP cleavage and caspase 3 and caspase 9 cleavage to their active forms, p17 and p37, respectively, but no caspase 8 cleavage to the active p18 form. C) Effect of treatment of pL-transfected cells with the pancaspase inhibitor qVD-OPh, showing a significant reduction ($P<0.01$) in cell death compared to treatment with PBS at 24 and 48 h. D) Immunoblot of pL-transfected cells treated with qVD-OPh, revealing a lack of PARP and caspase 3 cleavages at 20 to 24 h. E) Electron photomicrographs of pL (top)- and pEV (bottom)-transfected cells at 24 h showing an apoptotic cell with condensed nuclear chromatin, two cells in the early stages of apoptosis, one with loss of marginated nuclear chromatin, and necrotic cell fragments. Cells in the lower frame appear normal except for ruffling of the cell membrane. The photomicrographs are at the same magnification. Bar = 5 μm.

In BeAn virus infection of M1-D cells, intrinsic apoptosis is mediated by Bcl-2 multidomain proapoptotic Bax and not Bak [58]. However, expression of Bak was increased at 16 to 24 h, suggesting that Bak is activated, whereas levels of Bax decreased at 20 to 24 h during L-induced apoptosis in BHK-21 cells (Fig. 7). Although the apical pathway leading to activation of these Bcl-1 multi-BH-domain proapoptotic proteins, which permeabilize the outer mitochondrial membrane,

appears to differ in BeAn virus infection versus L transfection, this could merely reflect a difference in cell type.

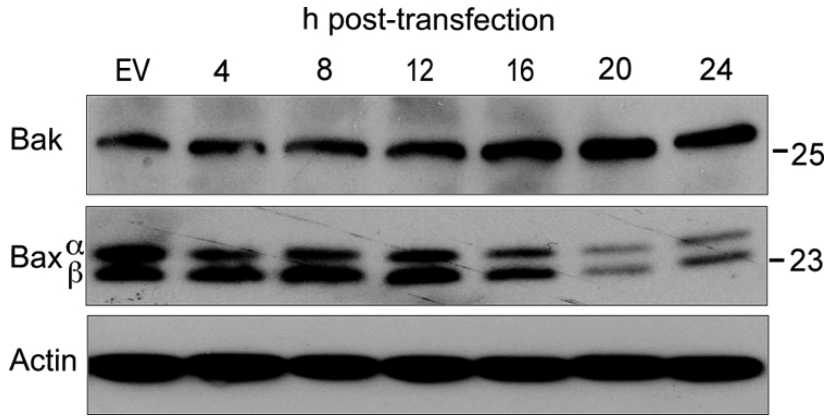

Figure 7 Bak and Bax expression in BHK-21 cells transfected with pL. The immunoblot reveals increased Bak expression at 12 to 24 h but decreased Bax over the same period.

4.2.6 BeAn virus L induces apoptosis in macrophages.

TMEV persists in the CNS of mice, primarily in macrophages, and infected macrophages provide an in vitro model for BeAn virus-induced apoptosis [58]. FACS analysis of PI- and annexin V-stained M1-D macrophages electroporated with pL or the pL mutant revealed an increased percent apoptotic cells only in the pL-transfected cells 20 h (Fig. 8A). The percent apoptotic cells for pEV, pL, and the pL mutant was 12.06 ± 5.29, 34.7 ± 13.41, and 13.38 ± 3.28 (mean ± SD for three experiments; $P < 0.01$ for differences between pEV and pL and between pL and the pL mutant). At this time, PARP cleavage was observed on immunoblots

(Fig. 8B), whereas cleavage of caspases 9 and 3 to their active forms was not observed, possibly due to a lower transient-transfection efficiency (55%) of this macrophage cell line. Nonetheless, these results suggest that L induces apoptosis in M1-D cells through a pathway that also requires an intact Zn finger.

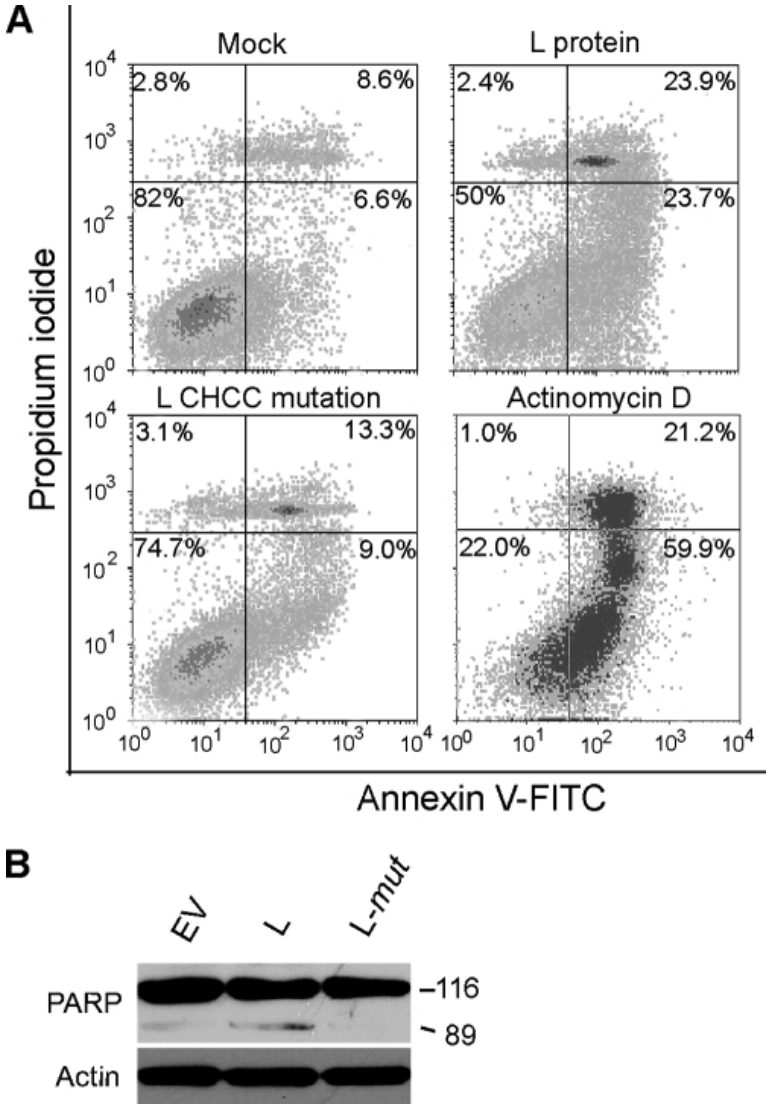

Figure 8 Effect of pL and the pL Zn finger mutant in transfected M1-D macrophages. A) FACS analysis of PI- and annexin V-stained cells at 24 h revealed increased numbers of apoptotic cells (right lower quadrant) after pL

transfection but not after transfection of the pL mutant. B) Immunoblot revealing PARP cleavage at 24 h.

4.3 Discussion

Our analysis of the ability of the TMEV nonstructural genes except that encoding 3B to induce apoptosis in transiently transfected BHK-21 cells showed that only L, which was first detected on immunoblots at 12 h posttransfection, induced progressive cell death between 24 and 48 h. Apoptosis occurred through the intrinsic apoptotic pathway, as demonstrated by FACS analysis of PI- and annexin V-stained transfected cells, immunoblot analysis of PARP and caspase cleavages, and the protection against apoptosis by the pancaspase inhibitor qVD-OPh.

The cardioviruses EMCV and TMEV regulate nuclear trafficking of cellular proteins and RNA through the L protein, which contains a Zn finger motif near the N terminus, an acidic domain with potential Thr and Tyr phosphorylation sites, and, only in TMEV, a C-terminal Ser/Thr domain [106, 113]. Unlike the L of aphthoviruses, the cardiovirus L does not have a proteolytic function. Recently, studies have shown that cardiovirus L binds Ran-GTPase and phosphorylates nucleoporins, leading to disruption of the nuclear pore complex that spans the nuclear envelope and the Ran gradient [114-116]. The inhibition of nuclear import allows measurement of the efflux of nuclear proteins into the cytoplasm after loading the nucleus with a marker protein (pGFPNLS). We detected efflux of GFP

from the nucleus to the cytoplasm after transfection of BeAn virus pL, confirming the functionality of its Zn finger, but not after transfection of the pL Zn finger mutant.

L-induced apoptosis was also dependent on a functional Zn finger, since mutation to remove the Zn finger abrogated apoptosis. Apoptosis following expression of L was associated with activation of caspases 9 and 3 but not caspase 8, indicating engagement of the intrinsic apoptotic pathway; however, a role for the extrinsic pathway has not been totally excluded. The increased expression of proapoptotic Bak but not Bax after transfection suggests differences between L-induced apoptosis in BHK-21 cells and BeAn virus infection in M1-D cells, where apoptosis is Bax dependent [58], or inherent differences in the apoptotic machinery in the two cell types. In L-induced apoptosis, the exact signaling events upstream of Bak, which is held in check by Bcl-2 antiapoptotic family proteins, remain to be determined.

Although inducible expression of poliovirus 2A and 3Cpro leads to apoptosis in mammalian cells [100, 101], we found that their TMEV counterparts did not induce progressive cytotoxicity. For cardiovirus 2A, this finding might stem from its lack of protease activity, in contrast to that of poliovirus 2A. Regarding TMEV 3Cpro, the mature form has a 26S proteasomal degradation signal near the N terminus which is not present in poliovirus 3Cpro, so that any 3Cpro diffusing away from replication complexes would likely be rapidly degraded and unavailable for induction of apoptosis. Finally, while the avian encephalomyocarditis virus 2C has been shown

to be apoptotic [98], BeAn virus 2C did not induce progressive cytotoxicity (Fig. 3A).

Preliminary studies in our laboratory indicate that BeAn virus infection in M1-D cells leads to phosphorylation of p53 at Ser15. In turn, Noxa, a Bcl-2 family BH3-only proapoptotic protein that binds to Mcl-1, a Bcl-2 antiapoptotic family member, is transcriptionally activated, releasing Bax, which then permeabilizes the outer mitochondrial membrane to activate caspase 9 (unpublished data). There is evidence that mitogenactivated protein kinases (MAPK) are involved in EMCV L induced phosphorylation of nucleoporins (A. C. Palmenberg, personal communication); therefore, it is conceivable that p53, a downstream target of MAPK, might be activated by L. In addition, since poliovirus 3Cpro cleaves transcription factors (TFIIIC, TFIID, Oct-1, and CREB) to inhibit cellular RNA synthesis [117-121], it is reasonable to consider whether TMEV 3Cpro may also activate p53. 3D proteins cardioviruses as well as other picornaviruses contain a basic NLS near the N terminus, enabling 3Cpro to enter the nucleus in the form of its precursors 3BCD and 3CD, which then generates 3Cpro by autoproteolysis [122-124]. Moreover, Lawson et al. [103] showed in in vitro translation reactions that the EMCV 3Cpro proteasomal ubiquitination signal is masked in 3CD rendering 3Cpro stable. Our RRL experiments indicated the analogous finding. However, we did not observe 3CD expression in BHK-21 cells transfected with our pIRES-3CD construct, possibly because of RNA splicing, although 3Cpro and 3D individually were not subject to RNA splicing. Expression of BeAn virus 3CD in the

cytoplasm of BHK-21 cells stably expressing T7 RNA polymerase might help enable 3CD expression and elucidate a potential role of 3CD in inducing apoptosis [125]. Expression of 3Cpro in the presence of MG132 as shown here indicates that BeAn virus 3Cpro is cytotoxic. Therefore, 3CD in addition to L are potential inducers of apoptosis during TMEV infection.

Finally, in contrast to L-induced apoptosis, BeAn virus infection of BHK-21 cells leads primarily to necrosis, with approximately only 20% of cell undergoing apoptosis [126], the apparent default cell death pathway from infection of this mammalian cell line by TMEV. Romanova et al. [127] have shown that the cell death pathway in poliovirus infection varies in different cell lines and that a rhabdomyosarcoma cell line did not have the “necessary machinery” to undergo apoptosis. BHK-21 cells are able to undergo apoptosis based on both nonviral (puromycin and actinomycin D) and viral stimuli in this study. Clearly, a balance between pro- and antiapoptotic virus genes determines the outcome of apoptosis. Since the TMEV out-of-frame L* protein has been reported to be antiapoptotic [94, 112], it is possible that apoptosis is held in check by L* during infection in BHK-21 cells. Insight into the potential antiapoptotic role of awaits analysis in transfected M1-D cells.

CHAPTER 5

THE ANTIAPOPTOTIC PROTEIN MCL-1 CONTROLS THE TYPE OF CELL DEATH IN THEILER'S VIRUS-INFECTED BHK-21 CELLS

5.1 Background

TMEV strains differ in neurovirulence following intracerebral inoculation of mice with the highneurovirulence GDVII strain, causing extensive infection of cerebral cortical and hippocampus neurons and producing a rapidly fatal encephalitis, whereas the low-neurovirulence DA and BeAn strains result in a CNS infection primarily in microglia/macrophages but also in oligodendrocytes, leading to immune-mediated demyelination. TMEV persistence in mice is recognized as a relevant experimental animal model for multiple sclerosis [8, 21].

Depending on the specific cell type infected, TMEV induces at least two distinct cell death programs, necrosis and apoptosis, which can result in substantial differences in infectious viral yields. All rodent cell types except for macrophages probably undergo necrosis because of the high viral yields produced [56]; murine macrophages undergo apoptosis with restricted viral yields, producing only a few PFU of virus per cell [128]. Moreover, TMEV infection of mouse M1-D macrophages induces apoptosis by activating the intrinsic apoptotic pathway [58, 128]. In these cells, TMEV infection results in activation of p38 mitogen-activated protein kinase by 2 to 3 h pi, followed by phosphorylation of tumor suppressor protein p53 Ser 15 at 3 to 6 h pi and stable p53 levels until 6 h pi; activated p53 upregulates the transcription of the proapoptotic puma and noxa genes at 2 to 4 h

pi, and the levels of prosurvival Mcl-1 and A1 proteins become undetectable at 4 to 10 h pi [58, 59]. Specific inhibition of phospho-p38 and inhibition of p53 by a genetic suppressor element led to a significant decrease in apoptosis [59]. Degradation of prosurvival proteins was also shown to release Bax [58, 59], which forms homo-oligomers and translocates into and permeabilizes the mitochondrial outer membrane, releasing cytochrome c and initiating the caspase cascade.

Antiapoptotic Mcl-1, initially isolated from a human myeloblastic leukemia cell line [35], predominates in differentiated human macrophages [36], protecting against apoptosis during the initial steps of differentiation [37, 38]. Overexpression of Mcl-1 in TMEV-infected M1-D cells reduced the cleavage of caspase-3 and caspase-9 to their active forms and inhibited apoptosis [59]. Whether Mcl-1 endogenously regulates TMEV-induced cell death in other cells remains to be determined.

In the present study, BeAn virus infection in BHK-21 cells led to necrosis of the majority of cells but to apoptosis in ca. 20% of the cells through the intrinsic apoptotic pathway in a p53-dependent manner. Mcl-1, an antiapoptotic Bcl-2 family member, was highly expressed in BHK-21 cells, and infection resulted in gradual loss of Mcl-1, which is consistent with the onset of apoptosis. Mcl-1 knockdown by silencing RNAs (siRNAs) increased apoptotic cell death by ~3-fold and concomitantly reduced infectious viral yields by at least 12-fold, indicating that Mcl-1 is an important regulator of cell death in infected BHK-21 cells. The availability

of BHK-21 cells with stably knocked-down Mcl-1 expression provides a convenient tool to further define the step(s) in the viral life cycle impacted by apoptosis.

5.2 Results

5.2.1 BeAn virus infection induces both necrotic and apoptotic cell death pathways in BHK-21 cells.

Since TMEV infection of BHK-21 cells is highly productive, with infectious virus yields on the order of 200 to 500 pfu/cell (27), these cells have been widely used to study the molecular virology and to purify the virus. Analysis of cell viability in BHK-21 cells infected with the BeAn strain of TMEV at (MOI=10) revealed progressive virus-induced cell death, with 85% of the cells dying by 24 h p.i. (Fig. 1A). FACS analysis revealed that cell death was due to a combination of necrosis and apoptosis (Fig. 1B), with most cells dying by necrosis and 20% by apoptosis at 24 h pi (Fig. 1B). Moreover, the very high levels of ROS observed by 10 to 12 h pi (Fig. 1C) were consistent with necrosis since its production in cell death is thought to be higher in necrosis than apoptosis (10). Figure 1D shows representative electron micrographs of a more normal appearing cell early in infection (left) and of necrotic (center) and apoptotic (right) cells at 16 h pi. The necrotic cell is intact but markedly swollen, with little recognizable cytoplasmic and nuclear architecture remaining (in most such cells the cell membrane was ruptured); the apoptotic cell is slightly shrunken with condensed nuclear chromatin, blebbing of a part of its nucleus, and proliferation of vesicular membranes or viroplasm in the cytoplasm, the site of viral genome replication. Thus, infection of

BHK-21 cells resulted primarily in necrosis, with only a minority of cells undergoing apoptosis.

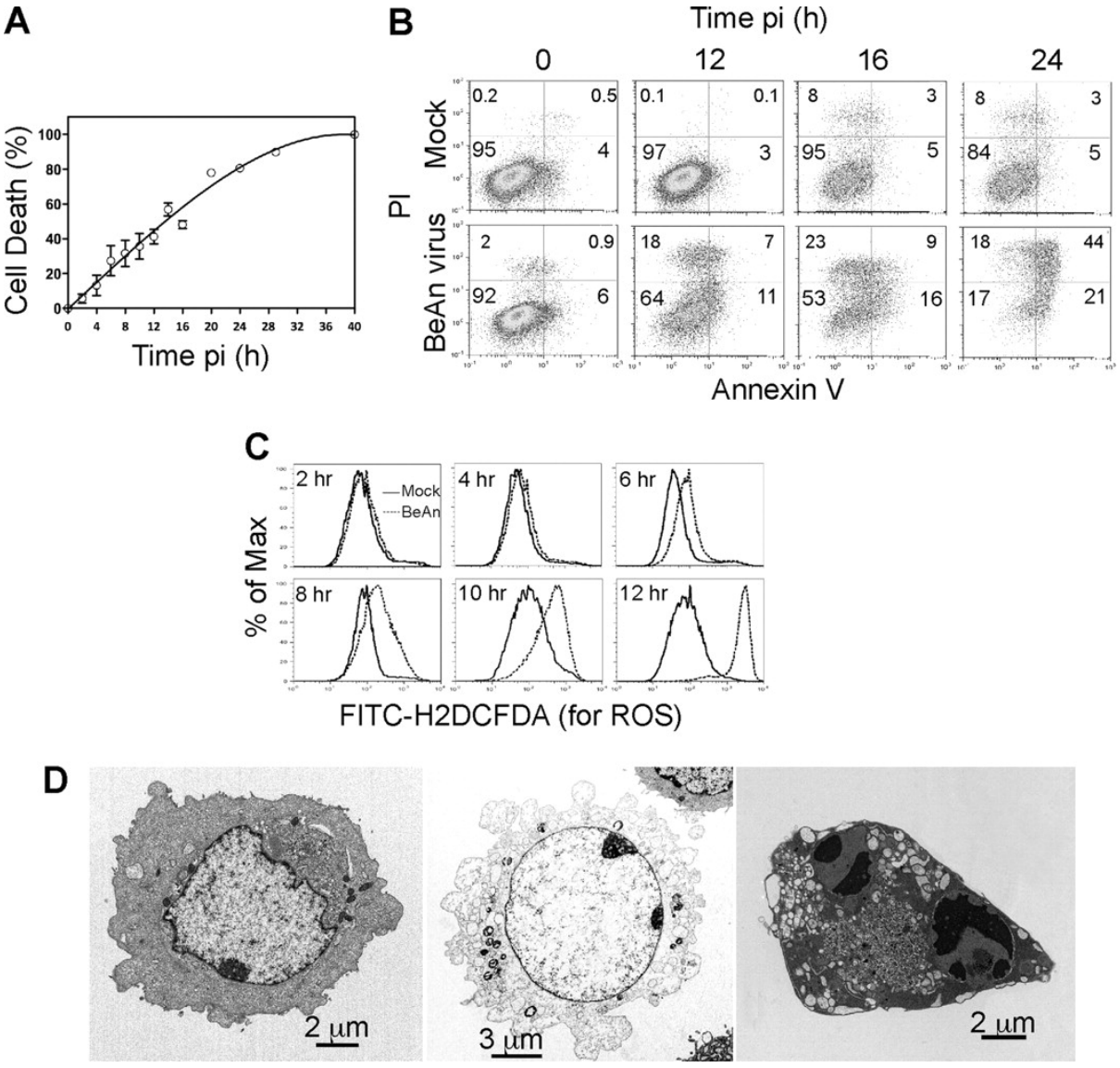

Figure 1. BeAn virus infection of BHK-21 cells (MOI=10) led primarily to necrosis, with a minority of cells undergoing apoptosis. A) Representative WST-1 cell

survival assay revealed progressive cell death to 40 h p.i. Error bars indicate the standard deviations (SD). B) FACS analysis of PI- and annexin V-stained cells showing a temporal profile of PI-positive cells, probably necrotic (majority of cells; upper quadrants) and apoptotic cells (minority of cells; lower right quadrant). C) FACS analysis showing that infected cells develop high levels of reactive oxygen species (ROS) at 10 to 12 h pi. D) Electron microscopy of infected BHK-21 cells showing (i) a relatively normal-appearing cell prior to onset of apoptosis at 8 h p.i. (left), (ii) a necrotic cell at 16 h pi, appearing swollen with little recognizable cytoplasmic or nuclear architecture (center), and (iii) an apoptotic cell at 16 h p.i., appearing mildly shrunken, with condensed nuclear chromatin and blebbing of part of its nucleus and perinuclear proliferating membranes representing viroplasm ("viral factory") (right).

5.2.2 Mcl-1 expression in BHK-21 and mouse cell lines.

Based on the antiapoptotic role of Mcl-1 in BeAn virus-infected M1-D macrophages (32, 33), we examined Mcl-1 expression in mouse cells, including five Macrophage and two fibroblast cell lines and in BHK-21 cells. Immunoblotting analysis revealed low levels of Mcl-1 in the murine cells compared to abundant expression in the hamster-derived BHK-21 cells (Fig. 2A). Because BHK-21 cell Mcl-1 consistently migrated above the mouse species in polyacrylamide gels, the nucleotide sequence was determined; Syrian hamster Mcl-1 has one less one amino acid (319 amino acids) and shares 93% sequence identity with its mouse counterpart (GenBank accession number U35623). Assessment of the expression of the five

Bcl-2 antiapoptotic family members demonstrated abundant Bcl-xL expression in both BHK-21 and M1-D cell lines and Mcl-1 in BHK-21 cells but minimal expression of the other antiapoptotic proteins in BHK-21 cells (Fig. 2B). Because Mcl-1 expression was abundant and might not be regulated, BHK-21 cells were maintained for 36 h in medium containing 0.1% FBS before immunoblotting; Mcl-1 expression decreased at 24 to 36 h (Fig. 2C), indicating that Mcl-1 is regulated by other signaling pathways, such as ERK (reviewed in reference 16). Following BeAn virus infection (MOI=10), Bcl-xL expression remained stable from 0 (end of adsorption period) to12 h pi, while that of Mcl-1 decreased by ~50% at 10 to 12 h p.i. (Fig. 2D, 2E). Assuming steady-state Mcl-1 synthesis and degradation, this decrease in Mcl-1 expression at 10 to 12 h is consistent with the onset of apoptosis.

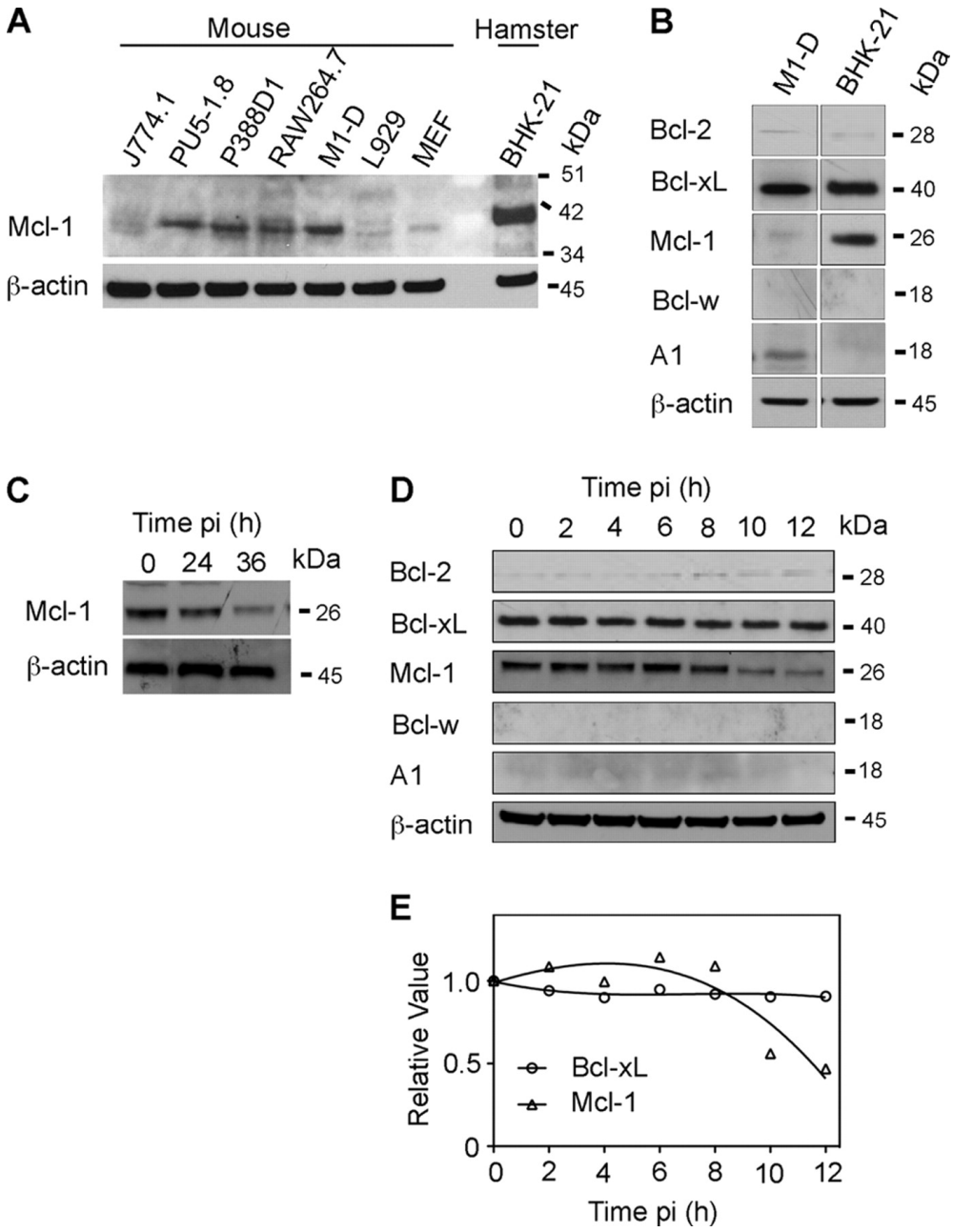

Figure 2. Expression profile of Bcl-2 family antiapoptotic members determined by immunoblotting. A) Mcl-1 expression in five mouse Macrophage cell lines, mouse L929 and murine embryonic fibroblasts (MEFs), and Syrian hamster BHK-21 cells. B) Comparison of the expression of the five Bcl-2 family antiapoptotic proteins in BHK-21 and M1-D macrophages, not the abundant Bcl-xL and Mcl-1 expression

in BHK-21 cells. C) Loss of Mcl-1 expression in BHK-21 cells grown in 0.1% FBS for 24 and 36 h. D) Expression of Bcl-2 antiapoptotic proteins in BeAn virus-infected BHK-21 cells (MOI=10) at the indicated times pi; the substantial reduction of Mcl-1 levels at 10 to 12 h pi is consistent with the induction of apoptosis at this time. E) Densitometric analysis of Bcl-xL and Mcl-1 immunoblot data in infected BHK-21 cells over time pi normalized to β-actin.

5.2.3 Mcl-1 is antiapoptotic in BeAn virus-infected BHK-21 cells.

To further examine the role of Mcl-1 in apoptosis of virus-infected BHK-21 cells, we tested whether siRNA Mcl-1 knockdown would result in increased apoptosis. Mcl-1 expression was inhibited by ~90% with Mcl-1-specific siRNAs, as determined by immunoblotting (Fig. 3A and B) in experiments where the transfection efficiency was ~90% (data not shown). A representative FACS analysis of four experiments revealed a significant increase ($P < 0.048$) in apoptotic cell death in BeAn virus-infected cells transfected with Mcl-1-specific compared to scrambled siRNAs (Fig. 3C). Analysis of viral replication in BHK-21 cells with siRNA knocked-down expression of Mcl-1 revealed an ~70-fold reduction in virus titers (Fig. 3D), indicating that apoptosis inhibited BeAn viral replication. siRNA knockdown of Bcl-xL expression also resulted in a substantial increase in apoptosis (Fig. 3E), indicating that Bcl-xL may also play an antiapoptotic role in infected BHK-21 cells.

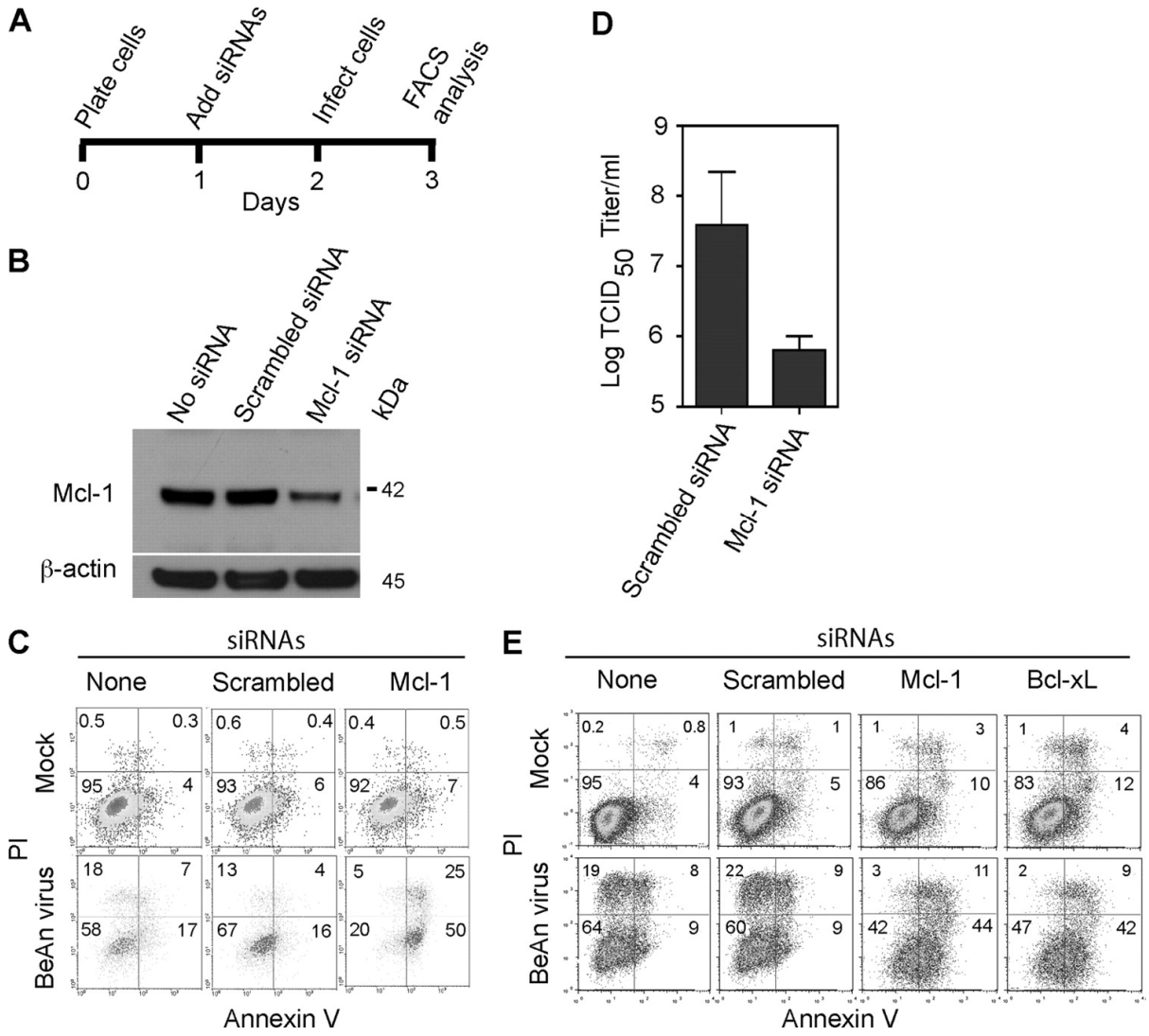

Figure 3. siRNA knockdown demonstrates an antiapoptotic role of Mcl-1 and Bcl-xL in BeAn virus-infected BHK-21 cells. (A) Timeline of cell death analysis in siRNA experiments. B) Immunoblot analysis revealing 90% knock down of the amount of Mcl-1 with specific compared to scrambled siRNAs. C) Representative FACS analysis of PI- and annexin V-stained cells revealed an ~3-fold increase in

apoptotic cells (right lower quadrant) after infection of Mcl-1 knockdown cells at 16 h p.i. D) Infectious virus yields of Mcl-1 siRNA-transfected cells was significantly decreased at 16 h p.i. ($P<0.01$) compared to viral yields of scrambled siRNA-transfected cells. Error bars indicate the SD. E) FACS analysis of PI- and annexin V-stained cells demonstrated that both Mcl-1 and Bcl-xL function as antiapoptotic proteins in infected BHK-21 cells.

To further study the effect of Mcl-1 knockdown on BeAn virus replication, 22 stable, puromycin-resistant BHK-21 clones were generated, and two clones (clones 8 and 10) showing the greatest decrease in Mcl-1 expression (Fig. 4A) were infected with virus and assessed for apoptosis. Both clones showed increased levels of apoptosis at 6 and 8 h p.i. ($P<0.05$) and levels were significantly higher at 10 h p.i. ($P=0.02$) compared to infected parental cells (Fig. 4B) in an assay based on nuclear morphology of attached cells; because of CPE, the assay was not reliable ≥ 12 h pi. BeAn infection of both clones resulted in PARP, caspase-9 and caspase-3 cleavage (shown for clone 10 in Fig. 4C) but not caspase-8 cleavage at 6 to 10 h pi, suggesting that TMEV infection in BHK-21 cells activates the intrinsic signaling pathway similar to its action in murine macrophages (14, 32). A caspase activity assay using a commercial luminescent reagent revealed an ~3-fold activation of caspase-9 compared to ~1.7-fold for caspase-8 ($P=0.01$) (Fig. 4D); however, the increases in activity were probably minimal because of the still limited extent of apoptosis. In contrast to the immunoblotting results, knockdown of Mcl-1 did not lead to significantly increased initiator caspase activity (Fig. 4D).

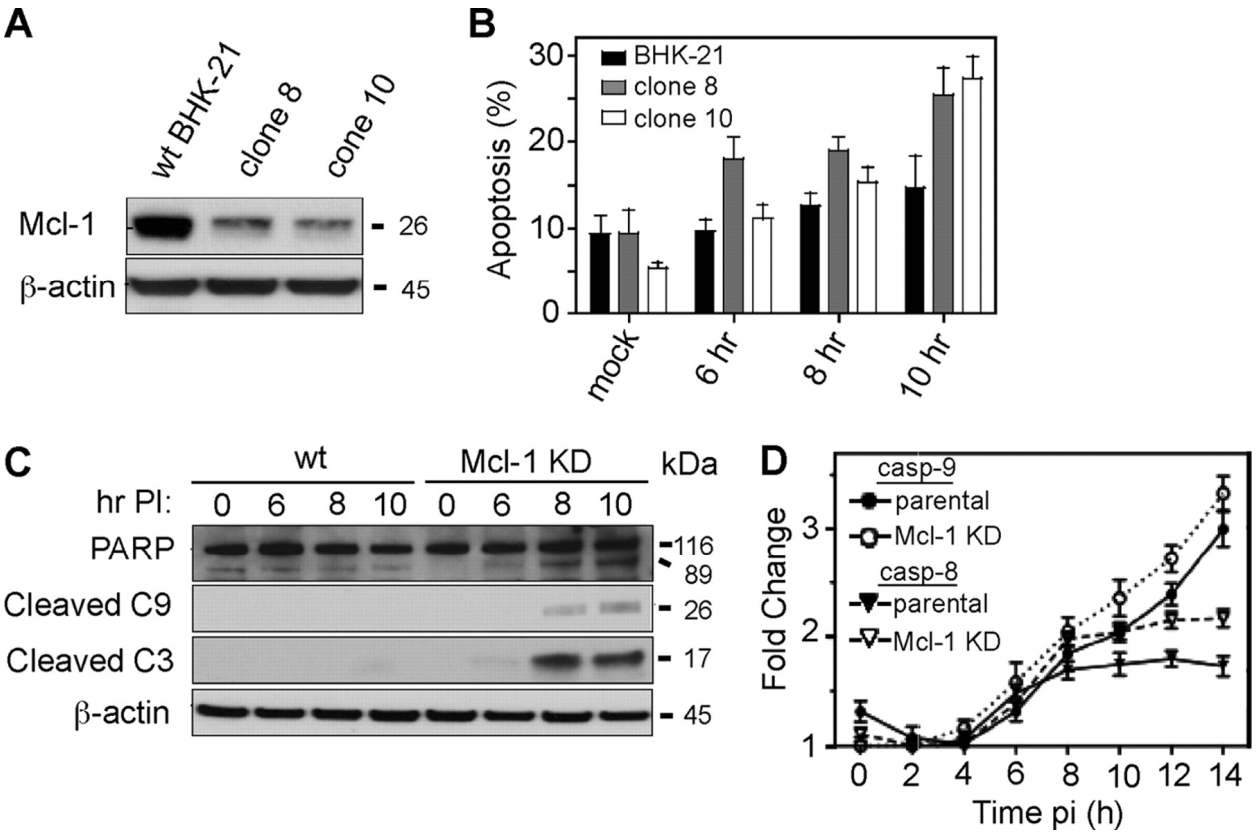

Figure 4. BeAn virus infection of BHK-21 cells with stable Mcl-1 knock-down induces apoptosis through the intrinsic pathway. A) Two stable Mcl-1 knockdown clones (clones 8 and 10) showed a 90% reduction in Mcl-1 expression. B) BeAn infection (MOI=10) of clones 8 and 10 induced apoptosis beginning at 6 h p.i., as assessed based on nuclear morphology (DAPI staining) (error bars indicate the SD). C) Immunoblot analysis revealed PARP and caspase-9 and caspase-3 cleavage in infected parental and Mcl-1 knockdown BHK-21 cells (shown for clone 10) at 8 and 10 h p.i. Note that the 17-kDa caspase-3 cleavage product is barely detectable at 10 h in parental cells but is clearly seen with a longer exposure time

of the autoradiogram (data not shown). D) Activation of caspase-9 but not caspase-8 over time in a Luc assay of parental and Mcl-1 knockdown BHK-21 cells (error bars indicate the SD).

Temporal analysis of virus titers in infected parental and Mcl-1 knockdown cells, indicated a shortened virus growth phase for infected clone 10 cells, peaking at 8 to 10 h p.i. and resulting in 90% reduction in infectious virus yields compared to parental cells (Fig. 5A). BeAn virus grown in knock-down cells yielded more defective virus particles per cell, i.e., a 16-fold increase in the ratio of physical particles to infectious particles (PFU) than in parental cells (5.2×10^4 versus 3.1×10^3) determined from virus purified at 24 h from infected cells (representative of three experiments). Northern blot analysis to determine whether the kinetics of single-stranded viral RNA (ss viral RNA) replication was also affected revealed no significant differences in parental and knockdown cells (Fig. 5B); Fig. 5C shows the densitometric scan of the Northern blot. Pulse-chase analysis at 5 h p.i. showed similar viral protein synthesis and polyprotein processing (Fig. 5D). These results indicate that Mcl-1 is an essential prosurvival factor that enables increased infectious virus yields by inhibiting apoptosis and by its impact on a step in the viral life cycle later than viral RNA replication, protein synthesis, or polyprotein processing.

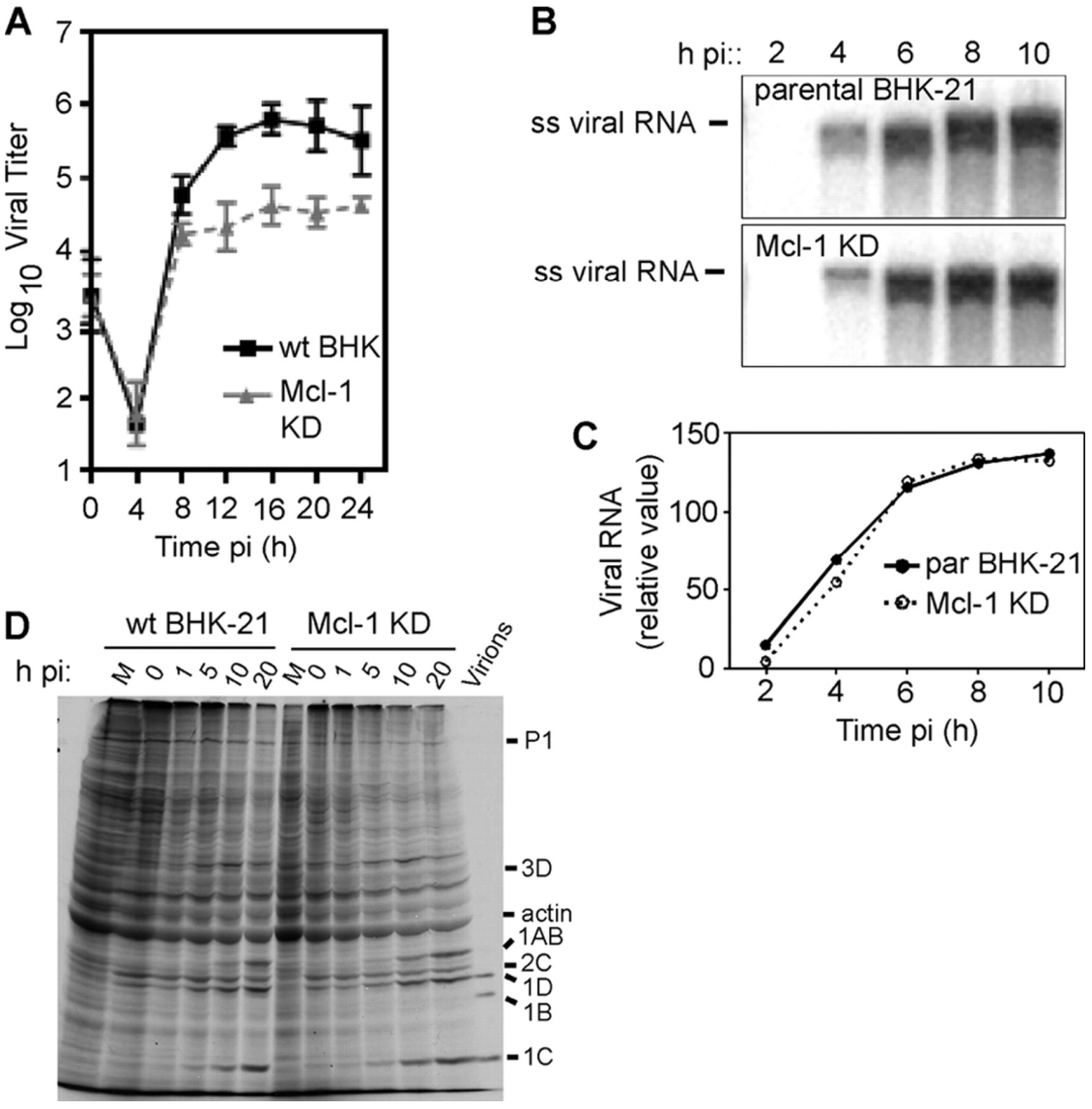

Figure 5. Stable Mcl-1 knockdown in BHK-21 cells does not affect viral RNA synthesis or translation but reduces infectious virus production of compared to parental cells. A) Temporal kinetics of BeAn infection showing that peak virus titers in knock-down cells were significantly reduced at 8 to 12 h pi compared to parental cells (P=0.04 at 12 h; error bars indicate the SD). B) Northern blot analysis showing similar replication of ss viral RNA in both parental and knockdown cell lines. C) Cells lines pulsed with [^{35}S]methionine at 5.5 h pi for 5 min, followed by chases at

the indicated times revealed similar protein synthesis, including polyprotein processing into the final structural and nonstructural viral proteins (labeled on the right).

5.2.4 Activation of p53 in infected BHK-21 cells.

Mcl-1 expression is regulated by a variety of cytokines and growth factors through a number of signaling pathways [128, 129]. Mcl-1 is also regulated by the p53 tumor suppressor protein [130], the activation of which is required for the induction of apoptosis in BeAn virusinfected M1-D macrophages [59]. Immunoblotting to determine whether p53 was also activated in infected BHK-21 cells showed increased p53 expression as early as 15 min p.i. (Fig. 6A). Ser-15 and Ser-20, two common p53 phosphorylation sites that are induced in BeAn infected M1-D cells [59], did not differ in phosphorylation levels (not shown), suggesting that p53 may be activated by phosphorylation at other sites. Immunoblot analysis of immunoprecipitated p53 with monoclonal antibody to phospho-Ser, phospho-Tyr, and phospho-Thr residues showed that p53 was phosphorylated in infected BHK-21 cells but not in BHK-21 cells incubated with UV-inactivated virus (Fig. 6B). Similar analysis of the BH3-only proapoptotic proteins Noxa and Puma, which are transcriptionally upregulated by p53 [42, 130, 131] and activated in BeAn-infected M1-D macrophages [59], revealed upregulation of only Noxa in infected BHK-21 cells (Fig. 6C). Immunoblotting analysis for Bax and Bak expression showed increased expression and activation of only Bax (Fig. 6D; Bak data not shown) at

30 min p.i. These data demonstrate the close similarity of the apoptotic cell death pathway in BHK-21 cells and M1-D macrophages.

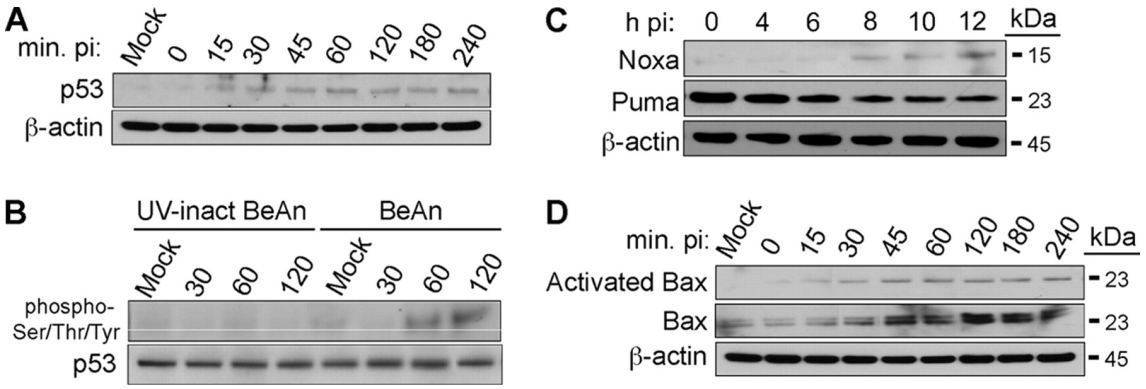

Figure 6. BeAn virus-infected parental BHK-21 cells show p53 and Noxa activation upstream and Bax downstream of Mcl-1. A) Immunoblot analysis showing after infection (MOI=10) of parental BHK-21 cells detectable p53 from 15 to 240 min pi but not in mock-infected cells (later is not shown). B) Immunoblot of p53 immunoprecipitated from infected cells early pi and incubated with mouse monoclonal antibody to phosphoserine/threonine/tyrosine demonstrated phosphorylation of p53 at 60 and 120 min p.i., whereas control, parental BHK-21 cells infected with UV-inactivated BeAn virus showed no p53phosphorylation. C, D) Immunoblots showing that BeAn infection leads to activation of Noxa, but not Puma at 8 to 10 h and to activation of Bax at 30 min p.i. and increased amounts of total Bax (D).

5.2.5 BeAn infection induces necrosis in immature N20.1 oligodendrocytes.

Unlike the restricted infection of macrophages, infection of oligodendrocytes in mice appears to be highly productive [132]. Analysis of cell death in the undifferentiated murine oligodendrocyte cell line N20.1 which is productively infected [133], showed a temporal profile similar to that in BHK-21 cells (Fig. 7A); however, FACS analysis of PI- and annexin V-stained cells indicated that essentially all of the cells underwent necrosis (Fig. 7B). As expected, virus infection of both cell lines resulted in one-step growth kinetics with similar high viral yields (Fig. 7C). Immunoblotting to examine the expression profile of the Bcl-2 antiapoptotic proteins in BHK-21, N20.1, and M1-D cells showed high levels of Mcl-1 only in BHK-21 cells, with just detectable levels in N20.1 and M1-D cells (Fig. 7D). Bcl-w was expressed at high levels in N20.1 cells, suggesting that Bcl-w may be a critical prosurvival protein in oligodendrocytes; however, the results of siRNA knockdown of Bcl-w were not conclusive (not shown).

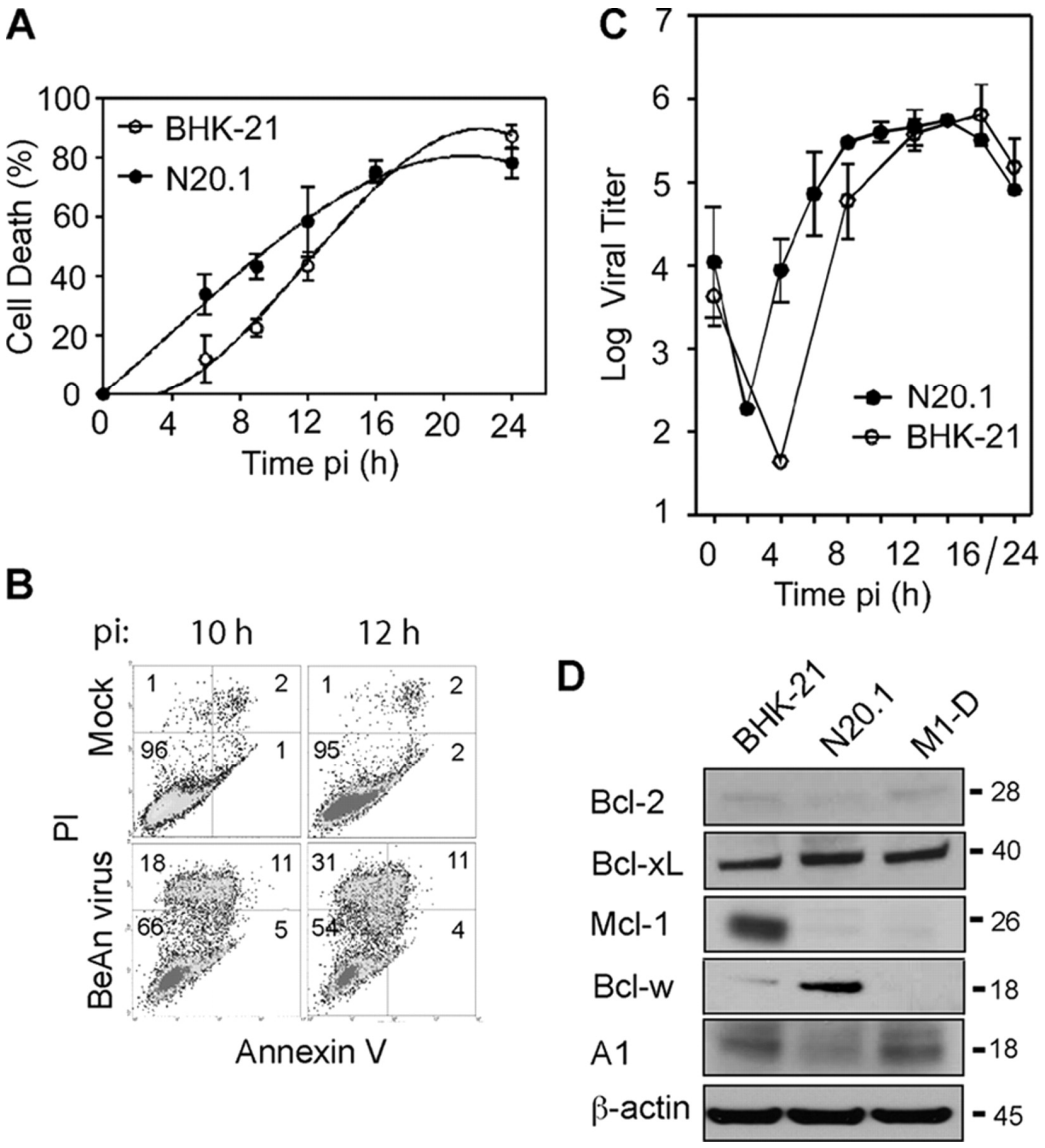

Figure 7. BeAn virus-induced necrosis in N20.1 oligodendrocyte cells. A) Comparison of the temporal profile of virus induced-cell death of N20.1 and parental BHK-21 cells in a representative experiment using the Wst-1 assay. Error bars indicate the SD. B) BeAn virus infection of N20.1 cells resulted primarily in necrotic cell death; 42% of the cells stained PI positive by 12 h pi, whereas only 4% underwent apoptosis. C) Comparison of one-step growth kinetics of BeAn virus in N20.1 and BHK-21 cells showed similar peaks of high virus titers by 12 to 14 h

pi. Error bars indicate the SD. D) Immunoblot analysis of the five Bcl-2 family antiapoptotic proteins showed that Bcl-w was highly expressed in the N20.1 oligodendrocytes compared to BHK-21 and M1-D cells. The low expression level of Mcl-1 in M1-D cells was not detected in this immunoblot.

5.3 Discussion

The mode of virus-induced cell death is critical in determining host range of a virus, i.e., the extent of virus production and viral spread in an animal host and dissemination to other animal hosts. In picornavirus infections where rapid viral replication kinetics usually predominate, necrosis generally has been associated with productive infections and apoptosis with restricted infections [56, 99, 134-136]. TMEV infection has been shown to induce necrosis in rodent cells, such as BHK-21 and L929 cells, in association with high viral yields [56, 58], whereas murine macrophages undergo apoptosis exclusively, with interruption of virus production and decreased yields of infectious virus progeny. An in-depth characterization of infection in BHK-21 cells has not been carried out, and the mechanism by which BeAn virus induces host-specific cell death to affect viral yields is not well understood. In the present study, we examined the mode of BeAn virus-induced cell death in BHK-21 cells, the role of Bcl-2 family prosurvival proteins, particularly Mcl-1, in regulating cell death, and the effect of apoptosis and necrosis on TMEV replication.

Our studies revealed the apoptosis of only a minority of BHK-21 virus-infected cells (~20%), while a majority were PI positive (~60%) and underwent necrosis (Fig. 1). The Bcl-2 multidomain, antiapoptotic protein Mcl-1 was highly expressed in BHK-21 cells, with a decrease in expression at 10 to 12 h p.i., which is consistent with the onset of apoptosis. siRNA knockdown of Mcl-1 resulted in an ~3-fold increase in apoptosis (Fig. 2 and 3), indicating that Mcl-1 is important in regulating apoptosis in BHK-21 cells. Bcl-xL was also expressed at high levels (Fig. 2D) and, when knocked down by siRNAs, led to a similar increase in apoptosis (Fig. 3E). Knockdown of both Mcl-1 and Bcl-xL did not result in a greater percentage of apoptotic cells than either prosurvival molecule alone (not shown), possibly because either Mcl-1 or Bcl-xL is sufficient to counter most of the proapoptotic activity of Bax.

The apoptotic program that switched on at the time of exponential TMEV replication in BHK-21 cells was similar to that M1-D macrophages [58, 59], with hallmarks of activation of the intrinsic apoptotic pathway in a tumor suppressor protein p53-dependent manner (Fig. 6A and B). Experiments in which Mcl-1 was stably knocked down to increase the otherwise low level of apoptosis in parental BHK-21 cells suggested that the subsequent activation of the Bcl-2 BH-only proapoptotic Noxa protein led to degradation of Mcl-1 (Fig. 6C and D), activation of Bax and, after the release of cytochrome c into the cytoplasm (not shown), the cleavage of caspase-9 and caspase-3 (Fig. 4C). The early activation of Bax, in contrast to its later activation in infected M1-D cells, was surprising but might be

explained by the direct interaction of Bax with p53 inducing its homo-oligomerization and activation [137].

Analysis of one-step viral growth kinetics in Mcl-1 knockdown BHK-21 cells demonstrated a peak in viral growth at 8 to 10 h p.i. (~2 h earlier than in parental cells), leading to 90% reduction in infectious viral yields at 24 h p.i. (Fig. 5A). While finding that viral RNA replication, protein synthesis, and polyprotein processing did not differ between stable Mcl-1 knockdown and parental cells (Fig. 5B and C) pointed to a defect in virion assembly possibly due to capsid protein cleavage from activated caspases, our preliminary experiments provide insufficient evidence of differences in the assembly of 5S protomers and 14S pentamers (assembly intermediates) or in 150S mature virions in cells with stable knockdown of Mcl-1 (unpublished data). Capsid proteins of feline calicivirus and Aleutian mink disease virus, a parvovirus, have been shown to be cleaved by caspases during infections in cell culture [138, 139]. Recently, Bryant and Clem [140] reported that a p35 mutant of Autographa californica multiple nucleopolyhedrovirus, a baculovirus that infects lepidopteran insects, did not induce apoptosis despite caspase activity but did produce progeny virus with defects in stability and infectivity. This defect was rescued in the producer cells when virus was grown in the presence of zVAD-fmk [140]. Caliciviruses, parvoviruses, baculoviruses, and TMEV are all nonenveloped viruses. Studies are in progress to identify a defect in TMEV virions or the capsid proteins grown in BHK-21 cells with stable knockdown of Mcl-1.

During persistent infection in the mouse CNS TMEV replication is observed primarily in macrophages [91, 141, 142] and, to a lesser extent, in oligodendrocytes [16, 132]. Blakemore et al. [132] found paracrystalline arrays of virions in oligodendrocytes by electron microscopy in chronically infected spinal cords, indicating that oligodendrocytes are productively infected and probably undergo necrosis. However, Tsunoda et al. [143] detected some TUNEL (terminal deoxynucleotidyltransferase-mediated dUTP-biotin nick end labeling)-positive oligodendrocytes in mice chronically infected with another low-neurovirulence TMEV, DA virus. Our in vitro analysis using the N20.1 cell line, which consisted of primarily of immature oligodendrocytes (undifferentiated cells when grown at 37°C), showed that infection with BeAn virus led to necrosis with the production of high virus titers, similar to BHK-21 cells. N20.1 cells expressed high levels of another Bcl-2 antiapoptotic family protein, Bcl-w (Fig. 7D), which is highly expressed in brain and spinal cord tissues [144] and in neurons and glia [144], 25). Further studies of primary murine oligodendrocytes and other murine oligodendrocyte cells lines are needed.

CHAPTER 6

TMEV INDUCES NECROPTOTIC CELL DEATH IN A RIP1-DEPENDENT MANNER, RESULTING IN HIGH YIELDS OF INFECTIOUS VIRUS

6.1 Background

Cellular sensing of viral pathogens by the host activates inflammatory gene expression and triggers cell death. Apoptosis is a well-established caspase-dependent host defense pathway triggered through cell-intrinsic or/and cell-extrinsic signals in response to pathogens [60, 61]. On the other hand, caspase-independent cell death, or programmed necrosis, has emerged as an alternative death pathway that dominates under specific conditions [62]. Necroptosis is a form of programmed necrosis induced by death receptors (DR) that is independent of caspases but dependent on receptor-interacting protein kinase 1 (RIP1; also known as RIPK1) [63, 64] and RIP3 (also known as RIPK3) [65-67], and its execution involves the active disintegration of mitochondrial, lysosomal and plasma membranes. It has been shown that necrosis can also be induced by multiple viruses such as human immunodeficiency virus type-1 (HIV-1) [75, 76], herpes simplex virus type-1 (HSV-1) [78], West Nile virus (WNV) [74], vaccinia virus (VV) [65], and murine cytomegalovirus (MCMV) [77]. Cell viability upon viral infection is increased when the infection is preceded by treatment with the RIPK1 kinase inhibitor Nec-1 [78]. It is known that viral infection induces the formation of a pro-necrotic RIPK1–RIPK3 complex [65, 77, 81, 82, 145]. Studies have shown that, RIPK3-deficient mice do not develop virus infection-induced necrosis and liver

inflammation, suggesting that RIPK1- and RIPK3-dependent necroptosis is important for the inflammatory response against virus infections.

TMEV infection results in two distinct cell death programs, necrosis and apoptosis, leading to substantial differences in infectious viral yields. While TMEV infection of mouse M1-D macrophages induces apoptosis by activating the intrinsic apoptotic pathway, infection of other rodent cells including neurons and oligodendrocytes undergo necrosis resulting in high viral yields [56, 146], i.e., ~500 pfu/cell [133]. BeAn virus infection of BHK-21 cells leads primarily to necrosis, with at most 20% of cell undergoing apoptosis [146], the apparent default cell death pathway from infection of this mammalian cell line by TMEV. The mechanism by which BeAn virus induces host-specific cell death, affecting viral yields is not well understood.

In this section, we investigated the necrotic pathway after TMEV infection of BHK-21 cells that is associated with productive infection. We showed that BeAn virus infection in BHK-21 cells led to programmed necrosis (necroptosis) through the activation of the RIP1 pathway. Knock down of RIP1 resulted in reduced virus titers, indicating that necroptosis to a more virulent infection.

6.2 Results

6.2.1 Nec-1 promoted survival of BeAn-infected BHK-21 cells.

The mechanism of cell death (or cell survival) and the regulated signaling pathways in TMEV-induced necrosis are largely unknown. It has been

demonstrated that mitochondrial energy metabolism is linked to the execution of necrosis in which ROS production plays an important role for the necroptotic response [147, 148]. Previous studies have shown that BeAn infection of BHK-21 cells induces significant amounts of ROS [146]. To study whether infected BHK-21 cells undergo necroptosis and induce ROS, we used Nec-1, an inhibitor of RIPK1 activity required for necroptosis [32, 68]. DAPI staining showed that Nec-1 treatment of BeAn infected cells results in a delay of cell death (Fig. 1A). Nec-1 did not affect the nuclear morphology (Fig. 1A) and revealed that caspase-3 was not cleaved (data not shown). These data indicate that cell survival was not due to inhibition of apoptosis. Nec-1 treatment resulted led to ~25% increase ($p<0.05$) in cell survival of BeAn infected BHK-21 cells (Fig. 1B, 1C) suggesting that RIP1-dependent necroptosis play a role in regulating BeAn virulence.

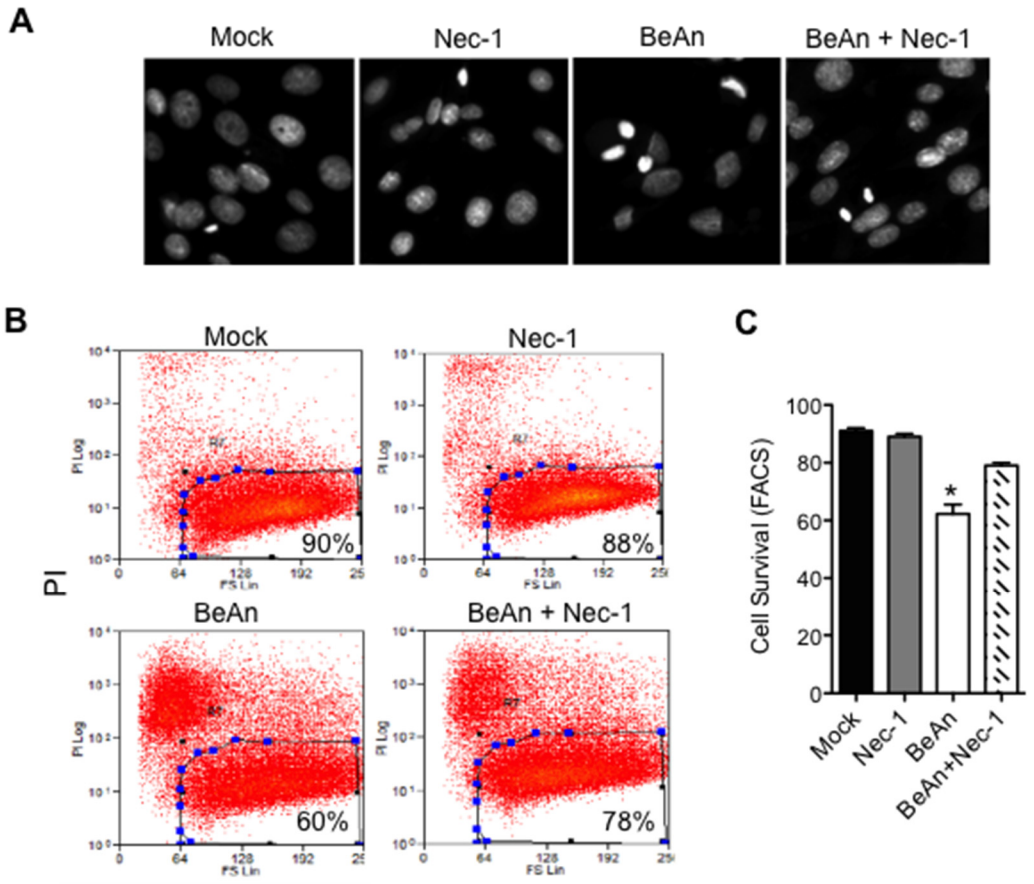

Figure 1. Nec-1 provides increased survival of BeAn-infected BHK-21 cells (MOI=10). A) BeAn infected BHK-21 cells (12 h pi) treated with Nec-1 (100 µM) shown by DAPI staining B) PI-staining showed significantly increased cell survival of infected cells in the presence of Nec-1 ($p<0.05$). These data are shown in the bar graph on the right (C).

6.2.2 BeAn induced RIP1 phosphorylation.

Necroptosis depends on autophosphorylation of RIP1, Ser161 and direct RIP1-mediated phosphorylation of RIP3 [32, 66]. We then examined the possibility that RIP1 and RIP3 might be recruited to a pronecrotic complex via phosphorylation by labeling BHK-21 cells with [^{32}P]-orthophosphate. RIP1

phosphorylation was detected when cells were infected with BeAn virus at 10h pi (Fig. 2A, 2B). We found that BeAn virus infection also induced RIP3 phosphorylation. Nec-1 treatment of BeAn virus infected cells (12 h pi) resulted in reduced phosphorylation levels of RIP3, suggesting that the kinase activity of RIP1 is required for RIP3 phosphorylation and possibly necrosome formation.

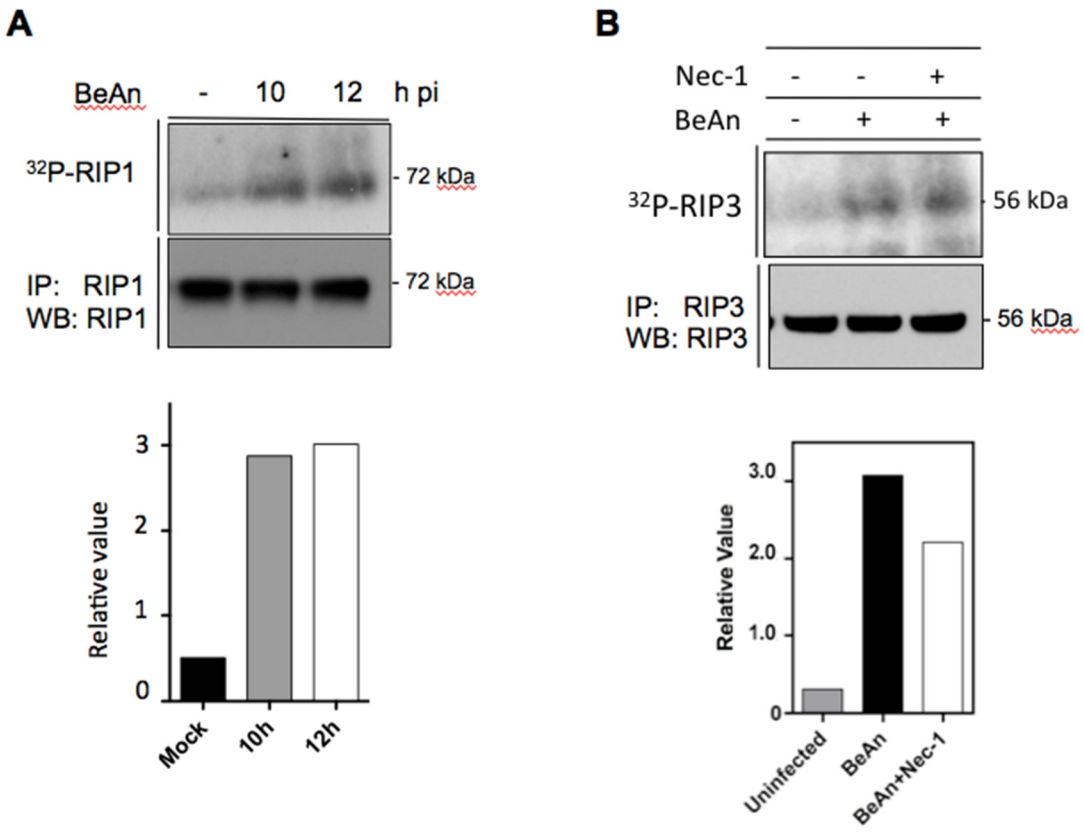

Figure 2. BeAn virus infection in BHK-21 cells induced RIP1 and RIP3 phosphorylation required for necroptosis. A) Infected BHK-21 cells were labeled with [^{32}P]-orthophosphate (top panel) and RIP1 was immunoprecipitated with specific antibody to RIP1 (bottom panel). Virus infection induced RIP1 phosphorylation at 10 h and 12 h pi. These data are shown in the bar graph on the bottom. B) RIP3 was also phosphorylated in infected cells, and phosphorylation

was reduced in the presence of Nec-1 (top panel). Relative values of RIP3 phosphorylation were shown on the bottom.

6.2.3 BeAn induced ROS during necroptosis.

A major effort have been exerted to understand how the RIP1-RIP3 necrosome complex activates necrotic cell death. Recent studies have shown that RIP3 acts upstream to regulate ROS production during necroptosis [65]. On the other hand, c-Jun NH2-terminal kinase (JNK) leads to necrosis by producing ROS, potentially by impacting mitochondrial function [149], whereas intracellular production of ROS activates the pro-necrotic effect of JNK [150]. While Nec-1 inhibits necroptosis, it does not have any effect on other RIP1 functions, such as mitogen-activated protein kinase p38, and JNK [32]. Our results demonstrated that BeAn infection of BHK-21 cells resulted in elevated ROS production [146]. Since the infection induced RIP1 and RIP3 activation, we determined whether RIP1-RIP3 might function upstream of ROS to promote necroptosis. Elevated ROS were detected at 6 h pi by staining with 2′,7′-dichlorodihydrofluorescein diacetate (H_2DCFDA) (Fig. 3A), and Nec-1 treatment of BeAn virus infected cells resulted in reduced ROS levels (Fig. 3B, 3C). Moreover, the phosphorylation levels of JNK were increased upon virus infection in a temporal manner (Fig. 3D), suggesting that JNK and ROS may form a positive feedback loop to enhance necrosis. As expected, JNK levels were not affected when virus infected cells were treated with Nec-1 (data not shown). These results indicate that BeAn virus induces RIP1-RIP3

activation that may act upstream to regulate ROS production during programmed necrosis.

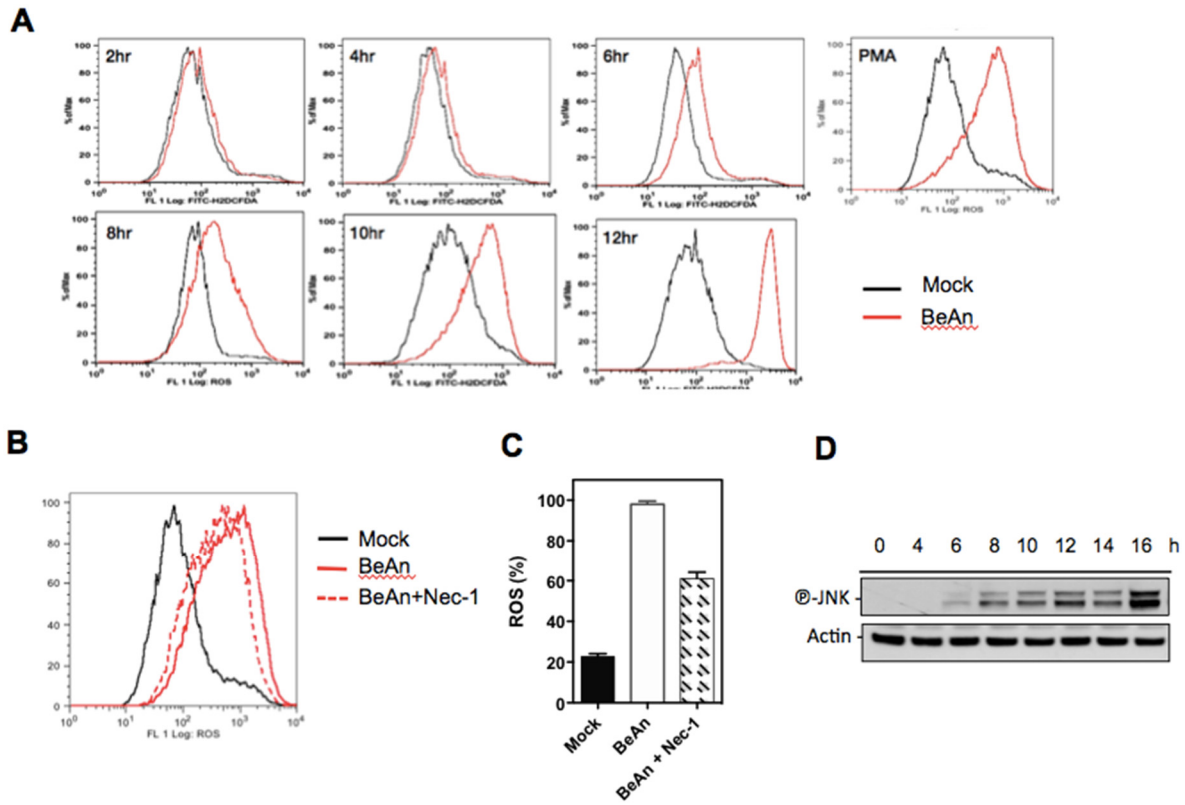

Figure 3. BeAn virus infection induced ROS during necroptosis. A) ROS levels in BeAn infected BHK-21 cells were measured by 2′ ,7-dichlorodihydrofluorescein diacetate (H_2DCFDA) staining and FACS analysis. BeAn virus infection of BHK-21 cells resulted in a significant increase in ROS at 6h pi indicated by a shift of the solid red peak. B) ROS levels decreased when BeAn virus infected cells were incubated with Nec-1 (50 μM) and analyzed at 12 h pi. C) Quantitation of three experiments demonstrating a significant decrease ($p<0.05$) in ROS at 16h pi in the presence of Nec-1. D) BeAn virus infection induced phosphorylation of JNK beginning at ~6 h pi.

6.2.4 RIP1-dependent necroptosis is required for productive infection

BeAn virus infection in BHK-21 cells is associated with high virus titers, resulting in productive infection [146]. To determine whether RIP1-dependent necroptosis is required for increased viral yields in infected BHK-21 cells, RIP1 siRNA was used to knock-down endogenous RIP1 expression at 24h pi before infection (Fig. 4A). Silencing of RIP1 (Fig. 4B) resulted in a significant decrease in virus titers ($p<0.05$) (Fig. 4C), indicating that RIP-1 mediated necroptosis is critical for maintaining BeAn virus production.

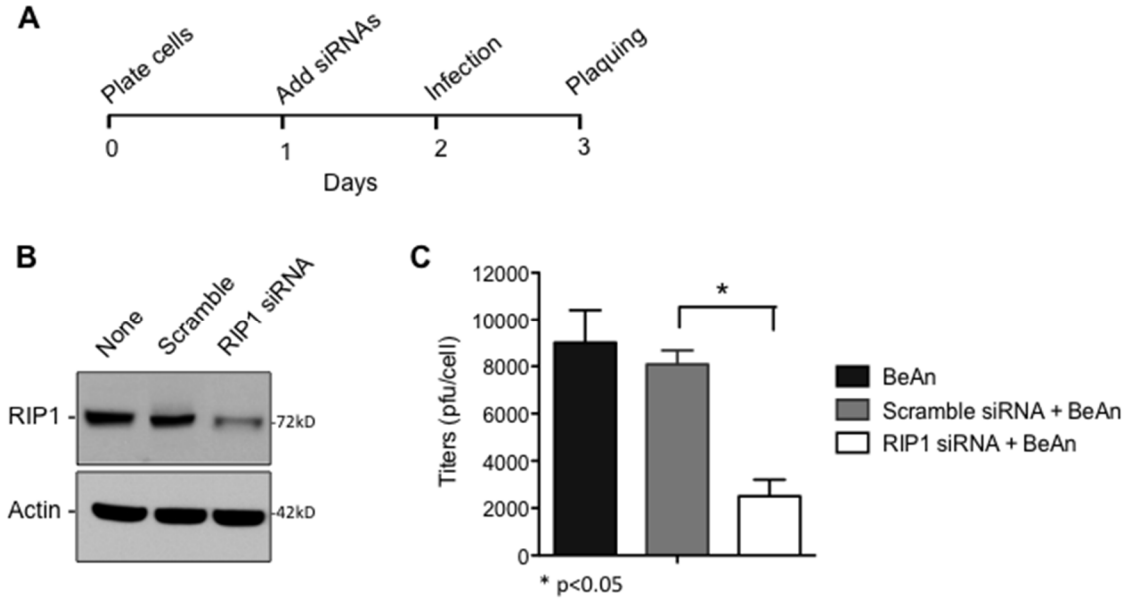

Figure 4. Knock-down of RIP1 reduced BeAn virus titers by increasing apoptosis. A) Cells were transfected with siRNA on day 1, infected with virus on day 2 and plaque assay was performed on day 3. B) siRNA transfection of BHK-21 cells shows decreased levels of endogenous RIP1 protein after 24h. C) Knock-down of RIP1 resulted in a significant decrease on BeAn virus titers ($p<0.05$).

6.3 Discussion

Necroptosis, or programmed necrosis, plays an important role in the response to viral infection by serving as a backup mechanism of cell death to apoptosis [151-153]. Virus-infected cells, which are resistant to apoptosis, are found to be highly sensitive to necroptosis [75, 76, 78, 82]. As yet, there is no knowledge about necroptosis in TMEV infection. Nec-1, which inhibits apoptosis, blocks the interaction between RIP1 and RIP3, which indicates that the kinase activity of RIP1 is indispensable for assembly of the RIP1-RIP3 complex [65, 66] required for necroptosis. Our studies showed that BeAn virus induces RIP1 and RIP3 phosphorylation, suggesting that infected BHK-21 cells undergo- necroptosis or programmed necrosis. It is known that RIP3 accelerates recruitment of RIP1 to the necrosome, and the kinase activity of both proteins is required in this process [65]. Treatment of BeAn infected cells with Nec-1 resulted in reduced levels of RIP3 phosphorylation suggesting that kinase activity of RIP1 is required for RIP3 activation (Fig 2). Whether RIP3 kinase activity induces RIP1 phosphorylation of infected BHK-21 remains to be determined.

Evidence has shown that necroptosis is induced by a class of death receptors that include TNFR1, TNFR2, and Fas [154]. One physiological situation in which caspases are inhibited and necroptosis might be important is during viral infections [155]. While the RIP1-RIP3 complex was only detected when cells were stimulated with TNFα/zVAD, TNFα alone was sufficient to trigger RIP1-RIP3 association in VV-infected MEFs [65, 81, 82]. This is in contrast to uninfected cells, in which TNFα

did not trigger a RIP1 and RIP3 interaction, indicating that RIP1-dependent necroptosis is an important cell death mechanism when the cellular apoptosis machinery is inhibited by broad- spectrum caspase inhibitors. On the other hand, MCMV and HSV-1 strains induce necrosis that relies on RIPK3 but not on RIPK1 or endogenous TNFα production [77, 78, 156]. Whether BeAn infection is sensitizing cells for necroptosis by inducing TNFα or directly inducing RIP1 and RIP3 remains to be determined. The extent of apoptosis observed following virus infection is cell type-dependent, indicating that virus-induced apoptosis is regulated by different cellular factors, such as Bcl-2 family members [157-161]. High endogenous levels of Mcl-1 in BHK-21 cells favors necroptosis when infected with BeAn virus, replacing a need of caspase inhibitors in infection of BHK-21 cells ([146], also see chapter 5).

Both RIP3 and kinase activity of RIP1 are essential for stable formation of RIP1-RIP3 pronecrotic complexes, which regulate the production of downstream ROS [65]. Indeed, our results showed that BeAn virus infection generated high levels of ROS which may act downstream of the RIP1 and RIP3 pathways. TMEV-induced necroptosis may also play a role in triggering inflammation as it has been demonstrated that inflammation caused by VV infection is evidently reduced in $RIP3^{-/-}$ mice [162]. Our results also showed that BeAn virus infection induce RIP1-dependent necroptosis since knock-down of RIP1 resulted in a significant decrease in viral titers due to increased apoptosis [146]. This suggests that necroptosis contributes to the TMEV virulence and in part to chronic inflammation in mice.

CHAPTER 7

VIRION CAPSID PROTEIN(S) ARE PERTURBED DURING APOPTOSIS, RESULTING IN LOSS OF INFECTIOUS VIRUS, ENABLING PERSISTENT INFECTION OF THIS HIGHLY CYTOLYTIC PICORNAVIRUS BY REDUCING ITS NEUROVIRULENCE.

7.1 Background

Low-neurovirulence TMEV strains (BeAn and DA) produce a persistent CNS infection in susceptible strains of mice that results in immune-mediated damage as well as viral destruction of oligodendrocytes, leading to demyelination [16, 132, 163]. Autoreactive CD4+ T-cells specific for myelin protein epitopes have been detected in TMEV-infected mice more than 1 month after onset of demyelination, suggesting a potential additional role for autoimmune damage to myelin at later times post-infection (pi) [22, 164, 165]. These features make infection of mice with low-neurovirulence TMEV a relevant experimental animal model for multiple sclerosis.

A central issue in TMEV pathogenesis relates to the dynamics of the persistent infection in the CNS. While persistence of noncytopathic RNA viruses is readily understood, that of cytolytic RNA viruses, such as picornaviruses, is enigmatic, since continuous cell-to-cell spread would seem to be required to perpetuate the infection. Although limited by host anti-viral immune responses, TMEV is nonetheless somehow able to spread to and infect macrophages and glia during

the persistent phase of infection. The ability of TMEV to persist in the mouse CNS has traditionally been demonstrated by recovering infectious virus from the spinal cord. Results of infectivity assays led to the notion that TMEV persists at low levels, usually with $\leq 10^3$ pfu detected in the spinal cord [166, 167]. However, real-time RT-PCR to quantitate TMEV RNA revealed $>10^9$ viral genomes per spinal cord between 1 and 8 months pi [168], demonstrating a ratio of 10^6:1 viral RNA copies to pfu during persistence or three orders of magnitude higher than the ratio in acutely infected spinal cords (5×10^3:1) [133]. The disparity between viral genome load and infectious virus during persistence *in vivo* remains unexplained, but may reflect the neutralization of infectious virus by virus-specific antibodies, clearance by virus-specific CD4+ and CD8+ T cells and restricted production of infectious virus by CNS macrophages, a principal cell type supporting TMEV replication during persistent infection [141, 142, 169].

TMEV has been shown to selectively induce apoptosis in murine macrophages *in vitro* in contrast to infection of other somatic cells, both primary and transformed, that undergo necrosis, and in the case of BHK-21 cells, necroptosis [58, 128, 146]. TMEV-induced apoptosis occurs via the intrinsic pathway, initiated by activation of MKKK3/6 and p38 MAPK leading to phosphorylation and activation of p53, in turn upregulating expression of the pro-apoptotic BH3-only proteins Noxa and Puma that bind the BH-multidomain anti-apoptotic proteins Mcl-1 and A1 [59]. This interaction alters the conformation of these prosurvial proteins resulting in the release of the BH-multidomain pro-apoptotic proteins Bak and Bax, which form

homo-oligomers and translocate into and permeabilize the mitochondrial outer membrane, releasing cytochrome C to activate the caspase cascade [59].

Apoptosis of M1-D macrophages induced by TMEV infection at high moi occurs toward the end of the viral growth kinetics (one-step) 10 to 12 h pi and is associated with a dramatic decline in infectious virus titers from ~200 pfu/cell to ~1 pfu/cell by 24 h pi [58, 128]. No appreciable change in viral RNA replication, polyprotein processing and expression of the final gene products that takes place between 1 and 10 h pi has been observed in M1-D macrophages undergoing apoptosis compared to a productive TMEV infection in BHK-21 cells leading to necroptosis [146].

In the present study using temporal analyses of capsid protein expression, capsid assembly and virion formation and TMEV infection in BHK-21 cells for comparison, we observed no alteration in the assembly of protomers and pentamers in M1-D cells. However, we found that mature 160S virions formed at 10 to 12 h pi contained incompletely cleaved VP0 (to VP4 and VP2) and a faster migrating virion species or aggregates that contained in addition to the capsid proteins, minor amounts of novel capsid fragments of 21- and 17-kDa in immunoblots with polyclonal rabbit antisera to BeAn virus. The faster migrating virion peak although first detected at 12 h pi, predominated at later times pi and had ~100-fold greater particle to pfu ratios than in the 160S virion peak at 12 h pi, indicating that these

virions were defective. BeAn virions incubated with recombinant caspase 3 *in vitro* revealed the novel capsid fragments as well as loss of VP4.

7.2 Results

7.2.1 Apoptosis resulted in the appearance of small amounts of two novel capsid fragments.

Analysis of BeAn virus-infected M1-D cells at high moi which undergo apoptosis with restricted viral yields [58] revealed that viral RNA replication, viral protein synthesis and polyprotein processing into the final protein products were similar to infection in BHK-21 cells which undergo necroptosis with high viral yields [146] (data not shown). Although SDS-PAGE analysis of [35S]met-radiolabeled BeAn virus proteins in infected M1-D cells did not show lower MW capsid fragments, immunoblots developed with polyclonal rabbit antiserum revealed 21- and 17-kD bands that were prominent pi in M1-D cells (Fig. 2A) but were not observed in BHK-21 cells (repeated 3 times; Fig. 2B). VP3 recognized by this antibody was faint compared to the VP0, VP1 and VP2 bands. The fact that these novel capsid fragments were principally seen on over-exposure of the immunoblots indicates that they were present in diminishing small amounts. The 21 kDa band was present in mock-infected cells but increased pi, possibly indicating it may be an artifact, whereas the 17-kDa band appeared de novo at ~8 h pi. Moreover, algorithms predicting cleavage sites within proteins by cysteine-dependent aspartate-directed proteases, i.e. caspases 3/7 indicate that there are two cleavage sites exposed on the surface of the BeAn virion (Fig. 1B, 1C). They are

in VP2 puff A (2153) and the VP3 first corner (3077), producing VP2 N-terminal and VP3 C-terminal 17-kDa species. Additional caspase cleavage sites are present internally in the three major capsid proteins (data not shown).

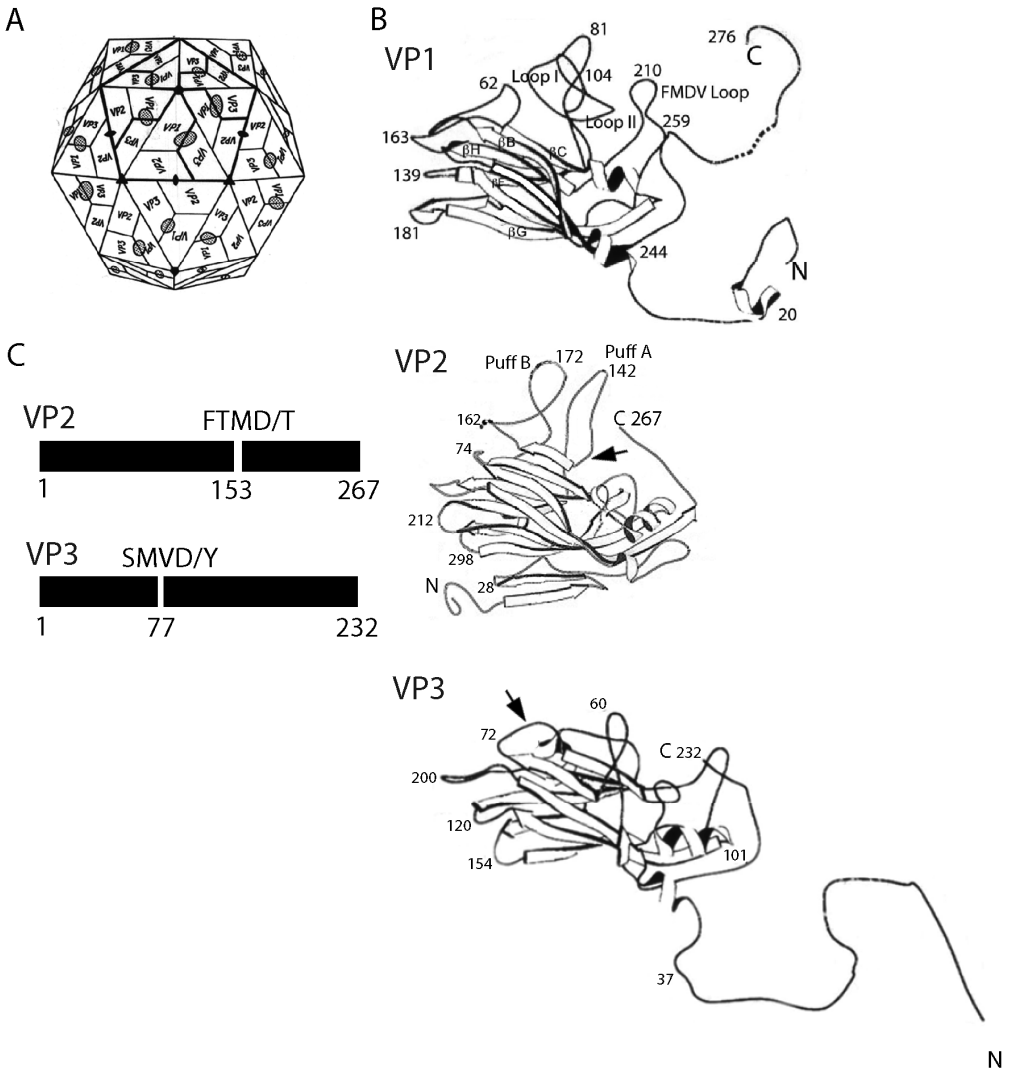

Figure 1. Icosahedral symmetry of picornavirion (top left) showing a pentamer (outlined in heavier lines) surrounding the five-fold axis, asymmetric protomers

formed by VP1, VP2 and VP3 shown as a triangular face within the protomer, and the receptor binding site, depicted as hatched ovals at the interface of VP1 and VP3. B) Ribbon drawings of the major capsid proteins VP1, VP2 and VP3 with the arrows showing exposed caspase cleavage sites predicted in VP2 and VP3 from SVM (www.casbase.org) [170]. C) Predicated caspase cleavage products of VP2 and VP3, showing that cleavage of both capsid proteins produces 17-kDa fragments.

7.2.2 Active recombinant caspase-3 cleaved BeAn capsid protein(s) to yield a 17-kDa product.

Since the 21- and 17-kD capsid species may have arisen from caspase cleavage of one or more of the capsid proteins, purified BeAn virions were incubated with active recombinant caspase-3 and immunoblots of SDS-PAGE gels were analyzed. Effector caspase-3 was chosen because the major impact on virus titers occurs after 12 h pi [58]. As shown in immunoblots that were overexposed (Fig. 2B, 2C; not present in Fig. 2A from shorter immunoblot exposure), a 21-kDa band was not detected, whereas a faint 17-kDa band was seen after 1 and 5 h of incubation at 37^{o}C with 5U of active recombinant caspase-3. However, after 5 h of incubation with 5 and 10U of enzyme, the band's intensity was faint, but was clearly observed with incubation of 20U of enzyme. Possibly this result is due to degradation of the 21-kDa band from longer incubation. In addition, the amount of VP4 decreased with 1 h of incubation and was virtually lost from virions with 5 h of incubation (Fig. 2C). These results support the restricted yields of BeAn virus in

M1-D cells being due to partial cleavage of one or more capsid protein(s) by caspases during apoptosis without substantail degradation of the major capsid proteins.

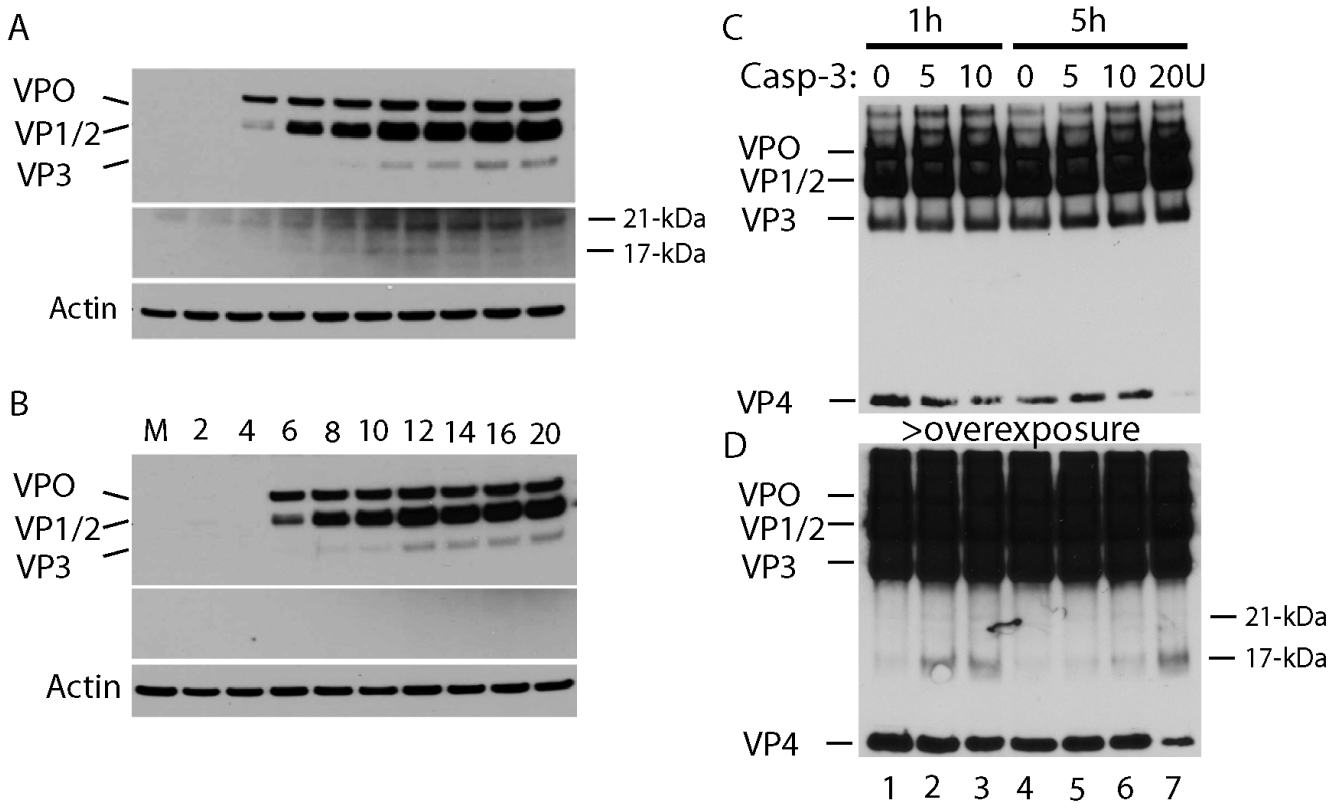

Figure 2. Novel capsid protein fragments in infected M1-D cells and with incubation of active recombinant caspase-3 with virions were observed in SDS-PAGE gels. A, B) Immunoblots developed with polyclonal rabbit antiserum revealed 21- and 17-kD bands in M1-D cells (A) but not in BHK-21 cells (B); note that the 21-kDa band was seen in mock-infected cells. VP3 recognized by this antibody was faint compared to the VP0, VP1 and VP2 bands. C, D) BeAn virions were incubated with active recombinant caspase-3 and SDS-PAGE gels were immunoblotted. In only the overexposured immunoblot (D) was a faint 17-kDa

band seen after incubation for 1 and 5 h with active recombinant caspase-3, but the 21-kDa band was not detected. Note that the VP4 band decreased in intensity with 1 h of incubation and was virtually lost from virions with 5 h of incubation.

7.2.3 Apoptosis did not alter protomer and pentamer assembly intermediates.

To determine whether apoptosis had an impact on assembly of protomers and pentamers, infected BHK-21 or M1-D cells were labeled with ^{35}[S]met, centrifuged in 5 to 20% sucrose gradients, and the gradients fractionated and compared. Both protomer (5S) and pentamer (14S) peaks were found to be identical when ^{35}[S]met-labeled virus from cells undergoing different types of cell death was centrifuged in parallel gradients (Fig. 3A, representative of 3 experiments) or radiolabeled with ^{35}[S]met and ^{3}[H]leu, and centrifuged in the same gradient (Fig. 3B, representative of 3 experiments). SDS-PAGE of gradient fractions revealed the presence of the 1ABC capsid precursor in protomers along with the major capsid proteins, including VP0 while pentamer fractions contained only the major capsid proteins, including VP0 (Fig. 3C). Thus, any minor perturbation of capsid proteins from infection of M1-D cells observed by immunoblotting did not affect protomer and pentamer assembly.

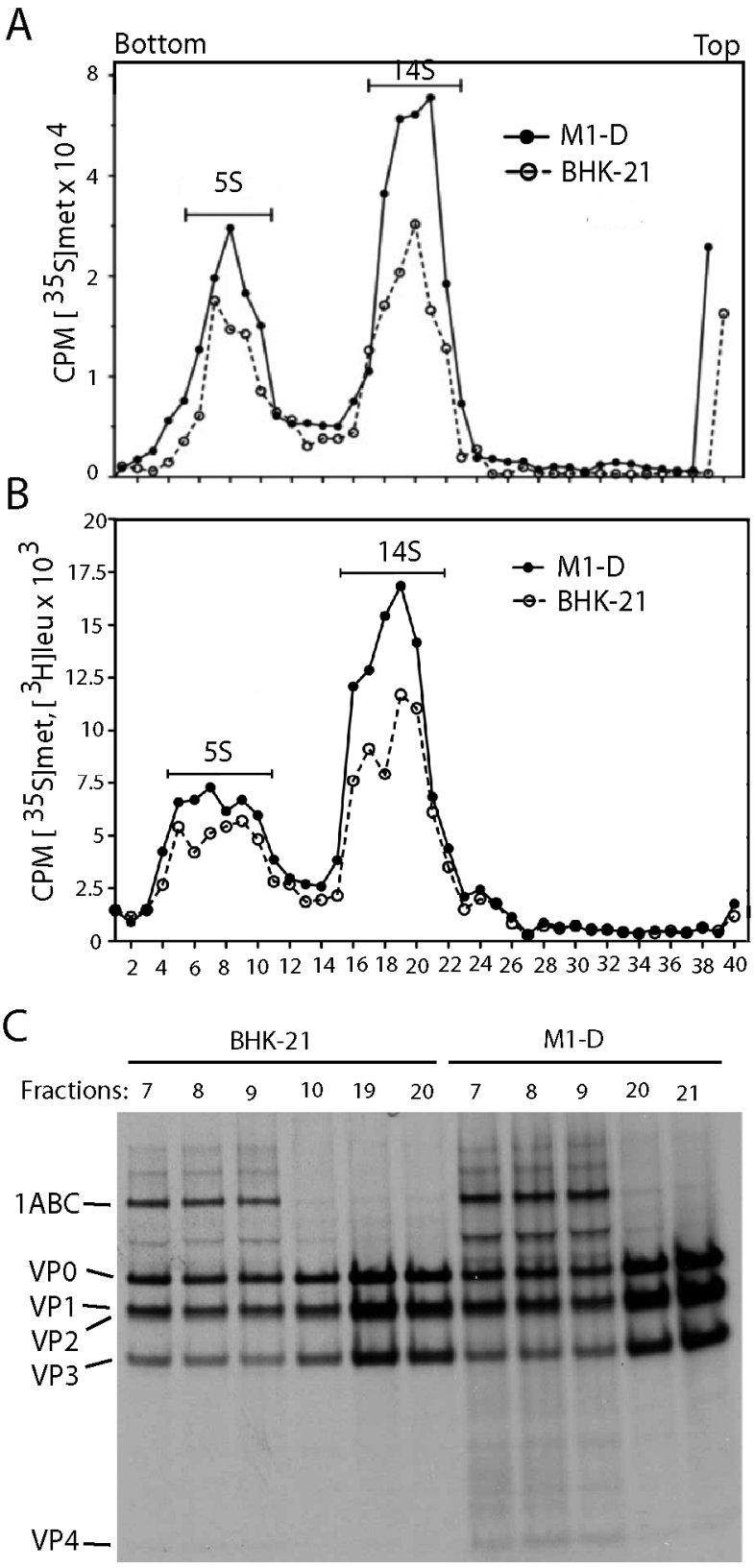
A
Bottom
Top
14S
5S
M1-D
BHK-21
CPM [35S]met x 10 4
B
14S
5S
M1-D
BHK-21
CPM [35S]met, [3H]leu x 10 3
C
BHK-21
M1-D
Fractions: 7 8 9 10 19 20 7 8 9 20 21
1ABC
VP0
VP1
VP2
VP3
VP4

Figure 3. BeAn virus-infected M1-D cells (MOI=10) which induces apoptosis did not reveal alteration in virus assembly intermediates by comparison with infected BHK-12 cells which undergo necroptosis. Infected cells were radiolabeled with [^{35}S]methionine or [^{3}H]leucine from 4.5 to 5.5h pi, lysates were centrifuged on 5 to 20% gradients, fractions immunoprecipitated with rabbit polyclonal anti-BeAn antibodies, and aliquots counted in a scintillation counter. A) 5S protomer (fractions 5 to 10) and 14S pentamer (fractions 16 to 22) peaks were identical in infected BHK-21 and M1-D cell monolayers radiolabeled with [^{35}S]methionine and centrifuged in separate gradients. B) Similarly, 5S protomer and 14S pentamer peaks were identical when the cells from infected BHK-21 and M1-D cells were radiolabeled with [^{35}S]methionine and [^{3}H]leucine, respectively, and fractionated in the same gradient. C) SDS-PAGE analysis showed similar protein species in virus from BHK-21 and M1-D cells; the 1ABC capsid precursor was observed only in protomers while the capsid proteins, VP0, VP1 and VP3, were present in protomers and pentamers. VP0 is largely uncleaved in assembly intermediates; however, minor amounts VP2 and VP4 were seen; note that VP1 and VP2 almost comigrate in 12% polyacrylamide gels.

7.2.4 Apoptotic cell death in infected M1-D cells results in a faster migrating virion peak in sucrose gradients.

Since viral assembly intermediates in infected M1-D cells were not affected by apoptosis, the formation of mature virions was analyzed. Examination of ^{35}[S]met-

labeled BeAn virus from infected BHK-21 cells harvested at 12 and 24 h pi and centrifuged through 20 to 70% sucrose gradients revealed 160S particles in fractions 25 to 29 of the gradient (Fig. 4A, representative of 5 experiments). SDS-PAGE of peak virion fractions showed the expected mature capsid proteins (Fig. 4B, representative of 3 experiments). In contrast, analysis of ^{35}[S]met-labeled BeAn virons produced in M1-D cells revealed an identical 160S mature virion peak in fractions 25 to 30 at 10, 11, 12 and 16 h pi that decreased over time pi and a second faster migrating peak in fractions 41 to 44 beginning at 11 h pi and increasing in prominence at 12, 16 and 24 h pi. The ratio between the two distinct peaks changed during infection, with equivalent peaks observed at 16 h and with only the faster sedimenting peak seen at 24 h pi (Fig. 4C, representative of 3 experiments). In addition, SDS-PAGE analysis revealed a different capsid protein profile with a prominent VP0 band and less VP2 and VP4 cleavage products in M1-D compared to BHK-21 cells (Fig. 4D). The faster migrating virion peak from M1-D cells undergoing apoptosis may have caused a conformational change resulting in virion aggregation to account for the faster migrating peak.

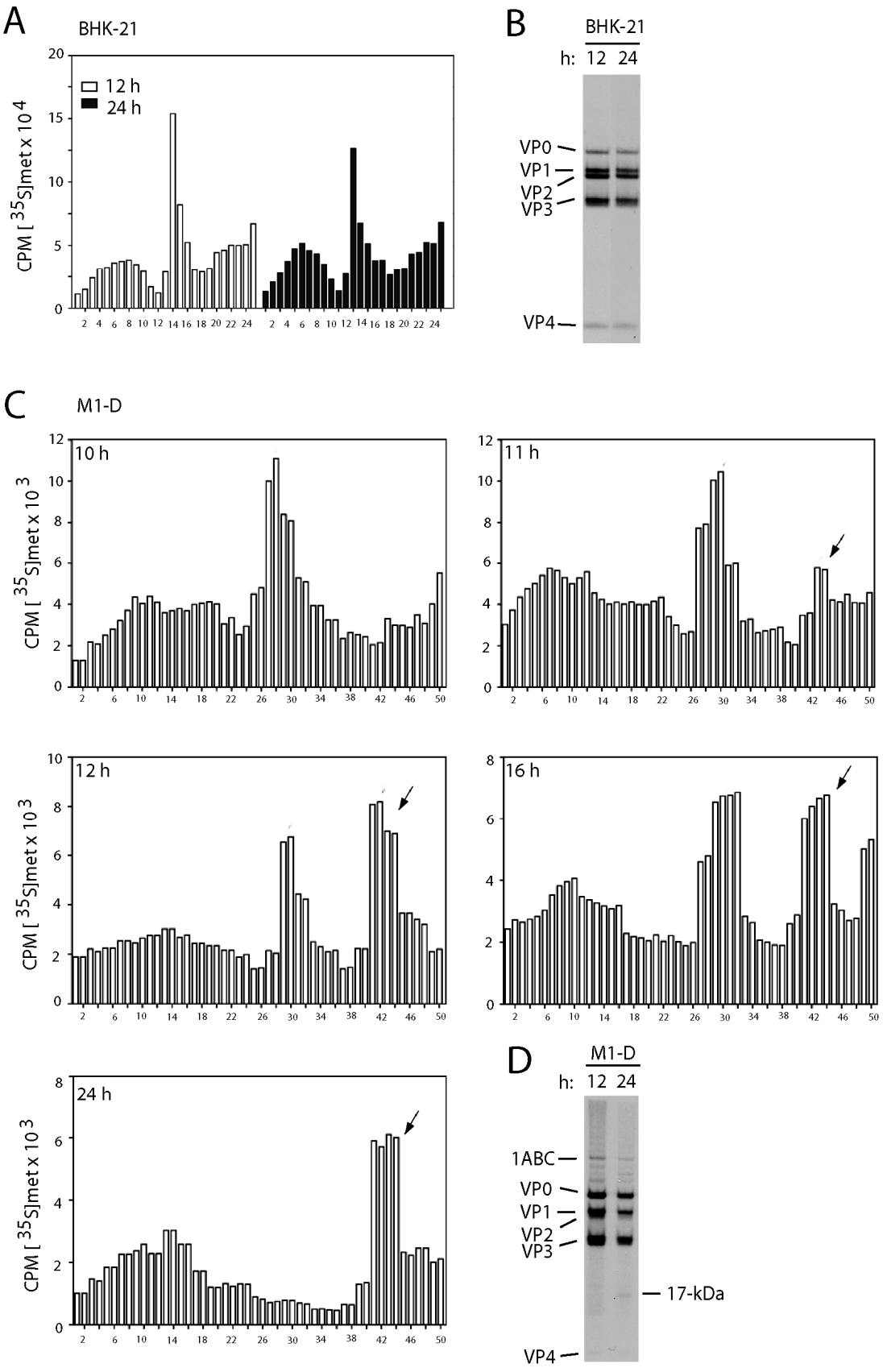
A
BHK-21
12 h
24 h
CPM [35S]met x 10 4
B
BHK-21
h: 12 24
VP0
VP1
VP2
VP3
VP4
C
M1-D
10 h
11 h
12 h
16 h
24 h
CPM [35S]met x 10 3
D
M1-D
h: 12 24
1ABC
VP0
VP1
VP2
VP3
17-kDa
VP4

Figure 4. BeAn virus infection in BHK-21 cells produced a 160S mature virion peak at 12 and 24 h pi, indicating stability of mature virions during cellular death from necroptosis, while infection in M1-D cells revealed essentially a similar migrating mature virion peak at 10-11 h pi and a faster migrating and increasingly prominent defective virion peak at ≥12 h pi, suggesting that apoptosis had perturbed already formed virions. A) Virion peaks in 20 to 70% sucrose gradients from infected BHK-21 cells were similar at 12 and 24 h pi. B) SDS-PAGE from (A) showed that virions had equimolar amounts of each of the capsid proteins. Note that VP3 consistently migrates as a "doublet." C) Virion peaks from infected M1-D cells demonstrated a gradual loss of mature virions between 12 and 24 h pi which was replaced with a faster migrating virion species. D) SDS-PAGE of virion fractions and the faster migrating virion species revealed similar capsid profile at 12 and 24 h pi; however, there was substantially more VP0.

7.2.5 Apoptosis resulted in formation of defective virus particles.

Measurement of viral infectivity from plaque assays and calculation of the number of virus particles (OD260/280) in the 160S and faster migrating virion peaks enabled the determination of particle:pfu ratios. Previously, Hertzler et al. [90] found that the particle:pfu ratio of BeAn virus grown in BHK-21 cells was 3.1×10^3. In the present study, we found that the particle:pfu ratios of the 160S virion peak from infected BHK-21 cells was ~1.5×10^3 at 12 and 24 h pi (Table 1), and the ratio from infected M1-D cells ranged from 2.5×10^3 at 10 h pi to 0.9×10^3 at 16 h pi, but fell to background levels of >1.4×10^4 observed in non-peak fractions of the

gradients (Table 2). In contrast, the faster migrating virion peak from M1-D cells, first assayed at 10 h, revealed a particle:pfu ratio of 0.27 x 10^4, or ~10-fold greater than that of the 160S peak. Moreover, the particle:pfu ratio of the faster migrating virion peak increased by ~100-fold at 24 h pi (Table 2). These results demonstrate that the 160S mature virions were converted to more defective virions, contemporaneously with the onset and progression of apoptosis in M1-D cells, suggesting that the virion structure is altered by apoptosis probably by caspase cleavage of amino acid(s) in predicted caspase cleavage sites in surface loops of VP2 and or VP3. In support of this hypothesis, knock-down of the anti-apoptotic Bcl-2 protein Mcl-1 in BHK-21 cells infected with BeAn virus increased apoptosis from 15% to 35% of total cell death and increased the particle:pfu ratio compared to infection in BHK-21 cells (5.20 x10^4) [146].

Table 1

Virus particle:pfu ratios for BeAn virion peak fractions from productive infection in BHK-21 cells

h post-infection	Gradient fractions	Particle:pfu ratio (n = 5)
12	14-16	1.46 $\pm$ 0.74 x 10^3 (n = 5)
24	13-15	1.50 $\pm$ 0.75 x 10^3

Table 2

Virus particle:pfu ratios for M1-D virion peak fractions from restricted infection in M1-D cells

h pi	Virion fractions	Particle:pfu ratio[a]	Defective virion fractions	Particle:pfu ratio[a]
0	27-30	$1.46 \pm 0.74 \times 10^3$	-	-
11	27-30	$1.50 \pm 0.75 \times 10^3$	43-44	$0.80 \pm 0.17 \times 10^5$
12	29-32	$1.20 \pm 0.32 \times 10^3$	41-44	$1.80 \pm 0.26 \times 10^5$
16	27-31	$0.90 \pm 0.11 \times 10^3$	41-44	$2.10 + 0.23 \times 10^5$
24	-	-	41-44	$2.56 + 1.60 \times 10^5$

[a](12, 24 h, n = 4; for other times, n = 3)

7.2.6 Incubation of BeAn virus with infected M1-D cell extracts or active recombinant caspase-3 increased particle:pfu ratios.

To further determine whether virions are subject to proteolysis by caspases, particularly the executioner caspasae-3 present later in the infection in M1-D cells, BeAn 160S virions were incubated with cytosolic extracts of infected M1-D cells (12 h pi) or 10U of active recombinant caspase-3 and analyzed by SDS-PAGE and immunoblotting. The units of caspase-3 were determined in preliminary experiments. Incubation of infected M1-D cytosolic extracts with purified BeAn virus from BHK-21 cells for 1 h at 37^{o}C induced an ~2-fold increase in the particle:pfu ratio ($p = 0.02$), and incubation with caspase-3 resulted in an ~7-fold increase in the particle:pfu ratio ($p = 0.001$; Table 3). Significant increases in the particle:pfu ratios in these *in vitro* experiments indicate that caspases cleave one or more of the viral capsid proteins in assembled virions, probably resulting in conformational changes in the capsid and concomitant loss of infectivity of virions (Table 3).

Table 3

Incubation of BeAn virus with infected cytosol extract or active recombinant caspase-3 increase virus particle:pfu ratios

Origin of BeAn virus[a]	Reagent added[b]	Particle:pfu ratio[c]	Significance
BHK-21 cells	buffer	$0.85 \pm 0.62 \times 10^3$	(n = 4)
BHK-21 cells	infected cytosol	$1.50 \pm 0.50 \times 10^3$	(n = 4) 0.02
BHK-21 cells	caspase-3	$5.70 \pm 0.73 \times 10^3$	(n = 4) 0.001
M1-D cells	buffer	$2.80 \pm 0.60 \times 10^3$	(n = 4)
M1-D cells	infected cytosol	$4.00 \pm 0.60 \times 10^3$	(n = 4)
M1-D cells	caspase-3	$9.00 \pm 0.52 \times 10^3$	(n = 3)

[a]BeAn virus purified from infections in either BHK-21 or M1-D
[b]Buffer for caspase; M1-D infected cytosol; active recombinant caspase-3 (Biovision)
[c](number of experiments)

7.2.7 Apoptosis results in loss of virus titers in L929 cells

Staurosporine (STS) has long been used in vitro as an initiator of apoptosis through activation of caspase-3 in many different cell types [171, 172]. It has been shown that treatment of L929 cells with STS induces intrinsic apoptosis by activation of caspase-9-like activity [172]. Induction of apoptosis by STS resulted

in a gradual decrease of cell survival, similar to one of BeAn infected cells (Fig 5A). We observed a significant increase in caspase-3 activity of BeAn infected L929 cells (MOI=10) treated with STS (Fig 5B). As expected, induction of apoptosis by varying concentration of STS resulted in a 100-fold decrease in BeAn virus titers (Fig 5C). Similar to BHK-21 cells, BeAn virus infection of L929 cells resulted in a productive infection with high virus titers. Analysis of one-step viral growth kinetics in STS treated cells demonstrated similar pattern as M1-D cells with a peak in viral growth at 8 to 12 h pi and loss of infectivity thereafter, leading to 90% reduction in infectious viral yields at 24 h pi (Fig. 6A and 6B). To determine which step of virus life cycle has been affected by apoptosis, STS (0.1 μM) were added to the infected L929 cells at different times pi. The results showed that STS induced loss of infectivity when added at 12 h pi, confirming that apoptosis affects mature virion and not early virus precursors (Fig. 6C). In conclusion, our data provide compelling evidence that apoptosis induction of infected L929 cells results in defective virus may lead to defective capsid proteins and, therefore, is deleterious to the virus.

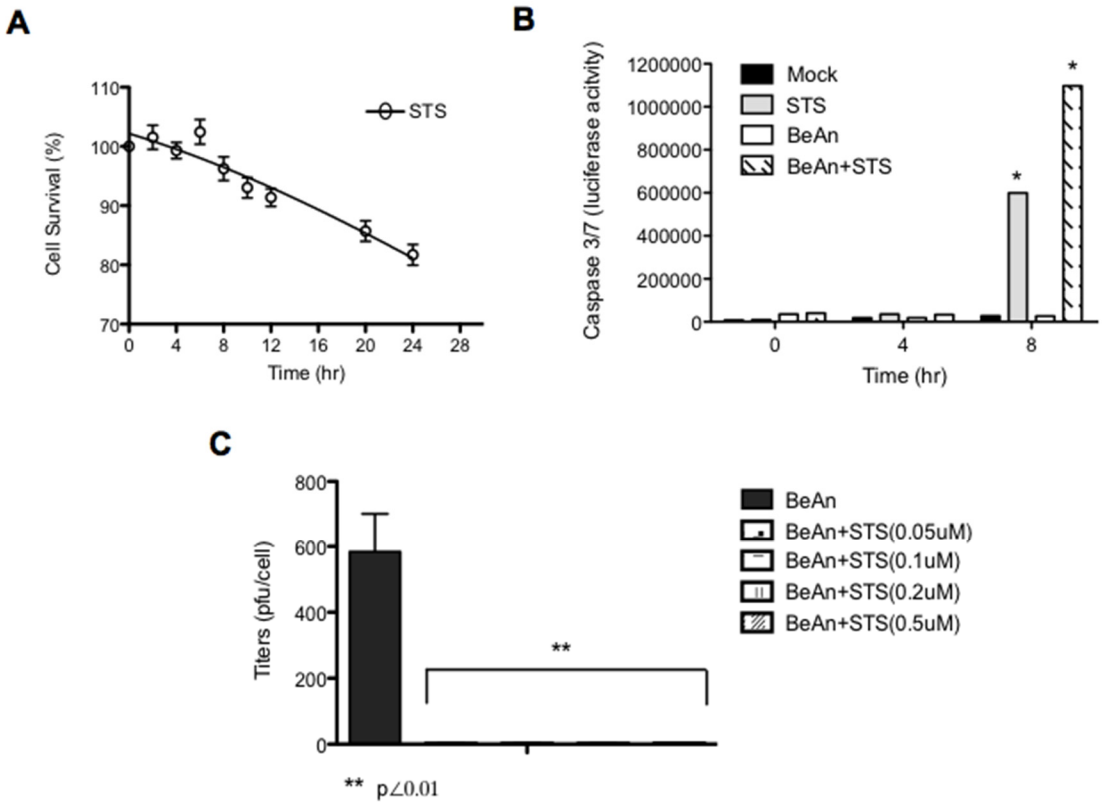

Figure 5. STS induces apoptosis of BeAn infected L929 cells A) Representative WST-1 cell survival assay revealed progressive cell death to 40 h pi. Error bars indicate the standard deviations (SD). B) L929 cells were infected with TMEV variants at various MOIs and incubated at 37°C. At 24 h pi, virus yields were determined by plaquing on BHK-21 monolayers.

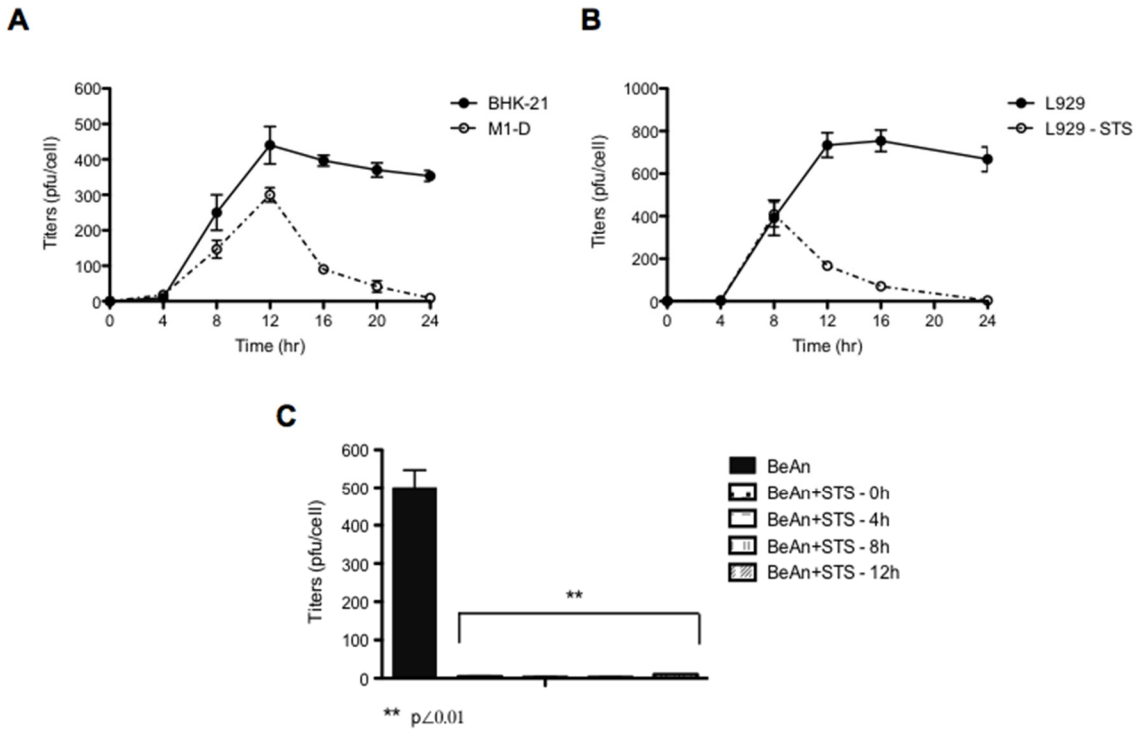

Figure 6. Apoptosis results in loss of virus titers. A) One step growth curve of BeAn in BHK-21 and M1-D cells B) One step growth curve of BeAn in L929 cells with and without STS (0.1 μM). C) L929 cells were infected with virus at an MOI of 10 and incubated at 37°C. STS at indicated concentrations were added to monolayers at various times pi, and plaquing were performed to determine the step of virus life cycle is affected by apoptosis.

7.3 Discussion

This study was designed to investigate whether apoptosis induction interrupts BeAn virus life cycle, resulting in the low virus titers. This is of importance since it has been reported that necrosis is associated the high viral yields while apoptosis results in restricted viral yields, producing only a few PFU of virus per cell [146]. We have shown that restricted BeAn virus infection in M1-D macrophages (~1

pfu/cell vs ~200 pfu/cell in a productive infection) may be due to caspase cleavage of virion surface loops of capsid proteins (VP2 and VP3), yielding a novel 17-kDa capsid fragment for both proteins. This new capsid protein species was seen in the infection in M1-D cells and was reproduced *in vitro* with active recombinant caspase-3 incubated with purified virions. This does not result in defective assembly intermediates (protomers and pentamers) but does produce a 160S mature virion peak at 10 to 12 h pi (end of one-step growth kinetics) and the appearance of a faster migrating species that predominates at $\geq$12 h pi in sucrose gradients. This faster migrating virion peak had a 100-fold increase in particle:pfu ratios, indicating that these virions were defective. In addition, these experiments were done in comparison with a productive infection in BHK-21 cells were these changes were not seen.

It is well known that caspases, key effectors of apoptosis recognize and cleave viral proteins at very characteristic motifs, resulting in either attenuation or progression of the virus [139, 173-175]. The expression of viral capsid proteins induces caspase activation, resulting in cleavage of capsid proteins and regulating persistent virus infection [139]. We discovered two putative cleavage sites exposed on the surface of the BeAn virion, VP2 puff A (2153) and VP3 first corner (3077), that corresponded with a ~17kD band generated upon in vitro incubation of BeAn virus with caspase-3. Since there were no significant differences in viral protein synthesis and processing and viral assembly intermediates between BHK-21 and M1-D macrophages, we aimed to test whether apoptosis affects the mature virion.

Viral gradient analysis of M1-D cells (24 h pi) resulted in virion peaks sedimented to the bottom of the gradient (fractions 41 to 44), generating low virus titers. Recently, Arzberger *et al.,* have shown that higher apoptotic stimulus generates noninfectious immature HBV, resulting in lower infectivity of the virus particles [174]. Other studies demonstrated that apoptotic stimulus in hepatoma cell lines releases two distinct populations of capsids sedimenting at different densities [174]. This has also been seen when mutations in the capsid proteins of picornavirus induce conformational changes to form 125S and 80S particles, resulting in loss of infectivity [176]. We found that BeAn virus infection of M1-D macrophages results in a faster sedimenting virion with low infectivity seen at 24 h pi (Fig. 4C), suggesting that apoptosis may possibly induce a structural change and generate a noninfectious virus with higher sedimentation rate. We also showed a different capsid protein profile with a prominent VP0 band and less VP2 and VP4 cleavage products in M1-D compared to BHK-21 cells (Fig. 4D). It is known that the structures of the poliovirus capsid changes at low temperature leading to the extrusion of VP4 from the capsids [177, 178]. In vitro incubation of BeAn virus with caspase-3 resulted in loss of VP4 (Fig. 2C, 2D) which may correspond to progressive conformational transitions of the capsid, causing aggregation and eventually low virus yields.

It has been demonstrated that caspase cleavages generate new viral products that act as dominant negatives of non-structural proteins (H-1PV NS1, KSHV ORF57) [179, 180] or conformational changes when structural proteins are concerned

(AMDV VP and possibly FCV capsid protein) [138, 139], resulting in the attenuation of the virus. When mutant capsid protein are expressed together with the authentic protein exertes a dominant-negative effect on the assembly of new virions, blocking the Cytomegalovirus (CMV) and poliovirus infection cycle [181, 182]. Thus, we hypothesize that caspase cleavage of one out of 60 capsid protein copies may induce a dominant-negative effect that may not be readily detectable, presumably because defective capsid proteins coassemble with functional capsid proteins and render the resulting capsid nonfunctional. Such attenuation at a cellular level might hold importance regarding the possibility for viruses to establish permissive and/or persistent infection. Our data provide compelling evidence that apoptosis induction of infected cells lead to defective capsid proteins and, therefore, is deleterious to the virus.

CHAPTER 8

8.1 REFERENCES

1. Theiler, M., *Spontaneous Encephalomyelitis of Mice--a New Virus Disease.* Science, 1934. **80**(2066): p. 122.
2. Bendiner, E., *Max Theiler: yellow jack and the jackpot.* Hosp Pract (Off Ed), 1988. **23**(6): p. 211-2, 214-5, 219-22 passim.
3. Lipton, H.L., A.S. Kumar, and M. Trottier, *Theiler's virus persistence in the central nervous system of mice is associated with continuous viral replication and a difference in outcome of infection of infiltrating macrophages versus oligodendrocytes.* Virus Res, 2005. **111**(2): p. 214-23.
4. Compston, A. and A. Coles, *Multiple sclerosis.* Lancet, 2008. **372**(9648): p. 1502-17.
5. Bedard, K.M. and B.L. Semler, *Regulation of picornavirus gene expression.* Microbes Infect, 2004. **6**(7): p. 702-13.
6. Fields BN, K.D., *Picornaviridae and Their Replication*, in *Fields Virology*. 1990, Raven Press: New York. p. 507-548.
7. van Eyll, O. and T. Michiels, *Non-AUG-initiated internal translation of the L* protein of Theiler's virus and importance of this protein for viral persistence.* J Virol, 2002. **76**(21): p. 10665-73.
8. Oleszak, E.L., et al., *Theiler's virus infection: a model for multiple sclerosis.* Clin Microbiol Rev, 2004. **17**(1): p. 174-207.

9. Lorch, Y., M. Kotler, and A. Friedmann, *Persistent and acute central nervous system infections are caused by Theiler's murine encephalomyelitis viruses which differ in RNA composition but code for only slightly different proteins.* J Virol, 1984. **52**(3): p. 960-5.

10. Lipton, H.L., *Theiler's virus infection in mice: an unusual biphasic disease process leading to demyelination.* Infect Immun, 1975. **11**(5): p. 1147-55.

11. Azoulay, A., M. Brahic, and J.F. Bureau, *FVB mice transgenic for the H-2Db gene become resistant to persistent infection by Theiler's virus.* J Virol, 1994. **68**(6): p. 4049-52.

12. Rodriguez, M. and C.S. David, *Demyelination induced by Theiler's virus: influence of the H-2 haplotype.* J Immunol, 1985. **135**(3): p. 2145-8.

13. Rodriguez, M. and C.S. David, *H-2 Dd transgene suppresses Theiler's virus-induced demyelination in susceptible strains of mice.* J Neurovirol, 1995. **1**(1): p. 111-7.

14. Borson, N.D., et al., *Brain-infiltrating cytolytic T lymphocytes specific for Theiler's virus recognize H2Db molecules complexed with a viral VP2 peptide lacking a consensus anchor residue.* J Virol, 1997. **71**(7): p. 5244-50.

15. Dethlefs, S., M. Brahic, and E.L. Larsson-Sciard, *An early, abundant cytotoxic T-lymphocyte response against Theiler's virus is critical for preventing viral persistence.* J Virol, 1997. **71**(11): p. 8875-8.

16. Rodriguez, M., J.L. Leibowitz, and P.W. Lampert, *Persistent infection of oligodendrocytes in Theiler's virus-induced encephalomyelitis.* Ann Neurol, 1983. **13**(4): p. 426-33.

17. Aubert, C., M. Chamorro, and M. Brahic, *Identification of Theiler's virus infected cells in the central nervous system of the mouse during demyelinating disease.* Microb Pathog, 1987. **3**(5): p. 319-26.

18. Dal Canto, M.C. and H.L. Lipton, *Ultrastructural immunohistochemical localization of virus in acute and chronic demyelinating Theiler's virus infection.* Am J Pathol, 1982. **106**(1): p. 20-9.

19. Clatch, R.J., et al., *Monocytes/macrophages isolated from the mouse central nervous system contain infectious Theiler's murine encephalomyelitis virus (TMEV).* Virology, 1990. **176**(1): p. 244-54.

20. Kumar, A.S., et al., *Virus persistence in an animal model of multiple sclerosis requires virion attachment to sialic acid coreceptors.* J Virol, 2004. **78**(16): p. 8860-7.

21. Brahic, M., J.F. Bureau, and T. Michiels, *The genetics of the persistent infection and demyelinating disease caused by Theiler's virus.* Annu Rev Microbiol, 2005. **59**: p. 279-98.

22. Miller, S.D., et al., *Persistent infection with Theiler's virus leads to CNS autoimmunity via epitope spreading.* Nat Med, 1997. **3**(10): p. 1133-6.

23. McMahon, E.J., et al., *Epitope spreading initiates in the CNS in two mouse models of multiple sclerosis.* Nat Med, 2005. **11**(3): p. 335-9.

24. Drescher, K.M., et al., *TGF-beta 2 reduces demyelination, virus antigen expression, and macrophage recruitment in a viral model of multiple sclerosis.* J Immunol, 2000. **164**(6): p. 3207-13.

25. Ai, X., et al., *Generation and characterization of antibodies specific for caspase-cleaved neo-epitopes: a novel approach.* Cell Death Dis, 2011. **2**: p. e205.

26. Fan, T.J., et al., *Caspase family proteases and apoptosis.* Acta Biochim Biophys Sin (Shanghai), 2005. **37**(11): p. 719-27.

27. Wickman, G., L. Julian, and M.F. Olson, *How apoptotic cells aid in the removal of their own cold dead bodies.* Cell Death Differ, 2012. **19**(5): p. 735-42.

28. Favaloro, B., et al., *Role of apoptosis in disease.* Aging (Albany NY), 2012. **4**(5): p. 330-49.

29. Saelens, X., et al., *Toxic proteins released from mitochondria in cell death.* Oncogene, 2004. **23**(16): p. 2861-74.

30. Elmore, S., *Apoptosis: a review of programmed cell death.* Toxicol Pathol, 2007. **35**(4): p. 495-516.

31. Youle, R.J. and A. Strasser, *The BCL-2 protein family: opposing activities that mediate cell death.* Nat Rev Mol Cell Biol, 2008. **9**(1): p. 47-59.

32. Degterev, A., et al., *Identification of RIP1 kinase as a specific cellular target of necrostatins.* Nat Chem Biol, 2008. **4**(5): p. 313-21.

33. Shore, G.C. and M. Nguyen, *Bcl-2 proteins and apoptosis: choose your partner.* Cell, 2008. **135**(6): p. 1004-6.

34. Ashkenazi, A. and V.M. Dixit, *Death receptors: signaling and modulation.* Science, 1998. **281**(5381): p. 1305-8.

35. Kozopas, K.M., et al., *MCL1, a gene expressed in programmed myeloid cell differentiation, has sequence similarity to BCL2.* Proc Natl Acad Sci U S A, 1993. **90**(8): p. 3516-20.

36. Liu, H., et al., *Constitutively activated Akt-1 is vital for the survival of human monocyte-differentiated macrophages. Role of Mcl-1, independent of nuclear factor (NF)-kappaB, Bad, or caspase activation.* J Exp Med, 2001. **194**(2): p. 113-26.

37. Zhou, P., et al., *Mcl-1, a Bcl-2 family member, delays the death of hematopoietic cells under a variety of apoptosis-inducing conditions.* Blood, 1997. **89**(2): p. 630-43.

38. Chao, J.R., et al., *mcl-1 is an immediate-early gene activated by the granulocyte-macrophage colony-stimulating factor (GM-CSF) signaling pathway and is one component of the GM-CSF viability response.* Mol Cell Biol, 1998. **18**(8): p. 4883-98.

39. Degterev, A. and J. Yuan, *Expansion and evolution of cell death programmes.* Nat Rev Mol Cell Biol, 2008. **9**(5): p. 378-90.

40. van Eyll, O. and T. Michiels, *Influence of the Theiler's virus L* protein on macrophage infection, viral persistence, and neurovirulence.* J Virol, 2000. **74**(19): p. 9071-7.

41. Marsden, V.S. and A. Strasser, *Control of apoptosis in the immune system: Bcl-2, BH3-only proteins and more.* Annu Rev Immunol, 2003. **21**: p. 71-105.

42. Villunger, A., et al., *p53- and drug-induced apoptotic responses mediated by BH3-only proteins puma and noxa.* Science, 2003. **302**(5647): p. 1036-8.

43. Noteborn, M.H., et al., *A single chicken anemia virus protein induces apoptosis.* J Virol, 1994. **68**(1): p. 346-51.

44. Sadzot-Delvaux, C., et al., *Varicella-zoster virus induces apoptosis in cell culture.* J Gen Virol, 1995. **76 (Pt 11)**: p. 2875-9.

45. Laurent-Crawford, A.G., et al., *The cytopathic effect of HIV is associated with apoptosis.* Virology, 1991. **185**(2): p. 829-39.

46. Levine, B., et al., *Conversion of lytic to persistent alphavirus infection by the bcl-2 cellular oncogene.* Nature, 1993. **361**(6414): p. 739-42.

47. Ubol, S., et al., *Neurovirulent strains of Alphavirus induce apoptosis in bcl-2-expressing cells: role of a single amino acid change in the E2 glycoprotein.* Proc Natl Acad Sci U S A, 1994. **91**(11): p. 5202-6.

48. Hinshaw, V.S., et al., *Apoptosis: a mechanism of cell killing by influenza A and B viruses.* J Virol, 1994. **68**(6): p. 3667-73.

49. Tyler, K.L., et al., *Differences in the capacity of reovirus strains to induce apoptosis are determined by the viral attachment protein sigma 1.* J Virol, 1995. **69**(11): p. 6972-9.

50. Rao, L., et al., *The adenovirus E1A proteins induce apoptosis, which is inhibited by the E1B 19-kDa and Bcl-2 proteins.* Proc Natl Acad Sci U S A, 1992. **89**(16): p. 7742-6.

51. Ink, B.S., C.S. Gilbert, and G.I. Evan, *Delay of vaccinia virus-induced apoptosis in nonpermissive Chinese hamster ovary cells by the cowpox virus CHOhr and adenovirus E1B 19K genes.* J Virol, 1995. **69**(2): p. 661-8.

52. Gregory, C.D., et al., *Activation of Epstein-Barr virus latent genes protects human B cells from death by apoptosis.* Nature, 1991. **349**(6310): p. 612-4.

53. Clem, R.J. and L.K. Miller, *Apoptosis reduces both the in vitro replication and the in vivo infectivity of a baculovirus.* J Virol, 1993. **67**(7): p. 3730-8.

54. Neilan, J.G., et al., *An African swine fever virus gene with similarity to the proto-oncogene bcl-2 and the Epstein-Barr virus gene BHRF1.* J Virol, 1993. **67**(7): p. 4391-4.

55. Agol, V.I., et al., *Competing death programs in poliovirus-infected cells: commitment switch in the middle of the infectious cycle.* J Virol, 2000. **74**(12): p. 5534-41.

56. Jelachich, M.L. and H.L. Lipton, *Theiler's murine encephalomyelitis virus kills restrictive but not permissive cells by apoptosis.* J Virol, 1996. **70**(10): p. 6856-61.

57. Jelachich, M.L. and H.L. Lipton, *Restricted Theiler's murine encephalomyelitis virus infection in murine macrophages induces apoptosis.* J Gen Virol, 1999. **80 (Pt 7)**: p. 1701-5.

58. Son, K.N., et al., *Theiler's virus-induced intrinsic apoptosis in M1-D macrophages is Bax mediated and restricts virus infectivity: a mechanism for persistence of a cytolytic virus.* J Virol, 2008. **82**(9): p. 4502-10.

59. Son, K.N., S. Pugazhenthi, and H.L. Lipton, *Activation of tumor suppressor protein p53 is required for Theiler's murine encephalomyelitis virus-induced apoptosis in M1-D macrophages.* J Virol, 2009. **83**(20): p. 10770-7.

60. Hengartner, M.O., *The biochemistry of apoptosis.* Nature, 2000. **407**(6805): p. 770-6.

61. Huang, D.C. and A. Strasser, *BH3-Only proteins-essential initiators of apoptotic cell death.* Cell, 2000. **103**(6): p. 839-42.

62. Festjens, N., T. Vanden Berghe, and P. Vandenabeele, *Necrosis, a well-orchestrated form of cell demise: signalling cascades, important mediators and concomitant immune response.* Biochim Biophys Acta, 2006. **1757**(9-10): p. 1371-87.

63. Meylan, E. and J. Tschopp, *The RIP kinases: crucial integrators of cellular stress.* Trends Biochem Sci, 2005. **30**(3): p. 151-9.

64. Festjens, N., et al., *RIP1, a kinase on the crossroads of a cell's decision to live or die.* Cell death and differentiation, 2007. **14**(3): p. 400-10.

65. Cho, Y.S., et al., *Phosphorylation-driven assembly of the RIP1-RIP3 complex regulates programmed necrosis and virus-induced inflammation.* Cell, 2009. **137**(6): p. 1112-23.

66. He, S., et al., *Receptor interacting protein kinase-3 determines cellular necrotic response to TNF-alpha.* Cell, 2009. **137**(6): p. 1100-11.

67. Zhang, D.W., et al., *RIP3, an energy metabolism regulator that switches TNF-induced cell death from apoptosis to necrosis.* Science, 2009. **325**(5938): p. 332-6.

68. Holler, N., et al., *Fas triggers an alternative, caspase-8-independent cell death pathway using the kinase RIP as effector molecule.* Nat Immunol, 2000. **1**(6): p. 489-95.

69. Sun, X., et al., *Identification of a novel homotypic interaction motif required for the phosphorylation of receptor-interacting protein (RIP) by RIP3.* J Biol Chem, 2002. **277**(11): p. 9505-11.

70. Kaiser, W.J., J.W. Upton, and E.S. Mocarski, *Receptor-interacting protein homotypic interaction motif-dependent control of NF-kappa B activation via the DNA-dependent activator of IFN regulatory factors.* J Immunol, 2008. **181**(9): p. 6427-34.

71. Rebsamen, M., et al., *DAI/ZBP1 recruits RIP1 and RIP3 through RIP homotypic interaction motifs to activate NF-kappaB.* EMBO Rep, 2009. **10**(8): p. 916-22.

72. Kelliher, M.A., et al., *The death domain kinase RIP mediates the TNF-induced NF-kappaB signal.* Immunity, 1998. **8**(3): p. 297-303.

73. Newton, K., X. Sun, and V.M. Dixit, *Kinase RIP3 is dispensable for normal NF-kappa Bs, signaling by the B-cell and T-cell receptors, tumor necrosis factor receptor 1, and Toll-like receptors 2 and 4.* Mol Cell Biol, 2004. **24**(4): p. 1464-9.

74. Chu, J.J. and M.L. Ng, *The mechanism of cell death during West Nile virus infection is dependent on initial infectious dose.* J Gen Virol, 2003. **84**(Pt 12): p. 3305-14.

75. Lenardo, M.J., et al., *Cytopathic killing of peripheral blood CD4(+) T lymphocytes by human immunodeficiency virus type 1 appears necrotic rather than apoptotic and does not require env.* J Virol, 2002. **76**(10): p. 5082-93.

76. Petit, F., et al., *Productive HIV-1 infection of primary CD4+ T cells induces mitochondrial membrane permeabilization leading to a caspase-independent cell death.* J Biol Chem, 2002. **277**(2): p. 1477-87.

77. Upton, J.W., W.J. Kaiser, and E.S. Mocarski, *Virus inhibition of RIP3-dependent necrosis.* Cell Host Microbe, 2010. **7**(4): p. 302-13.

78. Peri, P., et al., *Cathepsins are involved in virus-induced cell death in ICP4 and Us3 deletion mutant herpes simplex virus type 1-infected monocytic cells.* J Gen Virol, 2011. **92**(Pt 1): p. 173-80.

79. Bolton, D.L., et al., *Death of CD4(+) T-cell lines caused by human immunodeficiency virus type 1 does not depend on caspases or apoptosis.* J Virol, 2002. **76**(10): p. 5094-107.

80. Arjona, A., et al., *West Nile virus envelope protein inhibits dsRNA-induced innate immune responses.* J Immunol, 2007. **179**(12): p. 8403-9.

81. Chan, F.K., et al., *A role for tumor necrosis factor receptor-2 and receptor-interacting protein in programmed necrosis and antiviral responses.* J Biol Chem, 2003. **278**(51): p. 51613-21.

82. Li, M. and A.A. Beg, *Induction of necrotic-like cell death by tumor necrosis factor alpha and caspase inhibitors: novel mechanism for killing virus-infected cells.* J Virol, 2000. **74**(16): p. 7470-7.

83. Wu, W., P. Liu, and J. Li, *Necroptosis: an emerging form of programmed cell death.* Crit Rev Oncol Hematol, 2012. **82**(3): p. 249-58.

84. Rozhon, E.J., J.D. Kratochvil, and H.L. Lipton, *Analysis of genetic variation in Theiler's virus during persistent infection in the mouse central nervous system.* Virology, 1983. **128**(1): p. 16-32.

85. Reed, L.J.M., H. , *A simple method of estimating fifty per cent endpoints. .* Am J Hyg 1938. **27**: p. 493–497.

86. Qi, D. and K.B. Scholthof, *A one-step PCR-based method for rapid and efficient site-directed fragment deletion, insertion, and substitution mutagenesis.* J Virol Methods, 2008. **149**(1): p. 85-90.

87. Kumar, A.S., et al., *Amino acid substitutions in VP2 residues contacting sialic acid in low-neurovirulence BeAn virus dramatically reduce viral binding and spread of infection.* J Virol, 2003. **77**(4): p. 2709-16.

88. Kumar, A.S., et al., *Amino acid substitutions of low neurovirulence VP2 residues contacting sialic acid dramatically reduce viral binding and spread.* Journal of Virology, 2003. **77**: p. 2709-2716.

89. Higuchi, R., B. Krummel, and R.K. Saiki, *A general method of in vitro preparation and specific mutagenesis of DNA fragments: study of protein and DNA interactions.* Nucleic Acids Res, 1988. **16**(15): p. 7351-67.

90. Hertzler, S., M. Luo, and H.L. Lipton, *Mutation of predicted virion pit residues alters binding of Theiler's murine encephalomyelitis virus to BHK-21 cells.* J Virol, 2000. **74**(4): p. 1994-2004.

91. Schlitt, B.P., et al., *Apoptotic cells, including macrophages, are prominent in Theiler's virus-induced inflammatory, demyelinating lesions.* J Virol, 2003. **77**(7): p. 4383-8.

92. Jelachich, M.L. and H.L. Lipton, *Theiler's murine encephalomyelitis virus induces apoptosis in gamma interferon-activated M1 differentiated myelomonocytic cells through a mechanism involving tumor necrosis factor alpha (TNF-alpha) and TNF-alpha-related apoptosis-inducing ligand.* J Virol, 2001. **75**(13): p. 5930-8.

93. Obuchi, M., et al., *Theiler's murine encephalomyelitis virus subgroup strain-specific infection in a murine macrophage-like cell line.* J Virol, 1997. **71**(1): p. 729-33.

94. Jelachich, M.L., et al., *Theiler's virus growth in murine macrophage cell lines depends on the state of differentiation.* Virology, 1995. **209**(2): p. 437-44.

95. Henke, A., et al., *Apoptosis in coxsackievirus B3-caused diseases: interaction between the capsid protein VP2 and the proapoptotic protein siva.* J Virol, 2000. **74**(9): p. 4284-90.

96. Henke, A., et al., *The apoptotic capability of coxsackievirus B3 is influenced by the efficient interaction between the capsid protein VP2 and the proapoptotic host protein Siva.* Virology, 2001. **289**(1): p. 15-22.

97. Liu, J., T. Wei, and J. Kwang, *Avian encephalomyelitis virus induces apoptosis via major structural protein VP3.* Virology, 2002. **300**(1): p. 39-49.

98. Liu, J., T. Wei, and J. Kwang, *Avian encephalomyelitis virus nonstructural protein 2C induces apoptosis by activating cytochrome c/caspase-9 pathway.* Virology, 2004. **318**(1): p. 169-82.

99. Kuo, R.L., et al., *Infection with enterovirus 71 or expression of its 2A protease induces apoptotic cell death.* J Gen Virol, 2002. **83**(Pt 6): p. 1367-76.

100. Goldstaub, D., et al., *Poliovirus 2A protease induces apoptotic cell death.* Mol Cell Biol, 2000. **20**(4): p. 1271-7.

101. Barco, A., E. Feduchi, and L. Carrasco, *Poliovirus protease 3C(pro) kills cells by apoptosis.* Virology, 2000. **266**(2): p. 352-60.

102. Lawson, T.G., et al., *Identification and characterization of a protein destruction signal in the encephalomyocarditis virus 3C protease.* J Biol Chem, 1999. **274**(14): p. 9871-80.

103. Lawson, T.G., et al., *The encephalomyocarditis virus 3C protease is a substrate for the ubiquitin-mediated proteolytic system.* J Biol Chem, 1994. **269**(45): p. 28429-35.

104. Schlax, P.E., et al., *Degradation of the encephalomyocarditis virus and hepatitis A virus 3C proteases by the ubiquitin/26S proteasome system in vivo.* Virology, 2007. **360**(2): p. 350-63.

105. Wojcik, C., *Regulation of apoptosis by the ubiquitin and proteasome pathway.* J Cell Mol Med, 2002. **6**(1): p. 25-48.

106. Zoll, J., et al., *The mengovirus leader protein suppresses alpha/beta interferon production by inhibition of the iron/ferritin-mediated activation of NF-kappa B.* J Virol, 2002. **76**(19): p. 9664-72.

107. van Pesch, V., O. van Eyll, and T. Michiels, *The leader protein of Theiler's virus inhibits immediate-early alpha/beta interferon production.* J Virol, 2001. **75**(17): p. 7811-7.

108. Hato, S.V., et al., *The mengovirus leader protein blocks interferon-alpha/beta gene transcription and inhibits activation of interferon regulatory factor 3.* Cell Microbiol, 2007. **9**(12): p. 2921-30.

109. Lidsky, P.V., et al., *Nucleocytoplasmic traffic disorder induced by cardioviruses.* J Virol, 2006. **80**(6): p. 2705-17.

110. Delhaye, S., V. van Pesch, and T. Michiels, *The leader protein of Theiler's virus interferes with nucleocytoplasmic trafficking of cellular proteins.* J Virol, 2004. **78**(8): p. 4357-62.

111. Himeda, T., et al., *A lentiviral expression system demonstrates that L* protein of Theiler's murine encephalomyelitis virus (TMEV) has an anti-apoptotic effect in a macrophage cell line.* Microb Pathog, 2005. **38**(5-6): p. 201-7.

112. Ghadge, G.D., et al., *A protein critical for a Theiler's virus-induced immune system-mediated demyelinating disease has a cell type-specific antiapoptotic effect and a key role in virus persistence.* J Virol, 1998. **72**(11): p. 8605-12.

113. Dvorak, C.M., et al., *Leader protein of encephalomyocarditis virus binds zinc, is phosphorylated during viral infection, and affects the efficiency of genome translation.* Virology, 2001. **290**(2): p. 261-71.

114. Porter, F.W., et al., *A picornavirus protein interacts with Ran-GTPase and disrupts nucleocytoplasmic transport.* Proc Natl Acad Sci U S A, 2006. **103**(33): p. 12417-22.

115. Porter, F.W. and A.C. Palmenberg, *Leader-induced phosphorylation of nucleoporins correlates with nuclear trafficking inhibition by cardioviruses.* J Virol, 2009. **83**(4): p. 1941-51.

116. Ricour, C., et al., *Inhibition of mRNA export and dimerization of interferon regulatory factor 3 by Theiler's virus leader protein.* J Gen Virol, 2009. **90**(Pt 1): p. 177-86.

117. Das, S. and A. Dasgupta, *Identification of the cleavage site and determinants required for poliovirus 3CPro-catalyzed cleavage of human TATA-binding transcription factor TBP.* J Virol, 1993. **67**(6): p. 3326-31.

118. Shen, Y., et al., *DNA binding domain and subunit interactions of transcription factor IIIC revealed by dissection with poliovirus 3C protease.* Mol Cell Biol, 1996. **16**(8): p. 4163-71.

119. Yalamanchili, P., U. Datta, and A. Dasgupta, *Inhibition of host cell transcription by poliovirus: cleavage of transcription factor CREB by poliovirus-encoded protease 3Cpro.* J Virol, 1997. **71**(2): p. 1220-6.

120. Yalamanchili, P., et al., *Inhibition of basal transcription by poliovirus: a virus- encoded protease (3Cpro) inhibits formation of TBP-TATA box complex in vitro.* J Virol, 1996. **70**(5): p. 2922-9.

121. Yalamanchili, P., K. Weidman, and A. Dasgupta, *Cleavage of transcriptional activator Oct-1 by poliovirus encoded protease 3Cpro.* Virology, 1997. **239**(1): p. 176-85.

122. Aminev, A.G., S.P. Amineva, and A.C. Palmenberg, *Encephalomyocarditis virus (EMCV) proteins 2A and 3BCD localize to nuclei and inhibit cellular mRNA transcription but not rRNA transcription.* Virus Res, 2003. **95**(1-2): p. 59-73.

123. Amineva, S.P., et al., *Rhinovirus 3C protease precursors 3CD and 3CD' localize to the nuclei of infected cells.* J Gen Virol, 2004. **85**(Pt 10): p. 2969-79.

124. Sharma, R., S. Raychaudhuri, and A. Dasgupta, *Nuclear entry of poliovirus protease-polymerase precursor 3CD: implications for host cell transcription shut-off.* Virology, 2004. **320**(2): p. 195-205.

125. Buchholz, U.J., S. Finke, and K.K. Conzelmann, *Generation of bovine respiratory syncytial virus (BRSV) from cDNA: BRSV NS2 is not essential for virus replication in tissue culture, and the human RSV leader region acts as a functional BRSV genome promoter.* J Virol, 1999. **73**(1): p. 251-9.

126. Friedmann, A. and H.L. Lipton, *Replication of Theiler's murine encephalomyelitis viruses in BHK21 cells: an electron microscopic study.* Virology, 1980. **101**(2): p. 389-98.

127. Romanova, L.I., et al., *Variability in apoptotic response to poliovirus infection.* Virology, 2005. **331**(2): p. 292-306.

128. Jelachich, M.L., C. Bramlage, and H.L. Lipton, *Differentiation of M1 myeloid precursor cells into macrophages results in binding and infection by Theiler's murine encephalomyelitis virus and apoptosis.* J Virol, 1999. **73**(4): p. 3227-35.

129. Akgul, C., *Mcl-1 is a potential therapeutic target in multiple types of cancer.* Cell Mol Life Sci, 2009. **66**(8): p. 1326-36.

130. Haupt, S., et al., *Apoptosis - the p53 network.* J Cell Sci, 2003. **116**(Pt 20): p. 4077-85.

131. Fischer, S.F., G.T. Belz, and A. Strasser, *BH3-only protein Puma contributes to death of antigen-specific T cells during shutdown of an immune response to acute viral infection.* Proc Natl Acad Sci U S A, 2008. **105**(8): p. 3035-40.

132. Blakemore, W.F., et al., *Observations on demyelinating lesions induced by Theiler's virus in CBA mice.* Acta Neuropathol, 1988. **76**(6): p. 581-9.

133. Trottier, M., et al., *High numbers of viral RNA copies in the central nervous system of mice during persistent infection with Theiler's virus.* J Virol, 2001. **75**(16): p. 7420-8.

134. Carthy, C.M., et al., *Caspase activation and specific cleavage of substrates after coxsackievirus B3-induced cytopathic effect in HeLa cells.* J Virol, 1998. **72**(9): p. 7669-75.

135. Shih, S.R., et al., *Viral protein synthesis is required for Enterovirus 71 to induce apoptosis in human glioblastoma cells.* J Neurovirol, 2008. **14**(1): p. 53-61.

136. Tolskaya, E.A., et al., *Apoptosis-inducing and apoptosis-preventing functions of poliovirus.* J Virol, 1995. **69**(2): p. 1181-9.

137. Chipuk, J.E., et al., *Direct activation of Bax by p53 mediates mitochondrial membrane permeabilization and apoptosis.* Science, 2004. **303**(5660): p. 1010-4.

138. Al-Molawi, N., et al., *Caspase-mediated cleavage of the feline calicivirus capsid protein.* J Gen Virol, 2003. **84**(Pt 5): p. 1237-44.

139. Cheng, F., et al., *The capsid proteins of Aleutian mink disease virus activate caspases and are specifically cleaved during infection.* J Virol, 2010. **84**(6): p. 2687-96.

140. Bryant, B. and R.J. Clem, *Caspase inhibitor P35 is required for the production of robust baculovirus virions in Trichoplusia ni TN-368 cells.* J Gen Virol, 2009. **90**(Pt 3): p. 654-61.

141. Lipton, H.L., G. Twaddle, and M.L. Jelachich, *The predominant virus antigen burden is present in macrophages in Theiler's murine encephalomyelitis virus-induced demyelinating disease.* J Virol, 1995. **69**(4): p. 2525-33.

142. Rossi, C.P., et al., *Role of macrophages during Theiler's virus infection.* J Virol, 1997. **71**(4): p. 3336-40.

143. Tsunoda, I., C.I. Kurtz, and R.S. Fujinami, *Apoptosis in acute and chronic central nervous system disease induced by Theiler's murine encephalomyelitis virus.* Virology, 1997. **228**(2): p. 388-93.

144. Minami, M., et al., *Bcl-w expression is increased in brain regions affected by focal cerebral ischemia in the rat.* Neuroscience letters, 2000. **279**(3): p. 193-5.

145. Cookson, B.T. and M.A. Brennan, *Pro-inflammatory programmed cell death.* Trends Microbiol, 2001. **9**(3): p. 113-4.

146. Arslan, S.Y., K.N. Son, and H.L. Lipton, *The antiapoptotic protein Mcl-1 controls the type of cell death in Theiler's virus-infected BHK-21 cells.* J Virol, 2012. **86**(4): p. 1922-9.

147. Schulze-Osthoff, K., et al., *Cytotoxic activity of tumor necrosis factor is mediated by early damage of mitochondrial functions. Evidence for the involvement of mitochondrial radical generation.* J Biol Chem, 1992. **267**(8): p. 5317-23.

148. Vandenabeele, P., et al., *Molecular mechanisms of necroptosis: an ordered cellular explosion.* Nat Rev Mol Cell Biol, 2010. **11**(10): p. 700-14.

149. Davis, R.J., *Signal transduction by the JNK group of MAP kinases.* Cell, 2000. **103**(2): p. 239-52.

150. Morgan, M.J., Y.S. Kim, and Z. Liu, *Lipid rafts and oxidative stress-induced cell death.* Antioxid Redox Signal, 2007. **9**(9): p. 1471-83.

151. Degterev, A., et al., *Chemical inhibitor of nonapoptotic cell death with therapeutic potential for ischemic brain injury.* Nat Chem Biol, 2005. **1**(2): p. 112-9.

152. Tait, S.W. and D.R. Green, *Caspase-independent cell death: leaving the set without the final cut.* Oncogene, 2008. **27**(50): p. 6452-61.

153. Declercq, W., T. Vanden Berghe, and P. Vandenabeele, *RIP kinases at the crossroads of cell death and survival.* Cell, 2009. **138**(2): p. 229-32.

154. Fiers, W., et al., *TNF-induced intracellular signaling leading to gene induction or to cytotoxicity by necrosis or by apoptosis.* J Inflamm, 1995. **47**(1-2): p. 67-75.

155. Benedict, C.A., P.S. Norris, and C.F. Ware, *To kill or be killed: viral evasion of apoptosis.* Nat Immunol, 2002. **3**(11): p. 1013-8.

156. Walsh, J.G., et al., *Caspase-1 promiscuity is counterbalanced by rapid inactivation of processed enzyme.* J Biol Chem, 2011. **286**(37): p. 32513-24.

157. Ahmed, M., et al., *Regions of the herpes simplex virus type 1 latency-associated transcript that protect cells from apoptosis in vitro and protect neuronal cells in vivo.* J Virol, 2002. **76**(2): p. 717-29.

158. Asano, S., et al., *US3 protein kinase of herpes simplex virus protects primary afferent neurons from virus-induced apoptosis in ICR mice.* Neuroscience letters, 2000. **294**(2): p. 105-8.

159. Aubert, M. and J.A. Blaho, *Viral oncoapoptosis of human tumor cells.* Gene Ther, 2003. **10**(17): p. 1437-45.

160. Branco, F.J. and N.W. Fraser, *Herpes simplex virus type 1 latency-associated transcript expression protects trigeminal ganglion neurons from apoptosis.* J Virol, 2005. **79**(14): p. 9019-25.

161. Galvan, V. and B. Roizman, *Herpes simplex virus 1 induces and blocks apoptosis at multiple steps during infection and protects cells from exogenous inducers in a cell-type-dependent manner.* Proc Natl Acad Sci U S A, 1998. **95**(7): p. 3931-6.

162. Ruby, J., H. Bluethmann, and J.J. Peschon, *Antiviral activity of tumor necrosis factor (TNF) is mediated via p55 and p75 TNF receptors.* J Exp Med, 1997. **186**(9): p. 1591-6.

163. Gerety, S.J., et al., *Class II-restricted T cell responses in Theiler's murine encephalomyelitis virus-induced demyelinating disease. VI. Potentiation of demyelination with and characterization of an immunopathologic CD4+ T cell line specific for an immunodominant VP2 epitope.* J Immunol, 1994. **152**(2): p. 919-29.

164. Olson, J.K., T.N. Eagar, and S.D. Miller, *Functional activation of myelin-specific T cells by virus-induced molecular mimicry.* J Immunol, 2002. **169**(5): p. 2719-26.

165. Borrow, P., et al., *Investigation of the role of delayed-type-hypersensitivity responses to myelin in the pathogenesis of Theiler's virus-induced demyelinating disease.* Immunology, 1998. **93**(4): p. 478-84.

166. Chamorro, M., C. Aubert, and M. Brahic, *Demyelinating lesions due to Theiler's virus are associated with ongoing central nervous system infection.* J Virol, 1986. **57**(3): p. 992-7.

167. Lipton, H.L., et al., *Theiler's virus antigen detected in mouse spinal cord 2 1/2 years after infection.* Neurology, 1984. **34**(8): p. 1117-9.

168. Trottier, M., B.P. Schlitt, and H.L. Lipton, *Enhanced detection of Theiler's virus RNA copy equivalents in the mouse central nervous system by real-time RT-PCR.* J Virol Methods, 2002. **103**(1): p. 89-99.

169. Christophi, G.P., et al., *Modulation of macrophage infiltration and inflammatory activity by the phosphatase SHP-1 in virus-induced demyelinating disease.* J Virol, 2009. **83**(2): p. 522-39.

170. Wee, L.J., T.W. Tan, and S. Ranganathan, *SVM-based prediction of caspase substrate cleavage sites.* BMC Bioinformatics, 2006. **7 Suppl 5**: p. S14.

171. Chae, H.J., et al., *Molecular mechanism of staurosporine-induced apoptosis in osteoblasts.* Pharmacol Res, 2000. **42**(4): p. 373-81.

172. Gaddy, D.F. and D.S. Lyles, *Vesicular stomatitis viruses expressing wild-type or mutant M proteins activate apoptosis through distinct pathways.* J Virol, 2005. **79**(7): p. 4170-9.

173. Zhirnov, O. and A.G. Bukrinskaya, *Nucleoproteins of animal influenza viruses, in contrast to those of human strains, are not cleaved in infected cells.* J Gen Virol, 1984. **65 (Pt 6)**: p. 1127-34.

174. Arzberger, S., M. Hosel, and U. Protzer, *Apoptosis of hepatitis B virus-infected hepatocytes prevents release of infectious virus.* J Virol, 2010. **84**(22): p. 11994-2001.

175. Majerciak, V., et al., *Caspase-7 cleavage of Kaposi sarcoma-associated herpesvirus ORF57 confers a cellular function against viral lytic gene expression.* J Biol Chem, 2010. **285**(15): p. 11297-307.

176. Lee, W.M., S.S. Monroe, and R.R. Rueckert, *Role of maturation cleavage in infectivity of picornaviruses: activation of an infectosome.* J Virol, 1993. **67**(4): p. 2110-22.

177. Pelletier, I., et al., *Characterization of the poliovirus 147S particle: new insights into poliovirus uncoating.* Virology, 2003. **305**(1): p. 55-65.

178. Katpally, U., et al., *Antibodies to the buried N terminus of rhinovirus VP4 exhibit cross-serotypic neutralization.* J Virol, 2009. **83**(14): p. 7040-8.

179. Deleu, L., et al., *Inhibition of transcription-regulating properties of nonstructural protein 1 (NS1) of parvovirus minute virus of mice by a dominant-negative mutant form of NS1.* J Gen Virol, 2001. **82**(Pt 8): p. 1929-34.

180. Richard, A. and D. Tulasne, *Caspase cleavage of viral proteins, another way for viruses to make the best of apoptosis.* Cell Death Dis, 2012. **3**: p. e277.

181. Borst, E.M., et al., *Genetic evidence of an essential role for cytomegalovirus small capsid protein in viral growth.* J Virol, 2001. **75**(3): p. 1450-8.

182. Crowder, S. and K. Kirkegaard, *Trans-dominant inhibition of RNA viral replication can slow growth of drug-resistant viruses.* Nat Genet, 2005. **37**(7): p. 701-9.

VITA

NAME: Sevim Yildiz Arslan

EDUCATION: B.S., Molecular Biology and Genetics, Halic University, Istanbul, Turkey, 2004

PhD., Department of Microbiology and Immunology, College of Medicine, University of Illinois at Chicago, Chicago, Illinois, 2012

EXPERIENCE: Research Assistant, Department of Microbiology and Immunology, College of Medicine, University of Illinois at Chicago, 2007-2012

Research Associate, University of Illinois at Chicago, Department of Psychiatry, The Psychiatric Institute, Chicago, 2005-2006

Intern, Pfizer Inc. Medical Division, Istanbul, Turkey, 2004

Research Associate, University of Illinois at Chicago, Department of Psychiatry, The Psychiatric Institute, Chicago, 2003

Intern, Istanbul University, Department of Molecular Medicine, Institute of Experimental Medical Research, Istanbul, Turkey, 2002-2003

Bogazici University, Department of Medical Biology and Genetics, Istanbul, Turkey, 2001-2002

AWARDS AND

HONORS: American Heart Association Midwest Affiliate Predoctoral Fellowship, 2011-2013

Chicago Biomedical Consortium (CBC) Scholar Recipient, University of Illinois at Chicago, Chicago, 2010-2012

W.C. and May Deiss Award for Biomedical Research, University of Illinois at Chicago, Chicago, 2011-2012

Student Presenter Award, University of Illinois at Chicago, Chicago, 2011-2012

American Society for Virology (ASV) Student Travel Grant, 2010-2011

Graduate Student Council Travel Award, University of Illinois at Chicago, Chicago, 2009-2010

Student Presenter Award, University of Illinois at Chicago, Chicago, 2009-2010

Full scholarship for MS education awarded by the US Army Dental and Trauma Research Detachment at Great Lakes, IL, 2006-2008

PROFESSIONAL MEMBERSHIPS:

AHA Student Member

ASV Associate Member

EACR Student Member

AAPS Associate Member

AADR Associate Member

ISBOR Associate Member

FEBS Student Member

PUBLICATIONS: **Arslan SY.,** Son KN., Lipton HL. The antiapoptotic protein Mcl-1 controls the type of cell death in Theiler's virus-infected BHK-21 cells. J Virol. 2012 Feb;86(4):1922-9.

Arslan SY., Leung KP., Wu CD. The effect of lactoferrin on oral bacterial attachment. Oral Microbiol Immunol. 2009. **24**(5): p. 411-6.

Fan J, Son, K-N., **Arslan SY.**, Liang Z, Lipton, HL. The Theiler's murine encephalomyelitis virus leader protein is the only nonstructural protein tested that induces apoptosis when transfected into mammalian cells. J Virol. 2009. **83**(13): p. 6546-53.

Imbesi, M., **Yildiz, S**., Dirim Arslan, A., Sharma, R., Manev, H. and Uz, T., Dopamine receptor-mediated regulation of neuronal "clock" gene expression. Neuroscience, 2009. **158**(2): p. 537-44.

Imbesi, M., Arslan, A.D**.**, **Yildiz, S**., Sharma, R., Gavin, D., Tun, N., Manev, H. and Uz, T., The melatonin receptor MT1 is required for the differential regulatory actions of melatonin on neuronal 'clock' gene expression in striatal neurons in vitro. J Pineal Res, 2009. **46**(1): p. 87-94.

Imbesi M, Uz T, **Yildiz S**, Arslan AD, Manev H. Drug- and region-specific effects of protracted antidepressant and cocaine treatment on the content of melatonin MT(1) and MT(2) receptor mRNA in the mouse brain. Int J Neuroprot Neuroregener. 2006. **2**: p. 185-9.

Dimitrijevic N, Dzitoyeva S, Satta R, Imbesi M, **Yildiz S**, Manev H. Drosophila GABA(B) receptors are involved in behavioral effects of gamma-hydroxybutyric acid (GHB). Eur J Pharmacol. 2005. **519**(3): p. 246-52.

ABSTRACTS: **Arslan SY.** and Lipton HL., The anti-apoptotic Bcl-2 family member Mcl-1 controls the type of cell death in BeAn virus-infected BHK-21 cells. 9th Annual Meeting on Cell Death, Cold Spring Harbor Laboratory (CSHL), 2011, Cold Spring Harbor, NY.

Arslan SY. and Lipton HL., Regulation of Theiler's virus-induced cell death. 30th Annual American Society for Virology Meeting (ASV), 2011, Minneapolis, MN.

Arslan SY. and Lipton HL., Mcl-1 is an essential factor that protects against apoptosis in p53-dependent manner, restricting the production of Theiler's virus. Chicago Biomedical Consortium (CBC) Science Day, 2011, Chicago, IL.

Arslan SY. and Lipton HL., Mcl-1 is an essential factor that protects against apoptosis in p53-dependent manner, restricting the production of Theiler's virus. Student Research Forum, UIC, 2011, Chicago, IL.

Arslan SY. and Lipton HL., Regulation of Theiler's virus-induced cell death. College of Medicine Research Forum, UIC, 2010, Chicago, IL

Arslan SY. and Lipton HL., 9th International Symposium on Positive-Strand RNA Viruses, 2010, Atlanta, GA.

Yildiz S., Leung KP. and Wu CD., 37th Annual Meeting of American Association for Dental Research (AADR), 2008, Dallas, TX.

Yildiz S., Leung KP. and Wu CD., Student Research Forum, UIC, 2007, Chicago, IL.

Yildiz S., Leung KP. and Wu CD., 20th Annual Meeting of College of Dentistry's Clinic and Research Day, UIC, 2007, Chicago, IL.

Coulburn, J., Chin, Y-W., Parekh, H., **Yildiz, S**., Beavers, R.,

Kinghorn, AD., and Wu, CD., 35th Annual Meeting of International Association for Dental Research (IADR), 2006, Orlando, Florida.

Toepke, TRS., Drahos, P., **Yildiz, S.,** and Wu, CD., 35th Annual Meeting of International Association for Dental Research (IADR), 2006, Orlando, Florida.